The importance of H2O in arc magmas for the formation of porphyry Cu deposits

The importance of H_2O in arc magmas for the formation of porphyry Cu deposits

Hervé Rezeau† and Oliver Jagoutz

Department of Earth, Atmospheric, and Planetary Sciences, MIT, Cambridge, USA

†Corresponding author: hrezeau@mit.edu

Keywords: Arc magmas; Calc-alkaline and tholeiitic series; Magmatic sulfides; Melt water content; Ore-forming potential; Porphyry copper deposits.

ABSTRACT

Porphyry copper deposits (PCDs) hosted in subvolcanic intrusions at convergent margins are the primary world's copper resources. However, the set of magmatic processes that lead to the generation of ore-bearing magmatic provinces remains unclear. In this paper we review the systematic of Cu evolution during arc magmatic differentiation using new and existing global compilations of whole rock geochemistry data. We trace the Cu evolution from primitive arc magmas through lower crustal plutonic to volcanic rocks. We focus on the well-known tholeiitic and calc-alkaline fractionation sequences, where arc tholeiitic series represents damp primitive melts (<2 wt% H_2O) evolving with iron enrichment, and calc-alkaline series are wet primitive melts (>2 wt% H_2O) that differentiate with iron depletion.

Our study shows that the Cu concentration in primitive arc melts (~80 ppm) is indistinguishable from that of primitive melts formed at mid-ocean ridges (MORBs) implying that Cu is mainly sourced from the mantle wedge in arcs with a limited contribution from the subducted oceanic lithosphere. A global compilation of plutonic rocks whole rock geochemistry (lower crustal cumulates and derivative melts) indicate no systematic difference in Cu concentrations between cumulates associated with tholeiitic or calc-alkaline series. Yet a complementary global compilation of arc volcanic whole rock geochemistry highlights the contrasting behavior of Cu in tholeiitic and calc-alkaline series during magmatic differentiation in arc. In tholeiitic series, Cu shows an incompatible and/or compatible behavior during magma differentiation influenced by the crustal thickness. In calk-alkaline series, Cu is compatible during magma differentiation independently to the crustal thickness. This relates to the timing of sulfide saturation, which is controlled by the

liquid lines of descent (LLD) and/or crustal thickness at redox conditions relevant for arc magmas.

We demonstrate that the initial melt H_2O content in primitive arc melts controls the LLD and the volume of remaining melt mass at fluid saturation. We show that the remaining H_2O-saturated melt mass positively correlates with the total mass of Cu transferred into degassing fluids. The mass of extractable Cu ranges from ~3 to ~10 Mt (i.e., large PCD) for calc-alkaline series, and ranges from ~0.3 to ~2.5 Mt for tholeiitic series. The ore-forming potential of calc-alkaline arc magmas is at least ~4 to ~10 times higher relative to tholeiitic arc magmas. Despite the compatible behavior of Cu during magmatic differentiation, we propose that a single stage model for the formation of large economic PCDs (as opposed to multi-stage model for Cu-sulfides storage and remobilization) is most applicable for the calc-alkaline melts. The importance of the initial melt H_2O content ultimately reflects the key role of flux melting associated with wet calc-alkaline series and high ore-forming potential, in opposition to decompression melting associated with damp tholeiitic series.

1. Introduction

Porphyry copper deposits (PCDs) formed in arc setting represent ~75% of the global copper resources (Sillitoe, 2010). Large economic PCDs are dominantly associated with volatile-rich and oxidized calc-alkaline sub-volcanic intrusions in continental arcs, although some important ones are also formed in oceanic island arcs (Fig. 1; Kesler et al., 1975; Titley, 1975; Solomon, 1990; Richards, 2003, 2011a; Cooke et al., 2005; Sillitoe, 1997, 2010). Magmatic-hydrothermal processes directly associated with the formation of PCDs are reasonably well understood (e.g., Seedorff et al., 2005; Sillitoe, 2010; Kouzmanov and Pokrovski, 2012). In contrast, the role of precursor magmatism (and related source and crustal processes) to generate magmas able to form ore deposits remains less clear (e.g., Audétat and Simon, 2012; Wilkinson, 2013; Richards, 2015). Specifically, the importance of magmatic sulfide crystallization and saturation of a fluid phase acting as the main Cu scavengers during magmatic differentiation is unclear.

Copper is incompatible during magmatic differentiation in thin island arc (<20 km) dominated by tholeiitic series, whereas Cu is compatible during magmatic differentiation in thick continental arc (>30 km) dominated by calc-alkaline series (e.g., Lee et al., 2012;

Chiaradia, 2014). Crustal thickness is proposed to have a first-order control on arc magma differentiation (Miyashiro, 1974; Chiaradia, 2014) and hence the Cu evolution in arc magmas (Chiaradia, 2014; Lee and Tang, 2020). Furthermore, the different tholeiitic and calc-alkaline liquid lines of descent (LLD) control the evolution of the melt redox conditions (expressed in terms of oxygen fugacity, fO_2) in the crust, which in turn impact the solubility of sulfur and Cu through sulfide immiscibility (e.g., Lee et al., 2012), potentially linked to the onset of magnetite crystallization (Jenner et al., 2010; Chiaradia, 2014). Alternative views suggest that the initial H_2O in primitive magma primarily control the LLD (Sisson and Grove, 1993; Tatsumi and Susuki, 2009; Zimmer et al., 2010; Jagoutz et al., 2011; Müntener and Ulmer, 2018), and high initial melt H_2O contents (>4wt% H_2O) combined with high fO_2 in the source region are thought to play a major role for the formation of PCDs (Richards, 2003, 2009, 2011a, 2015; Sun et al., 2015, 2017). As a result, endmember models for PCDs formation in arcs can be grouped in two: (1) multi-stage models envision that early magmatic Cu-sulfide saturation in the deep arc crust represent a key pre-enrichment step to the formation of PCDs in continental arc dominated by calc-alkaline series. Subsequent events within the same or later magmatic cycle remobilize the Cu from these cumulates to form PCDs in the upper crust (e.g., Lee et al., 2012; Wilkinson, 2013; Chiaradia, 2014); alternatively (2) single-stage models consider PCDs formed from metal precipitated from hydrothermal fluids that are exsolved from differentiated mantle-derived, volatile-rich and oxidized calc-alkaline magmas (e.g., Richards, 2009, 2011a, 2015; Sun et al., 2015, 2017).

For both endmember models, a wide range of crucial parameters for the formation of PCDs have been proposed that include the initial metal endowment (McInnes et al., 1999; Mungall, 2002; Sun et al., 2017; Zheng et al., 2018), the melt water concentration (Richards, 2011a,b; Chiaradia et al., 2012; Loucks, 2014; Chiaradia and Caricchi, 2017), the melt redox conditions (Lee et al., 2012; Richards et al., 2015; Sun et al., 2015; Lee and Tang, 2020), the melt metal concentration and/or the melt volume at the time of magmatic fluid saturation (Cline and Bodnar, 1991; Richards, 2009; Park et al., 2019; Chelle-Michou et al., 2017), the duration of the precursor magmatism (Rezeau et al., 2016; Chelle-Michou et al., 2017; Chiaradia and Caricchi, 2017; Richards, 2018) and the overriding plate thickness (i.e.,

pressure of melt differentiation; Chiaradia, 2014; Matjuschkin et al., 2016; Cox et al., 2019; Lee and Tang, 2020).

The evolution of Cu during arc magma differentiation results from a complex interplay of processes occurring in the mantle source region and/or in the crust. Thus, it remains unclear which parameter(s) primarily control the ore-forming potential of arc magmas. This contribution aims to critically evaluate the role of source- and crustal-related magmatic processes related to the ore-forming potential, and examine their respective importance. Here, we use a global compilation of arc volcanic and plutonic (cumulates and derivative melts) whole rock geochemical analyses to systematically characterize the evolution of Cu in arc magmas during magmatic differentiation starting from primitive mantle derived arc magmas. Our global compilation aims to evaluate the role of primitive magma Cu concentration, initial water content, fO_2, pressure of melt differentiation and different LLD for the formation of economic PCDs in the light of the above mentioned two endmember models. Our results emphasize the primary role of the initial melt H_2O content regarding the ore-forming potential of arc magmas, whereas the initial melt Cu content is of secondary importance. We show that a single stage model can explain the formation of large economic PCDs associated with wet calc-alkaline arc series, whereas the multi-stage model is applicable form PCD formed from damp tholeiitic arc series. Ultimately, we propose that the initial melt H_2O content reflect the importance of the melting regime in the mantle wedge, i.e., flux melting in contrast to decompression melting.

2. Copper concentration in primitive arc magmas: implications for the source of Cu

2.1 Dataset and results

Previous studies reported Cu concentration in primitive arc basalts and mid-oceanic ridge basalts (MORBs) ranging from ~50 to ~100 ppm (Jenner et al., 2010; Jenner and O'Neill, 2012; Lee et al., 2012; Chiaradia, 2014; Richards, 2015). Here, we reevaluate the Cu concentration between the different types of primitive arc melts and geodynamic settings. We used the primitive arc melts compilation of Schmidt and Jagoutz (2017) with available whole rock Cu analyses (n=422) from 20 arcs including intra-oceanic, continental and back-arc settings (Supplemental Material Table A1). For this study, we present Cu concentration in primitive arc melts using the same classification scheme as Schmidt and Jagoutz (2017),

with the exception of primitive depleted tholeiitic andesites which are considered fractionated melts. Here, they are classified into five types: (1) primitive calc-alkaline basalts (n=82), (2) primitive tholeiitic basalts (n=50), (3) primitive low-Si basalts (n=64), (4) primitive shoshonites (n=78), and (5) primitive high-Mg andesites (n=148) (Fig. 2; Table A1). For the sake of comparison, we also compiled whole rock Cu analyses (n=58) in primitive MORBs using the data set of Gale et al. (2013). Primitive MORBs were selected based on the same criteria used by Schmidt and Jagoutz (2017) for arc primitive melts, i.e., Mg# of 0.65-0.75, Ni concentrations of 150-500 ppm, and Cr concentrations of < 1200 ppm (Table A1).

Our global compilation indicates that the Cu concentration of primitive arc melts range from 35 to 120 ppm with a global average of 78 ± 31 ppm (1σ) for primitive arc basalts and of 42 ± 17 ppm for primitive high-Mg andesites (Fig. 2). By comparison, the Cu concentration in primitive MORBs display a similar range from 50 to 130 ppm, with a global average of 81 ± 20 ppm (Fig. 2) indistinguishable from primitive arc basalts. Among primitive arc basalts, there is no systematics correlation between the Cu concentrations, the types of primitive melt and/or the geodynamic settings. Only the high-Mg andesites are characterized by systematically lower Cu concentrations.

2.2 The source of Cu in arc magmas

A magmatic origin for Cu in PCDs is widely accepted based on isotopic composition of hydrothermal and magmatic sulfides, ore-forming fluids, and the genetically related igneous intrusions (e.g., Hedenquist and Lowenstern, 1994; Rezeau et al., 2016; Zheng et al., 2018). However, there is no consensus whether Cu in arc magmas is directly derived from the mantle wedge/refertilized sub-continental lithospheric mantle (e.g., McInnes et al., 1999; Richards, 2009; Hou et al., 2017; Wang et al., 2018; Zheng et al., 2018) or dominantly inherited from the subducting oceanic lithosphere by slab-related fluid/melt (e.g., Mungall, 2002; Sun et al., 2017).

2.2.1 Mantle-derived vs. slab-related

The Cu concentrations in primitive arc basalts range from 50 to 120 ppm, with no systematics regarding the types of primitive melt and/or the geodynamic settings (Fig. 2). The range of Cu concentration in primitive arc basalts can be generated after 5 to 30% of melting of a mantle source having an initial Cu concentration of 30 ppm at fO_2 ranging from ΔFMQ = 0 to 2 (Lee et al., 2012), which could be reconciled with primitive arc basalts formed by variable degree of partial melting at different pressure in the mantle wedge (Schmidt and Jagoutz, 2017). Alternatively, the range of Cu in primitive melts may represent variable input of Cu from slab-related fluid and/or melt. In this case, we would expect a positive correlation between incompatible elements and Cu content. Our global compilation lacks of such systematics as demonstrated by similar average Cu contents (and a comparable range of Cu) for the different types of primitive basalts characterized by variable involvement of slab-related fluid and/or melts (Table A1; Schmidt and Jagoutz, 2017). This is consistent with the limited remobilization of chalcophile elements from subducted sulfide ore deposits during dehydration of the subducting oceanic lithosphere (Tomkins, 2010; Giacometti et al., 2015). More importantly, primitive arc basalts and MORBs are characterized by the same global average Cu concentration of ~80 ppm irrespective of the degree of subduction-related inputs (Fig. 2). Therefore, our observations are consistent with previous studies (McInnes et al., 1999; Jenner et al., 2010; Lee et al., 2012; Chiaradia, 2014; Richards, 2015) and strongly suggest the predominant contribution of Cu from the mantle without necessarily requiring additional input from slab-related fluids and/or melts.

2.2.2 Refertilization and Cu enrichment via melt-rock reaction

In arc setting, Cu and Os isotope studies suggest that Cu enrichment is linked to the refertilization of the sub-arc mantle through the redistribution of primary sulfides into sulfide-bearing metasomatic veins by slab-related oxidizing fluids (e.g., McInnes et al., 1999; Zheng et al., 2018). Our compilation reveals that primitive high-Mg andesites are characterized by the lowest Cu concentrations (Fig. 2), which are positively correlated with MgO (Supplemental Figure A1). Primitive high-Mg andesites has been proposed to represent lower temperature derivatives of primitive calc-alkaline basalts through melt-rock reaction (also known as refertilization) in the shallow mantle and/or arc lithosphere (Kelemen et

al.,1995; Kelemen et al., 2014; Schmidt and Jagoutz, 2017). Consequently, we suggest that the low Cu concentrations in primitive high-Mg andesites reflect Cu-sulfide fractionation, which occur during melt-rock reaction. Such mechanism has been documented in a suite of MORBs erupted at the Kane Megamullion, where Cu enrichment in the shallow mantle results from melt-peridotite reaction (Ciazela et al., 2017). Similarly, melt-rock reaction in the arc mantle region could represent an additional mechanism for local Cu enrichment in the sub arc mantle and/or arc lithosphere. We envision that subsequent remelting of these zones may account for unusually high Cu content in primitive arc basalts.

3. Copper concentration in volcanic arc rocks

3.1 Dataset

It has long been recognized that differentiation of arc magmas dominantly follow either a tholeiitic or calc-alkaline series with minor importance of an alkaline series (e.g., Miyashiro, 1974). Global whole rock compilation suggests that the crustal thickness of the overriding plates represents a first-order control on tholeiitic and calc-alkaline differentiation series (Miyashiro, 1974; Chiaradia, 2014, 2015). Yet, tholeiitic and calc-alkaline arc magmas are documented to coexist along the same arc segment from fore-arc to back-arc (e.g., Cascades, Baker et al., 1994; Mandler et al., 2014; Kamchatka, Portnyagin et al., 2007; Izu-Bonin-Mariana, Tatsumi and Susuki, 2009; Brounce et al., 2014; Aleutians, Zimmer et al., 2010). It has been proposed that the geochemical differences between tholeiitic and calc-alkaline series relate to different LLDs controlled by the initial H_2O content of the primitive arc melt (Sisson and Grove 1993; Zimmer et al., 2010; Jagoutz et al., 2011; Melekhova et al., 2013; Müntener and Ulmer, 2018). It has been proposed that primitive arc magmas with high initial H_2O content, that evolve along a calk-alkaline fractionation sequence are related to flux melting in the sub arc mantle (Grove et al., 2002, 2012; Cervantes and Wallace, 2003; Jagoutz et al., 2011). Flux melting occurs because the melting point of peridotite is significantly lowered due to the addition of water in the mantle wedge (e.g., Grove et al., 2012). The influx of slab-derived hydrous melts/fluids hence produces melts with high initial H_2O. Alternatively, the sub arc mantle can melt due to adiabatic decompression, which produces melts with lower initial H_2O content that evolve along a tholeiitic LLD (Grove et al., 2002, 2012).

Here, we produce a global compilation of whole rock analyses with available Cu of arc volcanic rocks from the georoc database (http://georoc.mpch-mainz.gwdg.de/georoc/) to evaluate the Cu evolution between tholeiitic and calc-alkaline magmatic series along individual arc segment. The discrimination between volcanic rock following a calc-alkaline (n=9,275) or tholeiitic (n=6,114) differentiation trend is based on the classical FeO/MgO versus SiO_2 relationship (Supplemental Figure B1; Miyashiro, 1974). Our global compilation includes volcanic rocks from 28 different magmatic arcs for a total of 15,389 entries (Figs. 1, 3, C1 and D1; Supplementary Table B1). The analyses included in the database fulfilled the following criteria: a loss of ignition (LOI) < 2 wt% (if provided), totals of 97-102 wt%, SiO_2 of 50-70 wt%, MgO of 0.5-10 wt% and FeO/MgO ratio < 15 to avoid any exotic melt compositions. Note that we screened and removed analyses from known mineralized porphyry district to avoid high Cu concentration influenced by ore-forming hydrothermal fluids overprint that are unrelated to the original melt Cu endowment. In the following, all the whole rock data have been recalculated on an anhydrous basis.

3.2 Results

Our global compilation of volcanic rocks shows a wide range of Cu concentrations. For MgO ranging from 0.5 to 10 wt%, most of the Cu data ranges from <10 to ~400 ppm in tholeiitic series and from <10 to ~150 ppm in calc-alkaline series (Fig. 3a,d). During magma differentiation (i.e., decreasing MgO concentration), the evolution of Cu concentrations in tholeiitic and calc-alkaline series differs significantly. In tholeiitic series, the Cu concentration increases from the typical primitive arc basalts value of ~80 ppm at 10 wt% MgO, to the highest values between 3.5 and 5 wt% MgO with a maximum median Cu concentration of ~110 ppm at ~4.2 wt% MgO. This is followed by a decrease of Cu concentration down to a median concentration of ~10 ppm at 0.5 wt% MgO (Fig. 3a). FeO_{tot} and V concentrations also exhibit the highest values between 3.5 and 5 wt% MgO (Fig. 3b,c). In calk-alkaline series, the median Cu concentration steadily decreases from the typical primitive arc magma value of ~80 ppm at 10 wt% MgO to ~10 ppm at 0.5 wt% MgO (Fig. 3d). Both FeO_{tot} and V concentration also mimics the evolution trend of Cu (Fig. 3e, f). This suggests an apparent broad correlation between Cu, FeO_{tot} and V for both tholeiitic and calc-alkaline series. Based on this correlation, the switch from incompatible to compatible

behavior of Cu at MgO ~3-5 wt% is ascribed to the late onset of Fe-oxides crystallization in tholeiitic series, whereas the compatible behavior of Cu relates to the early Fe-oxides crystallization in calc-alkaline magmas (Jenner et al., 2010; Chiaradia, 2014). In details, however, the correlation between the three elements is weak for 17 individual representative arc segments characterized by more than 300 whole rock analyses with available Cu (Fig. 4a, b; Fig. C1 and D1; Table B1). For calc-alkaline and tholeiitic series, FeO_{tot} and V are systematically positively correlated (Fig. 4b). Experiments for tholeiitic and calc-alkaline LLDs have demonstrated that the decrease of FeO_{tot} is closely related to the onset of crystallization of Fe-Ti-oxides (spinel hercynite, ilmenite, magnetite; Villiger et al., 2004; Nandedkar et al., 2014; Ulmer et al., 2018) for which V have a high partition coefficient (Kd>>1 up to 130; Luhr and Carmichael, 1980; Latourrette et al. 1991; Canil, 1999). In contrast, the evolution of Cu is generally poorly correlated with FeO_{tot} and V (Fig.4a), although few arcs display positive correlation (e.g., Izu-Bonin, Aleutians; Fig. C1 and D1). Thus, Fe-oxides crystallization may not necessarily have a large effect on Cu depletion.

We use the Cu concentration at MgO~4 wt% (Cu_4) relative to the initial average Cu concentration in primitive arc basalts of ~80 ppm to evaluate the Cu enrichment or depletion during magmatic differentiation (Fig. 4c, d). With the exception of one arc segment (Central America), calc-alkaline series show a systematic depletion of Cu during magma differentiation (Fig. 4c, d), while tholeiitic series are characterized by Cu enrichment and depletion during magmatic differentiation (Fig. 4c, d). For tholeiitic series, we observe a systematic Cu enrichment in thin arcs (<25 km), which ultimately correlates with the highest FeO_{tot} enrichment at MgO~4 wt% (i.e., Fe_4). For tholeiitic series formed in thicker arcs (>25 km), the Cu depletion dominates. These observations indicate that the evolution of Cu during magma differentiation is influenced by the LLD and the pressure of magma differentiation that are further discussed below among other parameters.

3. Copper concentration in plutonic rocks and derivative melts

Finally, based on the compilation of Jagoutz and Kelemen (2015) and Jagoutz and Klein (2018), we produced a compilation of whole rock Cu analyses for lower crustal cumulates and their derivative melts from the Kohistan arc in Pakistan, Talkeetna arc in Alaska, Sierra Valle Fértil–Sierra Famatina complex in Argentina, Fiordland in New Zealand

(Table C1). A complementary whole rock compilation of Cu-bearing cumulates from Chin et al., 2018 is also included in Table C1, which consist of deep crustal cumulates from Arizona and Sierra Nevada (Western USA), Bonanza arc (British Columbia), Colombia (North Volcanic Andean Zone), Kermadec islands (South Pacific Ocean), and Pontides (NE Turkey). The entire dataset consists in 1606 whole rock major elements analyses, of which 985 include Cu analyses (Table C1).

Our compilation of lower crust plutons that are cumulates and frozen melt compositions (Jagoutz, 2010, Jagoutz et al., 2011) is characterized by a range of SiO_2 from 40 to ~76 wt%, Mg# from 0.9 to 0.2, and Cu concentrations from <10 ppm to 250 ppm (Fig. 5, Table C1). The compiled cumulates are associated with differentiated melt of calc-alkaline signature (Famatina arc, e.g., Otamendi et al., 2009; Fiordland arc, e.g., Allibone et al., 2009; Jijal complex in Kohistan arc, e.g., Jagoutz et al., 2011), tholeiitic signature (Chilas complex in Kohistan arc, e.g., Jagoutz et al., 2011), or overlapping the tholeiitic and calc-alkaline fields (Talkeetna arc, e.g., Greene et al., 2006). Most of the compiled lower crustal plutons are characterized by a "Z" shape trend in the Mg# and SiO_2 space, except for the Chilas complex in Kohistan (Fig. 5a). The different patterns are related to different LLD such as the "Z" shape represents wet fractionation associated with calc-alkaline series, whereas the others represent dry fractionation linked to tholeiitic series (Jagoutz, 2010; Jagoutz et al., 2011; Müntener and Ulmer, 2018). Our global compilation of lower crustal cumulates do not show any systematics difference in whole rock Cu concentrations between cumulates associated with calc-alkaline or tholeiitic series (Fig. 5b).

4. Discussion

When melt reaches sulfide or water saturation during magmatic differentiation Cu is strongly partitioned into magmatic sulfides and/or the fluid phase. Therefore, we first discuss the systematic of magmatic sulfide saturation and its role for the different evolutions of Cu concentration observed between tholeiitic and calc-alkaline magmas (Figs. 3 and 4). Subsequently, we focus on the initial melt H_2O content and its role for the ore-forming potential in arc magmas.

4.1 Sulfide saturation in arc magmas

Magmatic sulfide minerals are known to be highly efficient Cu scavengers, and therefore, it is generally assumed that sulfide saturation plays a crucial role in the ore-forming potential of arc magmas. Indeed, magmatic sulfides are ubiquitous in mafic to felsic volcanic and plutonic rocks (e.g., Stavast et al., 2006; Lee et al., 2012; Zelenski et al., 2017; Georgatou and Chiaradia, 2019). The observed volume of magmatic sulfides in igneous rocks range from <0.1 to 0.6 vol% and directly influences the Cu budget during melt differentiation (Kiseeva and Wood, 2015; Georgatou et al., 2018; Cox et al., 2019). As copper is a highly chalcophile element ($D^{sulfide/melt}_{Cu}$ =~250-1000; Li and Audétat, 2012), its solubility in silicate melt strongly depends on sulfide saturation. Experiments have demonstrated a sharp transition from sulfide (S^{2-}) to sulfate (S^{6+}), where sulfide (S^{2-}) is the dominant sulfur species in hydrous silicate melts under more reducing conditions (fO_2), whereas sulfate (S^{6+}) dominates at higher redox conditions (Fig. 6a; Mavrogenes and O'Neill, 1999; O'Neill and Mavrogenes, 2002; Jugo, 2009; Jugo et al., 2010; Botcharnikov et al., 2011; Fortin et al., 2015; Matjuschkin et al., 2016). Furthermore, higher pressure of differentiation shifts the sulfide-sulfate transition towards higher fO_2 (Fig. 6a; Matjuschkin et al., 2016). The sulfur solubility in silicate melts strongly correlates with the sulfide-sulfate transition, such as the S solubility increases as a function of the fraction of oxidized species in the melt (Fig. 6a; Carroll and Rutherford, 1985; Jugo, 2009; Jugo et al., 2010; Botcharnikov et al., 2011; Matjuschkin et al., 2016). At convergent margins, the redox conditions in primitive arc basalts and sub-arc mantle are on average higher than MORBs, but varies over several log units above the fayalite-magnetite-quartz (FMQ) buffer assemblage from ΔFMQ ~0 to +4 (Fig. 6a; e.g., Carmichael, 1991; Lee et al., 2010, 2012; Evans et al., 2012; Kelley and Cottrell, 2012; Brounce et al., 2014; Bénard et al., 2018; Bucholz and Kelemen, 2019). Furthermore, the pressure of differentiation and the volatiles content (H_2O, S) of primitive melt composition vary within and among arcs (e.g., Grove et al., 2002; Rowe et al., 2009; Zimmer et al., 2010; Wallace and Edmonds, 2011; Brounce et al., 2014; Melekhova et al., 2019). In the following, we discuss the importance of sulfide saturation in terms of possible melt evolution paths at different pressures of differentiation, LLD, redox conditions, and initial sulfur concentrations (Fig. 6a-d) that could explain the Cu evolution in tholeiitic and calc-alkaline differentiation series (Fig. 3a, d).

The effect of variable pressure of differentiation on sulfide saturation

The contrasting Cu evolution trends between tholeiitic and calc-alkaline series could be related to different pressures of differentiation, as at low pressure sulfate stability increases towards lower fO_2, whereas higher pressure expands the sulfide stability field (Fig. 6a; e.g., Matjuschkin et al., 2016). Here we discuss arc melts with identical initial fO_2 of ΔFMQ ~ 1.5 and sulfur concentration that differentiate at 0.2 GPa and 1 GPa (Figs. 6a, b). As sulfur is highly incompatible during fractional crystallization (e.g., Ripley and Li, 2013), the sulfur concentration increases with 1/F (F is the remaining melt mass). At 0.2 GPa, hydrous basaltic melt will reach sulfide saturation at S ~0.5 wt% (Figs. 6a; Botcharnikov et al., 2011). At higher pressure, the sulfide-sulfate transition shift towards higher fO_2, and so does the S solubility curve (Matjuschkin et al., 2016). Considering the lack of available experimental data for hydrous basalt at 1 GPa, we shift the experimental sulfur solubility curve obtained at 0.2 GPa and correlate the highest S solubility with the transition of sulfate-only species curve (S^{6+}/S_{tot} =1) at 1 GPa (Figs. 6a). Thus, we can approximate that a hydrous basaltic melt will reach sulfide saturation at S ~0.15 wt%. Assuming the primitive melt has initially 0.12 wt% S (Fig. 6a; Wallace and Edmonds, 2011; Brounce et al., 2014), the high pressure melt will reach sulfur saturation after ~20% fractionation (F=0.8) whereas the low-pressure melt will reach sulfur saturation after 75% differentiation (F=0.25) (Fig. 6b, Table D1). If pressure of differentiation is the controlling parameter, then our data would indicate that tholeiitic melts on average fractionate shallower than calc-alkaline melts. This conclusion is supported by the empirical observation that the overriding plate thickness controls the Cu and FeO enrichment in thin island arc (<20 km) relative to Cu and FeO depletion in thick continental arcs (>30 km) (Chiaradia, 2014). This first-order observation would be consistent with the increase of sulfide stability with pressure (Matjuschkin et al., 2016; Cox et al., 2019). Furthermore, our results highlight that thicker crust and hence possible higher pressure of differentiation prevents Cu enrichment during magma differentiation even for tholeiitic series (Fig. 4d). This observation supports the idea that higher pressure lower crustal melt differentiation plays an important role to trigger early sulfide saturation. Yet, calc-alkaline series are characterized by early Cu depletion independently to the crustal thickness

suggesting that additional parameters control the timing of sulfide saturation during magma differentiation in these series.

The importance of different liquid line of descent on sulfide saturation

For a primitive melt that differentiates at a similar initial pressure, fO_2 and S concentrations, the contrasting Cu evolution trends could be explained by a progressive change of FeO content and redox conditions controlled by the different LLDs (e.g., Lee et al., 2012) due to different initial melt H_2O content (e.g., Sisson and Grove, 1993; Villiger et al., 2004; Nandedkar et al., 2014). Since the variations of redox conditions are sensitive to the melt $Fe^{3+}/\sum Fe$ ratio, the timing of crystallization of Fe-oxides (i.e., Fe^{3+}-bearing minerals) is expected to control the redox trajectories in a closed magmatic system, lowering the melt $Fe^{3+}/\sum Fe$ ratio and hence the oxygen fugacity (e.g., Ghiorso and Carmichael, 1987; Ulmer et al., 2018). The calc-alkaline series is characterized by an early crystallization of Fe-oxides on the LLD compared to the tholeiitic that crystallize Fe-oxide late on the LLD (Sisson and Grove, 1993). We test the evolution of fO_2 using Rhyolite-MELTS (Gualda et al., 2012) to simulate melt crystallization in a thick crust starting from P = 0.8 GPa to 0.15 GPa and in a thin crust starting from P = 0.4 GPa to 0.15 GPa for temperatures ranging from ~1220-1350°C (liquidus varies as a function of initial melt H_2O content) to ~750-800°C (Table D1). Each computation assumes melt differentiation through progressive decompression and cooling followed by cooling once the melt reaches 0.15 GPa (Table D1). We use a starting primitive melt composition of continental arc calc-alkaline basalt (Schmidt and Jagoutz, 2017) having different initial H_2O content of 4 wt%, 1wt% and 0.2 wt% H_2O to account for calc-alkaline and tholeiitic LLDs (e.g., Sisson and Grove 1993; Tatsumi and Susuki, 2009; Zimmer et al., 2010; Melekhova et al., 2013; Table D1).

The modelled melt evolution confirms that the onset of crystallization of ferric bearing minerals (magnetite) triggers the melt to evolve to lower fO_2. The onset of magnetite fractionation is dependent on the melt H_2O content and occurs at F~0.7 for the calc-alkaline series (4 wt% $H_2O_{initial}$) versus F~0.65-0.4 for the tholeiitic series (1 wt% and 0.2 wt% $H_2O_{initial}$). If both calc-alkaline and tholeiitic melt are S undersaturated at the time of magnetite crystallization, the melt evolves toward lower fO_2 as soon as the magnetite appears on the LLD to promotes sulfide saturation, which occur at higher melt fraction for

calc-alkaline magmas compared to tholeiitic ones (Fig. 6c). For tholeiitic series with 1 wt% $H_2O_{initial}$, magnetite crystallization occurs earlier on the LLD (F~0.65) indicative of the concomitant effect of pressure. Our calculations are consistent with Jenner et al. (2010) and Chiaradia (2014) suggestion that difference in Cu depletion trends between the calc-alkaline and tholeiitic differentiation series could be linked to the timing of magnetite crystallization within the respective LLDs, which is ultimately controlled by the initial H_2O content and the pressure of differentiation. This interpretation can explain the Cu enrichment and depletion observed for tholeiitic series in thin arcs (<25 km) and thick arcs (>25 km), while calc-alkaline series consistently displays Cu depletion irrespective of the crustal thickness (Fig. 4c, d).

The importance of variable initial redox conditions on sulfide saturation

The importance of the initial fO_2 of the melt is illustrated by the compatible character of Cu in MORB during differentiation (Jenner and O'Neill, 2012), where the initial fO_2 is ΔFMQ < 0 and sulfide saturation occurs at low S content (Jugo, 2009; Jugo et al, 2010; Botcharnikov et al., 2011; Matjuschkin et al., 2016). In comparison to MORBs, arc-related tholeiitic series are characterized by the early incompatible and compatible character of Cu in thin and thick arcs, respectively (Figs. 3a and 4c,d). According to the experimental sulfide-sulfate transition curves at different pressures (0.2-1 GPa, Fig. 6a), the incompatible character of Cu (i.e. delayed sulfide saturation) in thin arcs could be explained for initial fO_2 conditions of ΔFMQ > ~1 for the primitive arc melt. In contrast, the compatible character of Cu (i.e. early sulfide saturation) in thick arcs could be explained for initial fO_2 conditions of ΔFMQ < ~2 for the primitive arc melt (Figs. 6a,c). Such range of ΔFMQ~1-2 is consistent with estimates for tholeiitic and calc-alkaline arc basalts along the Aleutian arc (ΔFMQ~+0.4-2.1; Zimmer et al., 2010) and Mariana arc (ΔFMQ~+1-1.6; Brounce et al., 2014), for primitive lower crustal ultramafic cumulates in the Talkeetna arc (ΔFMQ~+0.4-2.3; Bucholz and Kelemen, 2019), and for sub-arc mantle xenoliths in Kamchatka arc (ΔFMQ~ +1-1.5; Bénard et al., 2018). If the initial melt fO_2 controls the different behavior of Cu in arc tholeiitic and calc-alkaline series in thin arcs, it would imply that the arc tholeiitic series differentiate at higher initial fO_2 than calc-alkaline series at the same initial S concentrations (Fig. 6c). Although H_2O itself

is a poor oxidant, the oxidation state of arc magmas is mainly affected by the proportion of subduction-related aqueous components added to the mantle wedge (e.g., Kelley and Cottrell, 2009), and more specifically to the chemical components associated with the slab-derived fluids or melts, i.e., Fe^{3+}, S^{6+}, C^{4+} (Mungall, 2002; Tomkins and Evans, 2015; Bénard et al., 2018; Brounce et al., 2019). A positive correlation between H_2O and fO_2 have been shown from mid-ocean ridges to back-arc tectonic settings (Kelley and Cottrell, 2009; Zimmer et al., 2010; Brounce et al., 2014), while melt inclusions from primitive arc basalts from fore-arc to back-arc in the Oregon Cascades do not show any significant differences in fO_2 between tholeiitic and calc-alkaline melts (Rowe et al., 2009). While the role of slab-derived fluids or melts for the oxidation of arc magmas remains unclear, there is no evidence to assume that arc tholeiitic melts have on average higher fO_2 than calc-alkaline melts. Consequently, the early sulfide saturation observed for calc-alkaline series in thin arcs should reflect other processes than a systematic difference in fO_2 in primitive melts.

The importance of variable initial sulfur concentrations on sulfide saturation

It has been proposed that slab-derived fluids/melts appear to be efficient transfer agent for the transport of sulfur from slab to mantle wedge (Jégo and Dasgupta, 2014), which is supported by higher range of S concentrations measured in arc basalts (up to ~0.9 wt%) compared to MORB (up to ~0.2 wt%; e.g., Jugo et al., 2010; Wallace and Edmonds, 2011). In this case, fluid flux melting should be characterized by higher contribution of an external input of S to the mantle wedge via the devolatilization of the subducting oceanic crust relative to decompression melting. Accordingly, we would expect higher initial S concentration in calc-alkaline series promoting early sulfide saturation compared to the tholeiitic series at similar pressure of differentiation and initial fO_2 (Fig. 6d). Positive correlations between melt H_2O content and S exist in arc magmas (e.g., Johnson et al., 2009; Zimmer et al., 2010; Kelley and Cottrell, 2012), although it is not systematic (e.g., Wallace, 2005). Furthermore, any apparent positive correlation from melt inclusions studies could be due to melt degassing (e.g., Wallace and Edmonds, 2011) rather than initial melt conditions. The relationship between the initial H_2O and S content of primitive arc magmas remains uncertain.

In conclusions, this section highlights the complex interplay of different parameters that control sulfide saturation and hence the evolution of melt Cu concentration during magmatic differentiation. Based on our compilation (Fig. 3), we propose that the liquid lines of descent have a large effect on the timing of sulfide saturation in thin arcs (<25 km), whereas the pressure of differentiation becomes the main controlling factor in thicker arcs (>25 km). Finally, more chemical data specifically on the sulfur content of arc magmas and plutons in combination with experimental studies are needed to better understanding sulfide saturation in natural magmatic systems.

4.2 The importance of initial melt H_2O content in arc magmas for the ore-forming potential of magmas

Most of the economic PCDs are preferentially associated with calc-alkaline subvolcanic intrusions (Sillitoe, 2010). Yet, our global compilation shows that the average melt Cu concentration in calc-alkaline series is systematically lower compared to tholeiitic series at a given MgO (Fig. 3a,d). This observation questions the primary importance of melt Cu content in the ore-forming potential. In the following, we evaluate the role of the initial melt water content and the Cu endowment in magmatic fluids for tholeiitic and calc-alkaline series.

4.2.1 Modeling the liquid lines of descent (LLDs)

Compelling lines of evidence suggest that the geochemical differences between tholeiitic and calc-alkaline series relate to different LLDs controlled by the initial H_2O content of the primitive arc melt showing that tholeiitic and calc-alkaline series are best reproduced by LLD of an H_2O-poor and H_2O-rich parental melt, respectively (Sisson and Grove 1993; Chaussidon and Sobolev, 1996; Villiger et al., 2004; Tatsumi and Susuki, 2009; Zimmer et al., 2010; Jagoutz et al., 2011; Melekhova et al., 2013; Brounce et al., 2014; Mandler et al., 2014; Nandedkar et al., 2014; Müntener and Ulmer, 2018). We use Rhyolite-MELTS (Gualda et al., 2012; Ghiorso and Gualda, 2015) to model LLDs with variable initial melt H_2O content from 0.2 wt% to 4 wt% representative of the spectrum of tholeiitic to calc-alkaline series emplaced at convergent margins (e.g., Sisson and Grove 1993; Tatsumi and Susuki, 2009;

Zimmer et al., 2010; Brounce et al., 2014; Melekhova et al., 2013; Mandler et al., 2014). We used an average primitive melt composition of intra-oceanic tholeiitic basalt and continental arc calc-alkaline basalt (Table D1; Schmidt and Jagoutz, 2017). Our models simulate melt differentiation in a thick crust starting from P = 0.8 GPa to 0.15 GPa and in a thin crust starting from P = 0.4 GPa to 0.15 GPa for temperatures ranging from ~1220-1350°C (liquidus varies as a function of initial melt H_2O content) to ~750-800°C at ΔFMQ +1 (Table D1). Each computation assumes melt differentiation through progressive decompression and cooling followed by cooling once the melt reaches 0.15 GPa (Table D1). The modelled LLDs reasonably reproduce the tholeiitic and calc-alkaline trends and show that the amplitude of Fe enrichment decreases as the initial H_2O melt increases (Fig. 7a). Tholeiitic trends are best reproduced by LLDs resulting from the differentiation of intra-oceanic tholeiitic primitive basalt with initial 0.2 to 1.5 wt% H_2O, whereas calc-alkaline trends are best reproduced by LLDs resulting from the differentiation of continental arc calc-alkaline primitive basalt with initial 2 to 4 wt% H_2O (Fig. 7a). For a given initial melt H_2O content, the absolute Fe enrichment depends on the initial melt composition, where LLDs resulting from the differentiation of intra-oceanic tholeiitic primitive basalt show more Fe enrichment compared to continental arc calc-alkaline primitive basalt. Our results also show that an increase of the initial pressure of differentiation slightly reduces the amplitude of Fe enrichment for damp LLDs (Fig. 7a), which is consistent with the broad tendency of having lower Fe_4 at higher crustal thickness (Fig. 4c). Higher redox conditions (ΔFMQ +2-3) significantly limit Fe enrichment and therefore obfuscate the effect of H_2O on the LLDs. Important is that our modeling allows us to quantify the melt composition in respect to the remaining melt fraction (F), the melt water content and the appearance of the aqueous liquid phases (i.e., fluid saturation) for the different LLDs. The latter is based on the fluid saturation model of Ghiorso and Gualda (2015) implemented to Rhyolite-MELT, where thermodynamic properties of the fluid phase are calculated from the model of Duan and Zhang (2006).

We also model the evolution of Cu concentration in the melt using the Rayleigh fractionation equation:

$$C_l = C_0*(F^{D-1}) \qquad [1]$$

where C_l is the concentration of Cu in the fractionated melt, C_0 is the Cu concentration in the parental melt. F is the remaining melt fraction computed from Rhyolite-MELTS. While Cu is incompatible in silicate minerals ($D^{silicates/melt}_{Cu}$ =<0.2; Liu et al., 2014; Hsu et al., 2017), it is highly compatible in sulfides ($D^{sulfide/melt}_{Cu}$ =~250-1000; Li and Audétat, 2012; Jenner, 2017). The bulk-partition coefficient (D) of Cu represents an average of partition coefficients related to the volume percent of saturated magmatic sulfide and rock-forming minerals. Here, we use $D^{sulfide/melt}_{Cu}$ =800 · and $D^{silicates/melt}_{Cu}$ =0.1, and an average of 0.25 vol% of magmatic sulfides (Kiseeva and Wood, 2015; Georgatou et al., 2018) corresponding to a bulk-partition coefficient D of 2.1 at sulfide saturation and a D of 0.1 assuming no sulfide saturation. For tholeiitic series in thin arc (<25 km), the evolution of the Cu is characterized by an initial incompatible behavior followed by a compatible behavior related to late magmatic sulfide saturation (Figs. 3a and 4c,d). In this case, we model the incompatible behavior of Cu assuming no sulfide saturation with an initial Cu concentration of ~80 ppm in the parental melt. The switch from incompatible to compatible behavior of Cu occurs at MgO ~4 wt% (Fig. 3a). At this point, we use the melt Cu concentration at MgO ~4 wt% as the initial Cu concentration in the parental melt (i.e., C_0 ranging from ~130 to 250 ppm) and we assume magmatic sulfide saturation to model the decrease of Cu concentration in tholeiitic series (Fig. 7b; Table D1). For tholeiitic series in thick arc (>25 km) and calc-alkaline series, we assume an early magmatic sulfides saturation to reproduce the steady decrease of Cu concentration (Fig. 7b; Table D1).

For melt differentiation starting at P=4kbars, the computed results indicate that the magmatic fluid phase saturates at H_2O=5.7-6.3 wt%, F=0.35-0.63, P=1.7-2.3 kbars and Cu ~25-50 ppm for the wet series with an initial H_2O content of 2, 2.5, 3, 3.5 and 4 wt%. Damp series with an initial H_2O content of 0.5, 1 and 1.5 wt% saturates magmatic fluid at H_2O=5.4-5.5 wt%, F=0.09-0.26, P=1.5-1.7 kbars and Cu ~15-30/~5-20 ppm (thin/thick arc model) (Figs. 7c,d; Table D1). For melt differentiation starting at P=8kbars, the computed results indicate that the magmatic fluid phase saturates at H_2O=5.5-6.8 wt%, F=0.36-0.59, P=1.8-2.5 kbars and Cu ~25-45 ppm for the wet series, and at H_2O=5.3-5.4 wt%, F=0.11-0.18, P=1.5 kbars and Cu ~15-20/~10 ppm (thin/thick arc model) for the damp series (Figs. 7c,d; Table D1). Independently to the initial pressure of melt differentiation, the wet calc-alkaline LLDs

reach fluid saturation at higher melt fraction, melt H_2O content and melt Cu content compared to damp tholeiitic LLDs (Table D1). Damp melt with initial H_2O content of 0.2 wt% does not reach H_2O saturation, and hence it is not further considered in the next section.

4.2.2 Assessing the ore-forming potential of tholeiitic vs calk alkaline magmas

The Cu endowment of fluids expelled during degassing of H_2O-saturated melt primarily depends on the melt H_2O and Cu content together with the volume of melt presentat fluid saturation (Cline and Bodnar, 1991; Chelle-Michou et al., 2017). As the mass of extractable Cu (Mt) correlates with the volume of water-saturated melt (Chelle-Michou et al., 2017) the remaining melt mass (F) of H_2O-saturated melt is a crucial parameter that determine how much total Cu could be extracted from a magmatic system and hence for the formation of economic PCDs. Because of the different initial H_2O content in the primitive magma, the melt mass remaining at H_2O saturation is different for calk-alkaline vs tholeiitic LLD. Our models presented above have shown that the melt mass remaining at fluid saturation for calk-alkaline LLD is ~1.5 to 7 times that of the tholeiitic LLD.

To illustrate this point, we use a simplified approach of Chelle-Michou et al. (2017) to quantify the mass of extractable Cu in fluids expelled during degassing of H_2O-saturated melt and to estimate the relative Cu endowment in expelled fluids between wet calc-alkaline and damp tholeiitic LLD. We estimate the volume of H_2O-saturated melt according to the Rhyolite-MELTS models presented above as it corresponds to the melt fraction at which an initial volume of primitive magma reached H_2O saturation. Here, we use an initial volume of primitive magma of 189 km^3 km^{-1} Myr^{-1} based on an average arc magma production rate for intra-oceanic arcs (Jicha and Jagoutz, 2015). Once the magma is H_2O-saturated, we calculate the remaining melt fraction of H_2O-saturated melt and the volume of fluids at degassing. Ultimately, the mass of Cu in fluid expelled at degassing corresponds to the volume and density of fluids and the Cu concentration in fluids at degassing. The latter varies according to the melt Cu concentration and the partition coefficient of Cu between the fluid and the melt. The melt Cu concentration is derived from our modelling presented above, while partition coefficients $D_{Cu}^{fluid/melt}$ in the literature range from ~15 to ~300 and strongly depends on the melt salinity, the presence of CO_2, redox conditions, and H_2S content (Zajacz

et al., 2008; Tattitch et al., 2015; Tattitch and Blundy, 2017). We use an intermediate value of $D_{Cu}^{fluid/melt}$ = 140 (Tattitch and Blundy, 2017). Our calculations yield a range of Cu concentration in fluids range from ~0.03 to ~0.1 wt% (Table D1), which correspond to a lower end estimate when compared to fluid inclusions data ranging from 0.002 to 2 wt% Cu with an average of ~0.26 wt% in PCDs (Kouzmanov and Pokrovski, 2012). Magma degassing occurs periodically during crystallization of H_2O-saturated melt, however the first degassing event accounts for ~50 to 75 wt% of the total fluid expelled with fluids enriched in Cu compared to the latest stages of degassing characterized by negligible amount of fluids (<25 wt%) depleted in Cu (Chelle-Michou et al., 2017). For this reason, we consider only a single degassing event, hence providing minimum estimates for the mass of extractable Cu in fluid expelled at degassing. In this simplified approach, we assume fixed parameters (percolation threshold, fluid and melt density, partition coefficient) to assess the role of the initial melt H_2O content and melt Cu concentration at degassing. The reader is referred to the Supplementary Material A1 and Table D1 for a detailed description of the calculations.

The results indicate a positive correlation between the relative mass of extractable Cu in fluids expelled from H_2O-saturated magmas and the initial melt H_2O content (Fig. 8). The mass of extractable Cu ranges from 2.6 to 9.6 Mt for wet calc-alkaline series modelled with initial melt H_2O between 2 and 4 wt%, whereas calculations for damp tholeiitic series modelled with initial melt H_2O between 0.5 and 1.5 wt% yield ranges from 0.3 to 2.3 Mt for and from 0.2 to 1 Mt for thin and thick arc models, respectively. The corresponding volumes of H_2O-saturated melt required to form PCDs >2 to ~10 Mt Cu (i.e., large to giant deposit) range from 50 to 120 km^3, which correspond to reasonable estimates compared to those reported for ore-bearing intrusions (e.g., Cline and Bodnar, 1991; Chelle-Michou et al., 2017; Du and Audétat, 2020). Overall, the ore-forming potential in typical calc-alkaline magmas (initial melt H_2O content of 4 wt%) is ~4-10 times higher relative to damp tholeiitic magmas (initial melt H_2O content of 1.5 wt%), and up to ~20-50 times relative to the dampest tholeiitic magmas (initial melt H_2O content of 0.5 wt%) (Fig. 8). If we assume the same melt Cu content of H_2O-saturated melt, the ore-forming potential in typical calc-alkaline magmas is ~3 to 8 times higher relative to damp tholeiitic magmas (Table D1). Such correlation reflects the crucial importance of the remaining H_2O-saturated melt mass, whereas the melt

Cu concentration is of secondary importance. Of course, higher melt Cu content at the time of fluid saturation increases the ore-forming potential of a given LLD, which can be envision with high fO_2 (e.g., Richards, 2015) and/or a source enriched in Cu (e.g., Zheng et al., 2018). Ultimately, our results are consistent with Chiaradia (2020a) suggesting that the highest ore-forming potential coincides with an initial H_2O content of 4 wt% in the parental basaltic melt, whereas lower ore-forming potential are modelled for initial melt H_2O content <2 wt% and >6 wt%. Although our modelling primarily aims to evaluate the effect of initial melt H_2O content on the ore-forming potential of arc magmas, we acknowledge that additional parameters including favorable tectonics, long-lived thermal sustainability, magma mingling, and metal precipitation efficiency play a complementary and important role to modulate the size of PCDs (Tosdal and Richards, 2001; Richards, 2003, 2011a; Caricchi et al., 2012; Wilkinson, 2013; Chiaradia and Caricchi, 2017; Chiaradia, 2020b).

5. Petrogenetic implications for the formation of giant PCDs

5.1 Models of formation for PCDs

In calc-alkaline series, the compatible behavior of Cu during magmatic differentiation (Fig. 3a,d) does not preclude the transfer of significant mass of Cu into the fluids expelled from H_20-saturated melts to form large economic PCDs in a single stage model (Fig. 9a), where fluid saturation occurs at ~1.5-2.5 kbars with an important volume of fluid-saturated melt at fairly low Cu concentrations of ~25-50 ppm. In contrast, a single stage model for the formation of large economic PCDs associated with damp tholeiitic series is unlikely because fluid saturation occurs late with a small volume of melt remaining and low Cu concentrations (Fig. 9b). Our results are consistent with the fact that large economic PCDs are predominantly associated with subvolcanic fluid-saturated calc-alkaline intrusions emplaced at ~2 kb (Richards, 2003; Sillitoe, 2010), whereas tholeiitic series are barren in the main arc (e.g., Kesler et al., 1977) and/or associated with shallow and smaller epithermal Cu-Au deposits associated with bi-modal suites in rift-related setting (e.g., Sillitoe and Hedenquist, 2003). In the case of the successive emplacement of damp tholeiitic series followed by wet calc-alkaline series, Cu-sulfide segregated in tholeiitic crustal cumulates could represent an additional source of Cu if remelting of lower crustal cumulates occurs during a subsequent hydrous magmatic event (Fig. 9c). Of course, Cu-sulfide segregated in

lower crustal cumulates formed from hydrous melts could equally be remobilized during a subsequent hydrous magmatic event (Fig. 9c; Richards, 2009, 2011a, 2015; Lee et al., 2012; Chiaradia, 2014; Hou et al., 2015). This scenario would increase the ore-forming potential and lead to the formation of large PCDs consistent with a multi-stage model that could occur in both subduction-related and post-subduction settings. In conclusions, we suggest that both scenarios are likely to occur in accretionary orogens, however, Cu-sulfide segregation and remobilization does not appear to be a prerequisite to form economic large PCDs in subduction-related setting.

5.2 Source vs. crustal processes

The importance of the melt H_2O content has long been recognized since large economic PCDs are predominantly associated with subvolcanic calc-alkaline intrusions characterized by high Sr/Y and La/Yb ratios ascribed to the early crystallization of amphibole in the deep crust (± garnet at high pressure) (Richards, 2011b; Chiaradia et al., 2012; Loucks, 2014). Furthermore, these ratios positively correlate with arc crustal thickness (Chiaradia, 2015; Profeta et al., 2015; Lieu and Stern, 2019), which ultimately correlates with tholeiitic and calc-alkaline differentiation series at the global scale (Miyashiro, 1974; Chiaradia, 2014). It has been proposed that the crustal thickness primarily controls the association of large PCDs, calc-alkaline magmas and thicker arc with a limited role for the composition of the mantle source (e.g., Chiaradia, 2014). Yet, at the arc scale, tholeiitic and calc-alkaline arc magmas are temporally and spatially related from fore-arc to back-arc and the different LLDs are controlled by the initial H_2O content of the primitive arc melt independently to the pressure of differentiation (Fig. 7a; Sisson and Grove 1993; Baker et al., 1994; Villiger et al., 2004; Tatsumi and Susuki, 2009; Zimmer et al., 2010; Melekhova et al., 2013; Brounce et al., 2014; Mandler et al., 2014; Nandedkar et al., 2014; Ulmer et al., 2018). Here, we suggest that the importance of the initial melt H_2O content in the ore forming potential of arc magmas reflects the primary role of flux melting in the mantle source associated with wet calc-alkaline series, in opposition to decompression melting associated with damp tholeiitic series (Fig. 9; Grove et al., 2002; Cervantes and Wallace, 2003; Jagoutz et al., 2011). The first order relationship between calc-alkaline

magmas and crustal thicknesses (Miyashiro, 1974; Chiaradia, 2014) illustrates that the crustal thickness controls the height of the mantle column and influences the relative importance of decompression melting versus flux melting (Grove et al., 2002; Jagoutz et al., 2011; Karlstrom et al. 2014; Turner and Langmuir, 2015). This makes intuitively sense as a thicker crust reduces the mantle wedge thickness and hence is associated with a shorter melting column, reducing the capability of the mantle to decompress. At the arc scale, the preferential association of PCDs with the episode of crustal thickening (e.g., Cooke et al., 2005) would be consistent with a shorter melting column and the dominance of flux melting regimes during internal tectonic and magmatic cycles. In conclusions, the role of flux melting at a given arc location remains of primary importance for the ore-forming potential in arc magmas and the formation of economic PCDs.

6. Conclusions

In this study, we reviewed the Cu concentrations in primitive arc melts, plutonic rocks and derivative melts, and volcanic rocks to discuss the role of mantle source and crustal magmatic processes to generate fertile magmatism associated with large economic PCDs. The compilation of primitive arc melt does not indicate any particular Cu endowment for a specific type of primitive arc melt and/or geodynamic setting. Our results are consistent with previous studies (Lee et al., 2012) showing an average Cu concentration in different types of primitive arc basalts similar to MORBs (~80 ppm) indicative of the predominant contribution of Cu from the mantle wedge and limited slab-related fluid/melts input. This suggests that the initial Cu endowment in the primitive arc melt is unlikely to represent a crucial prerequisite to form large economic PCDs. Our global compilation of plutonic rocks illustrates that Cu-rich arc (> 100 ppm) cumulates are associated with both calc-alkaline and tholeiitic series. In contrast, our global compilation of volcanic rocks documents systematically different Cu evolution during magma differentiation in calc-alkaline and tholeiitic series for each arc. The contrasting evolution of Cu in tholeiitic and calc-alkaline systematically correlates with FeO_{tot} and V, which is consistent with previous studies suggesting that the different timing of magmatic sulfide saturation relates to the onset of Fe-oxides crystallization on the respective LLDs (Jenner et al., 2010; Chiaradia, 2014). Additional parameters (pressure of magma differentiation, LLDs, fO_2, and/or sulfur

concentration) may locally play a role and account for the large range of Cu concentration observed in the compiled data. Although the average Cu concentrations during melt differentiation is systematically higher for tholeiitic series compared to calc-alkaline series, we propose that the melt Cu concentrations have minor implications for the ore-forming potential of arc magmas. Instead, we demonstrate that the initial melt H_2O content in primitive arc melts controls the LLD and the volume of remaining melt mass at fluid saturation. We showed that the melt mass remaining is a key parameter for calculating the total mass of Cu transferred into exsolving hydrothermal fluids. We propose that the single stage model for the formation of large economic PCDs is most applicable for melts from the calc-alkaline series. The importance of the initial melt H_2O content ultimately reflects the key role of flux melting associated with wet calc-alkaline series and high ore-forming potential, in opposition to decompression melting associated with damp tholeiitic series.

Acknowledgments

H. R. acknowledges the support by the Swiss National Foundation through the early post-doc mobility research grant P2GEP2_178008. The work of O. J and H. R. was supported by National Science Foundation under grant number EAR-1552202. The authors are grateful for the active discussions during group meetings at MIT that contribute to shape our ideas. The authors thank the reviewers for their insightful comments that helped to clarify and improve the manuscript.

Disclosure Statement

No potential conflict of interest was reported by the authors.

FIGURE CAPTION

Fig. 1: World map showing the distribution of arc magmatism and porphyry copper deposits. The location of calc-alkaline and tholeiitic magmatism compiled in this study is from the Georoc database (http://georoc.mpch-mainz.gwdg.de/georoc/). The location of porphyry copper deposits and the deposit size are from Singer et al. (2005). Phanerozoic felsic magmatism is after Jagoutz and Klein (2018). The location of active margins is from Hayes et al. (2018).

Fig. 2: Compilation of Cu concentrations in primitive arc melts and mid-oceanic ridge basalts (MORBs). (a) Whisker plot showing the Cu concentrations in primitive arc melt based on variable tectonic settings using the classification scheme of Schmidt and Jagoutz (2017). The ranges of Cu values for primitive MORBs are compiled from Gale et al. (2013). (b) Average Cu concentration and associated uncertainties (1 SD) for primitive arc basalts (blue), primitive arc high-Mg andesites (orange), and primitive MORBs (grey). (c) Histogram showing the distribution of Cu concentrations for primitive arc basalts, primitive arc high-Mg andesites (HMA), and primitive MORBs. Abbreviations in (a): C for continental arc, IO for Intra-oceanic arc, and BAB for back-arc basin.

Fig. 3: Plots of Cu, FeO_{tot} and V versus MgO for volcanic rocks of 28 arcs. (a–c) Tholeiitic rocks (n=6,114) (d-f) Calc-alkaline rocks (n=9,275). Median values for each compiled arc are also plotted at every MgO = 0.5 wt% for tholeiitic series (dark red circle) and calc-alkaline series (light blue circle) (see details in Fig. C1). Median values of Cu, FeO_{tot} and V for every MgO = 0.5 wt% are shown for the global compilation of tholeiitic and calc-alkaline series (yellow diamond). The average Cu concentration and associated uncertainties (1 SD) for primitive arc basalts (black bar) is shown in (a) and (d).

Fig. 4: Geochemical relationships between Cu, FeO_{tot}, V and crustal thicknesses for 17 volcanic arcs with representative whole rock geochemical data set (n>300). (a) Cu versus FeO_{tot}. (b) V versus FeO_{tot}. (c) Cu_4 versus Fe_4, where Cu_4 and Fe_4 correspond to the average of median values and associated uncertainties (1 SD) of Cu and Fe between MgO = 3 and MgO = 5 wt% (see Table B1). Circles and squares represent thin (<25 km) and thick arc (>25 km). (d) Cu_4 versus crustal thickness. References for crustal thicknesses and associated uncertainties (1 SD) are available in Table B1. The average Cu concentration and associated uncertainties (1 SD) for primitive arc basalts (black bar) is shown in (c) and (d).

Fig. 5: (a) Plots of Mg# (molar Mg/(Mg+Fe)) versus SiO_2 for compiled whole-rock compositions of plutonic rocks for four crustal sections (Famatina, Fjordland, Kohistan and Talkeetna; Jagoutz and Kelemen, 2015; Jagoutz and Klein, 2018 and references therein) together with other cumulates xenoliths from the Bonanza arc, Sierra Nevada, Arizona, Eastern Pontides and Kermadec (Chin et al., 2018 and references therein). Red dots are used for the Chilas complex in Kohistan arc as it represents a damp tholeiitic fractionation, whereas dots with different shades of blue represent plutonic rocks and cumulates xenoliths associated with wet calc-alkaline fractionation (Jagoutz et al., 2011; Jagoutz and Klein, 2018). (b) Histogram showing the density of Cu concentrations for the four crustal sections and other cumulates xenoliths. See discussion for details and the full data set and references in Table C1.

Fig. 6:

Sulfur speciation in melt and sulfur solubility as a function of oxygen fugacity, expressed log units relative to the fayalite-magnatite-quartz buffer (ΔFMQ). (a) The different black curves illustrates the changes in S6+/Stot in hydrous silicate melts with pressure from Jugo et al., (2010), Botcharnikov et al., (2011) and Matjuschkin et al. (2016). The brown line represents the sulfur solubility curve at sulfide and sulfate saturation at 0.2 GPa after Botcharnikov et al. (2011), whereas the brown dotted line represents an hypothetical similar sulfur solubility curve at higher pressure of 1 GPa. The upper inset indicates the redox ranges for mid-ocean ridge basalt (MORB), sub-arc mantle and arc basalts from Ballhaus (1993), Carmichael (1991), Parkinson and Arculus (1999), Arai and Ishimaru (2008), Wallace and Edmons (2011), Evans et al., (2012) and Bénard et al., (2018). We report a range of sulfur concentrations (orange whisker plot with a median values of 0.12 wt%) measured in olivine-hosted melt inclusions for arc-related basalts and basalt-andesites compiled from the Georoc database (n=456). (b-e) Sulfur solubility curves simplified from Figure 6a to illustrate the effect of different parameters on sulfide saturation, including (b) variable pressure of differentiation, (c) different liquid line of descent, (d) variable initial redox conditions, and (e) variable initial sulfur content $[S]_i$. In (b) and (c), the values of F and the timing of

magnetite is quantified in Table D1. The different scenarios are also discussed in details in the section 4.1 of the manuscript.

Fig. 7: Computed melt composition, melt Cu concentration, melt H_2O content, melt fraction (F), during magmatic differentiation for wet (2 to 4 wt% H_2O - blue) and damp (0.2 to 1.5 wt% H_2O - red) at ΔFMQ =1 for variable starting pressure of differentiation (i.e., 8-1.5 kbars (dotted lines) and 4-1.5 kbars (plain lines)) using Rhyolite-MELTS (Gualda et al., 2012). (a) Computed melt evolution of FeO_{tot} versus MgO. For damp LLDs, the highest and lowest Fe enrichment at MgO ~4-5 wt% corresponds to initial H_2O of 0.2 and 1.5 wt%, respectively. The black line corresponds to modelled LLD with initial H_2O of 1 wt% at ΔFMQ =1 from Zimmer et al. (2010), showing the effect of the initial primitive melt composition for the Fe enrichment. Shaded dots are single data and median data per arc from our global compilation of tholeiitic and calc-alkaline volcanic rocks in Figure 3b,e. (b) Evolution of the Cu concentration versus MgO in wet, damp and dry melt modelled using Rayleigh fractionation assuming 0.25 vol.% sulfide ($D^{sulfide/melt}_{Cu}$ =800) and 99.75 vol.% silicate ($D^{silicate/melt}_{Cu}$ =0.1). Shaded dots are single data and median data per arc from our global compilation of tholeiitic and calc-alkaline volcanic rocks in Figure 3a,d. The steady depletion assumes early sulfide saturation to simulate the trends observed in all calc-alkaline series and some tholeiitic series in thick arcs (>25 km). In contrast, the early enrichment in Cu followed by a sharp depletion simulates late sulfide saturation at MgO ~4 wt% to reproduce the evolution of Cu concentration displayed by tholeiitic series in thin arcs (<25 km). (c, d) Rhyolite-MELTS computed melt H_2O content versus the remaining melt mass (F) and pressure (P). See text for detailed discussion and Table D1 for full data sets.

Fig. 8: Relationship between the initial melt H_2O content and the ore-forming potential for the different liquid lines of descents modelled in Figure 7. The ore-forming potential is expressed as the relative Cu endowment in fluid expelled at degassing of a H_2O-saturated magma normalized to damp tholeiitic melts modelled with an initial H_2O content of 0.5 wt% (circles) and 1.5 wt% (squares) according to the variable pressure of differentiation from 4 to 1.5 kbars (4 kb – filled symbol) from 8 to 1.5 kbars (8 kb – empty symbol). The different

colors reflect melt Cu content at H_2O saturation in tholeiitic series assuming late sulfide saturation in thin arc (grey) and early sulfide saturation in thick arc (yellow). Details of the calculation is provided in Table D1 and Supplementary Material A1. See text for discussion.

Fig. 9: Conceptual cartoon of the single-stage and multi-stage models for the formation of porphyry Cu deposits (PCDs). (a) The single stage model assumes the formation of large economic PCDs associated with the generation of wet calc-alkaline melts, where flux melting is predominant in the main arc. (b) The single stage model assumes the formation of barren upper crustal intrusions associated with the generation of damp tholeiitic melts, where decompression melting is predominant in the main arc. (c) The multi-stage model assumes the remobilization of Cu-sulfide sequestered in crustal cumulates during a later hydrous and oxidized magmatic event in the main arc, which may result in the formation of large PCDs.

Fig. A1: Plots of Cu versus MgO for primitive arc basalts and primitive high-Mg Andesites using the classification scheme of Schmidt and Jagoutz (2017).

Fig. B1: Classification of tholeiitic and calc-alkaline volcanic rocks (n=15,389) based on the FeO/MgO versus SiO_2 after Miyashiro (1974).

Fig. C1: Plots of Cu, FeO_{tot} and V versus MgO for calc-alkaline and tholeiitic volcanic rocks for each compiled arc. Median Cu, FeO_{tot} and V values for each arc are plotted at every MgO = 0.5 wt%.

Fig. D1: Plots of Cu and V versus FeO_{tot} for calc-alkaline and tholeiitic volcanic rocks for each compiled arc.

.

REFERENCES

Allibone, A. H., Jongens, R., Scott, J. M., Tulloch, A. J., Turnbull, I. M., Cooper, A. F., Powell, N. G., Ladley, E. B., King, R. P., Rattenbury, M. S., 2009. Plutonic rocks of the Median Batholith in eastern and central Fiordland, New Zealand. Field relations, geochemistry, correlation, and nomenclature: New Zeal. J. of Geol. Geop. 52, 101–148.

Arai, S., Ishimaru, S., 2008. Insights into petrological characteristics of the lithosphere of mantle wedge beneath arcs through peridotite xenoliths: a review. J. Petrol. 49, 665-695.

Parkinson, I. J., Arculus, R. J., 1999. The redox state of subduction zones: insights from arc-peridotites. Chem. Geol. 160, 409-423.

Audétat, A., Simon, A. C., 2012. Magmatic Controls on Porphyry Copper Genesis. In Geology and Genesis of Major Copper Deposits and Districts of the World: A Tribute to Richard H. Sillitoe, eds. Jeffrey W. Hedenquist, Michael Harris, Francisco Camus. Society of Economic Geologists, Special Publication 16, 553-572.

Baker, M. B., Grove, T. L., Price, R., 1994. Primitive basalts and andesites from the Mt. Shasta region, N. California: products of varying melt fraction and water content. Contrib Mineral Petrol. 118, 111-129.

Ballhaus, C., 1993. Redox states of lithospheric and asthenospheric upper mantle. Contrib Mineral Petrol. 114, 331-348.

Bénard, A., Klimm, K., Woodland, A. B., Arculus, R. J., Wilke, M., Botcharnikov, R. E., Shimizu, N., Nebel, O., Rivard, C., Ionov, D. A., 2018. Oxidising agents in sub-arc mantle melts link slab devolatilisation and arc magmas. Nat. Commun. 9, 3500.

Botcharnikov, R. E., Linnen, R. L., Wilke, M., Holtz, F., Jugo, P. J., and Berndt, J., 2011. High gold concentrations in sulphide-bearing magma under oxidizing conditions. Nat. Geo. 4, 112-115.

Brounce, M. N., Kelley, K. A., and Cottrell, E., 2014. Variations in Fe3+/∑ Fe of Mariana Arc basalts and mantle wedge fO_2. J. Petrol. 55, 2513-2536.

Brounce, M., Cottrell, E., and Kelley, K. A., 2019. The redox budget of the Mariana subduction zone. Earth Planet. Sci. Lett. 528, 115859.

Bucholz, C. E., Kelemen, P. B., 2019. Oxygen fugacity at the base of the Talkeetna arc, Alaska. Contrib Mineral Petrol. 174, 79.

Canil, D., 1999. Vanadium partitioning between orthopyroxene, spinel and silicate melt and the redox states of mantle source regions for primary magmas Geochim. Cosmochim. Acta 63, 557-572.

Carmichael, I. S., 1991. The redox states of basic and silicic magmas: a reflection of their source regions?. Contrib Mineral Petrol. 106, 129-141.

Caricchi, L., Simpson, G., Schaltegger, U., 2014. Zircons reveal magma fluxes in the Earth's crust. Nature 511, 457-461.

Cervantes, P., and Wallace, P. J., 2003. Role of H2O in subduction-zone magmatism: new insights from melt inclusions in high-Mg basalts from central Mexico. Geology 31, 235-238.

Chelle-Michou, C., Rottier, B., Caricchi, L., Simpson, G., 2017. Tempo of magma degassing and the genesis of porphyry copper deposits. Sci. Rep. 7, 40566.

Chiaradia, M., 2014. Copper enrichment in arc magmas controlled by overriding plate Nat. Geo. 7, 43-46.

Chiaradia, M., 2015. Crustal thickness control on Sr/Y signatures of recent arc magmas: an Earth scale perspective. Sci. Rep. 5, 8115.

Chiaradia, M., 2020a. How much water in basaltic melts parental to porphyry copper deposits?. Frontiers in Earth Sciences, 8, 313.

Chiaradia, M., 2020b. Gold endowments of porphyry deposits controlled by precipitation efficiency. Nat. Commun. 11, 1-10.

Chiaradia, M., Caricchi, L., 2017. Stochastic modelling of deep magmatic controls on porphyry copper deposit endowment. Sci. Rep. 7, 44523.

Chiaradia, M., Ulianov, A., Kouzmanov, K., Beate, B., 2012. Why large porphyry Cu deposits like high Sr/Y magmas? Sci. Rep. 2, 685.

Chin, E.J., Shimizu, K., Bybee, G.M., Erdman, M.E., 2018. On the development of the calc-alkaline and tholeiitic magma series: a deep crustal cumulate perspective. Earth Planet. Sci. Lett. 482, 277–287.

Ciazela, J., Dick, H. J., Koepke, J., Pieterek, B., Muszynski, A., Botcharnikov, R., Kuhn, T., 2017. Thin crust and exposed mantle control sulfide differentiation in slow-spreading ridge magmas. Geology 45, 935-938.

Cline, J. S., Bodnar, R. J., 1991. Can economic porphyry copper mineralization be generated by a typical calc-alkaline melt?. J. Geophys. Res. Solid Earth 96(B5), 8113-8126.

Cooke, D. R., Hollings, P., Walshe, J. L., 2005. Giant porphyry deposits: characteristics, distribution, and tectonic controls. Econ. Geol. 100, 801-818.

Cox, D., Watt, S. F., Jenner, F. E., Hastie, A. R., Hammond, S. J., 2019. Chalcophile element processing beneath a continental arc stratovolcano. Earth Planet. Sci. Lett. 522, 1-11.

Du, J., Audétat, A., 2020. Early sulfide saturation is not detrimental to porphyry Cu-Au formation. Geology, 48, 519-524

Duan, Z., Zhang, Z., 2006. Equation of state of the H_2O, CO_2, and H_2O–CO_2 systems up to 10 GPa and 2573.15 K: molecular dynamics simulations with ab initio potential surface. Geochim Cosmochim Acta 70:2311–2324

Evans, K. A., Elburg, M. A., Kamenetsky, V. S., 2012. Oxidation state of subarc mantle. Geology 40, 783-786.

Fliedner, M. M., Klemperer, S. L., 1999. Structure of an island-arc: Wide-angle seismic studies in the eastern Aleutian Islands, Alaska. Journal of Geophysical Research: Solid Earth, 104(B5), 10667-10694.

Fortin, M. A., Riddle, J., Desjardins-Langlais, Y., Baker, D. R., 2015. The effect of water on the sulfur concentration at sulfide saturation (SCSS) in natural melts. Geochim Cosmochim Acta 160, 100-116.

Gale, A., Dalton, C. A., Langmuir, C. H., Su, Y., Schilling, J. G.,2013. The mean composition of ocean ridge basalts. Geochem Geophys Geosyst. 14, 489-518.

Georgatou, A., Chiaradia, M., 2019. Magmatic sulphides in high-K calc-alkaline to shoshonitic and alkaline rocks. Solid Earth. https://doi.org/10.5194/se-2019-106

Georgatou, A., Chiaradia, M., Rezeau, H., Wälle, M., 2018. Magmatic sulphides in Quaternary Ecuadorian arc magmas. Lithos 296, 580-599.

Ghiorso, M. S., Carmichael, I. S., 1987. Modeling magmatic systems; petrologic applications. Rev Mineral Geochem, 17, 467-499.

Ghiorso, M. S., Gualda, G. A., 2015. An H_2O–CO_2 mixed fluid saturation model compatible with rhyolite-MELTS. Contrib Mineral Petrol., 169, 1-30.

Duan Z, Zhang Z (2006) Equation of state of the H2O, CO2, and H2O–CO2 systems up to 10 GPa and 2573.15 K: molecular dynamics simulations with ab initio potential surface. Geochim Cosmochim Acta 70:2311–2324

Giacometti, F., Evans, K. A., Rebay, G., Cliff, J., Tomkins, A. G., Rossetti, P., Vaggelli, G., Adams, D. T. (2014). Sulfur isotope evolution in sulfide ores from Western Alps: Assessing the influence of subduction-related metamorphism. Geochem Geophys Geosyst 15, 3808-3829.

Greene, A. R., DeBari, S. M., Kelemen, P. B., Blusztajn, J., Clift, P. D., 2006. A detailed geochemical study of island arc crust: the Talkeetna arc section, south–central Alaska. J Petrol, 47, 1051-1093.

Grove, T., Parman, S., Bowring, S., Price, R., Baker, M., 2002. The role of an H_2O-rich fluid component in the generation of primitive basaltic andesites and andesites from the Mt. Shasta region, N California. Contrib Mineral Petrol. 142, 375-396.

Grove, T. L., Till, C. B., Krawczynski, M. J., 2012. The role of H_2O in subduction zone magmatism. Annu. Rev. Earth Planet. Sci, 40, 413-439.

Gualda, A.R., Ghiorso, M.S., Lemons, R. V., Tamara L., Carley, T. L., 2012. Rhyolite-MELTS: a Modified Calibration of MELTS Optimized for Silica-rich, Fluid-bearing Magmatic Systems, J Petrol. 53, 875–890.

Hayes, G. P., Moore, G. L., Portner, D. E., Hearne, M., Flamme, H., Furtney, M., Smoczyk, G. M., 2018. Slab2, a comprehensive subduction zone geometry model. Science 362, 58-61.

Hedenquist, J.W., Lowenstern, J.B., 1994. The role of magmas in the formation of hydrothermal ore deposits. Nature 370, 519.

Hou, Z., Yang, Z., Lu, Y., Kemp, A., Zheng, Y., Li, Q., Tang, J., Yang, Z. and Duan, L., 2015. A genetic linkage between subduction-and collision-related porphyry Cu deposits in continental collision zones. Geology 43, 247-250.

Hsu, Y. J., Zajacz, Z., Ulmer, P., Heinrich, C. A., 2017. Copper partitioning between silicate melts and amphibole: Experimental insight into magma evolution leading to porphyry copper ore formation. Chem. Geol. 448, 151-163.

Jagoutz, O. E., 2010. Construction of the granitoid crust of an island arc. Part II: a quantitative petrogenetic model. Contrib Mineral Petrol. 160, 359-381.

Jagoutz, O., Klein, B., 2018. On the importance of crystallization-differentiation for the generation of SiO_2-rich melts and the compositional build-up of arc (and continental) crust. Am. J. Sci, 318, 29-63.

Jagoutz, O., Kelemen, P. B., 2015. Role of arc processes in the formation of continental crust. Annu. Rev. Earth Planet. Sci, 43, 363-404.

Jagoutz, O., Müntener, O., Schmidt, M. W., Burg, J. P., 2011. The roles of flux-and decompression melting and their respective fractionation lines for continental crust formation: Evidence from the Kohistan arc. Earth Planet Sc Lett. 303, 25-36.

Jégo, S., Dasgupta, R., 2014. The fate of sulfur during fluid-present melting of subducting basaltic crust at variable oxygen fugacity. J. Petrol. 55, 1019-1050.

Jenner, F. E., 2017. Cumulate causes for the low contents of sulfide-loving elements in the continental crust. Nat. Geo. 10, 524-529.

Jenner, F. E., O'Neill, H. S. C., 2012. Analysis of 60 elements in 616 ocean floor basaltic glasses. Geochem, Geophys, Geosyst. 13.

Jenner, F.E., O'Neill, H.S.C., Arculus, R.J., Mavrogenes, J.A., 2010. The magnetite crisis in the evolution of arc-related magmas and the initial concentration of Au, Ag and Cu. J. Petrol. 51, 2445–2464.

Jicha, B. R., Jagoutz, O., 2015. Magma production rates for intraoceanic arcs. Elements 11, 105-111.

Johnson, E. R., Wallace, P. J., Delgado Granados, H., Manea, V. C., Kent, A. J., Bindeman, I. N., and Donegan, C. S., 2009. Subduction-related volatile recycling and magma generation beneath Central Mexico: insights from melt inclusions, oxygen isotopes and geodynamic models. J. Petrol. 50, 1729-1764.

Jugo, P. J., 2009. Sulfur content at sulfide saturation in oxidized magmas. Geology 37, 415-418.

Jugo, P.J., Wilke, M., Botcharnikov, R.E., 2010. Sulfur K-edge XANES analysis of natural and synthetic basaltic glasses: implications for S speciation and S content as function of oxygen fugacity. Geochim. Cosmochim. Acta 74, 5926–5938

Karlstrom, L., Lee, C.T., Manga, M., 2014. The role of magmatically driven lithospheric thickening on arc front migration. Geochem. Geophys. Geosyst. 15, 2655–2675.

Kelemen, P. B., Shimizu, N., Salters, V. J. M., 1995. Formation of harzburgite by pervasive melt/rock reaction in the upper mantle, Nature 358, 635–641.

Kelemen, P., Hanghøj, B., K., Greene, A. R., 2014. One view of the geochemistry of subduction-related magmatic arcs, with an emphasis on primitive andesite and lower crust. In The Crust, Treatise on Geochemistry, edited by H. D. Holland and K. K. Turekian, pp. 669–701, Elsevier-Pergamon, Oxford, U. K.

Kelley, K.A., Cottrell, E., 2009. Water and the oxidation state of subduction zone magmas. Science 325, 605–607

Kelley, K. A., Cottrell, E., 2012. The influence of magmatic differentiation on the oxidation state of Fe in a basaltic arc magma. Earth Planet. Sci. 329, 109-121.

Kesler, S.E., Jones, L.M., Walker, R.L., 1975, Intrusive rocks associates with porphyry copper mineralization in island arc areas. Econ. Geol. 70, 515-526.

Kesler, S. E., Sutter, J. F., Issigonis, M. J., Jones, L. M., Walker, R. L., 1977. Evolution of porphyry copper mineralization in an oceanic island arc; Panama. Econ. Geol. 72, 1142-1153.

Kiseeva, E. S., Wood, B. J., 2015. The effects of composition and temperature on chalcophile and lithophile element partitioning into magmatic sulphides. Earth Planet. Sci. 424, 280-294.

Kouzmanov, K., Pokrovski, G. S., 2012. Hydrothermal controls on metal distribution in porphyry Cu(–Au–Mo) systems. In Geology and Genesis of Major Copper Deposits and Districts of the World: A Tribute to Richard H. Sillitoe, eds. Jeffrey W. Hedenquist, Michael Harris, Francisco Camus. Society of Economic Geologists, Special Publication 16, 573–618.

La Tourrette, T. Z., Burnett, D. S., and Bacon, C. R., 1991. Uranium and minor-element partitioning in Fe-Ti oxides and zircon from partially melted granodiorite, Crater Lake, Oregon. Geochim. Cosmochim. Acta 55, 457-469.

Lee, C. T. A., Tang, M., 2020. How to make porphyry copper deposits. Earth Planet. Sci. 529, 115868.

Lee, C. T. A., Luffi, P., Le Roux, V., Dasgupta, R., Albaréde, F., Leeman, W. P., 2010. The redox state of arc mantle using Zn/Fe systematics. Nature 468, 681-685.

Lee, C.-T.A., Luffi, P., Chin, E.J., Bouchet, R., Dasgupta, R., Morton, D.M., Le Roux, V., Yin, Q.-z., Jin, D., 2012. Copper systematics in arc magmas and implications for crust–mantle differentiation. Science 336, 64–68.

Li, Y. Audétat, A., 2012. Partitioning of V, Mn, Co, Ni, Cu, Zn, As, Mo, Ag, Sn, Sb, W, Au, Pb, and Bi between sulfide phases and hydrous basanite melt at upper mantle conditions. Earth Planet. Sci. Lett. 355–356, 327–340.

Lieu, W. K., Stern, R. J., 2019. The robustness of Sr/Y and La/Yb as proxies for crust thickness in modern arcs. Geosphere 15, 621-641.

Liu, X., Xiong, X., Audétat, A., Li, Y., Song, M., Li, L., Sun, W., Ding, X., 2014. Partitioning of copper between olivine, orthopyroxene, clinopyroxene, spinel, garnet and silicate melts at upper mantle conditions. Geochim. Cosmochim. Acta 125, 1–22.

Loucks, R., 2014. Distinctive composition of copper–ore-forming arc magmas. Aust. J. Earth Sci. 61, 5–16.

Luhr, J. F., Carmichael, I. S., 1980. The colima volcanic complex, Mexico. Contrib Mineral Petrol. 71, 343-372.

Mandler, B. E., Donnelly-Nolan, J. M., Grove, T. L., 2014. Straddling the tholeiitic/calc-alkaline transition: the effects of modest amounts of water on magmatic differentiation at Newberry Volcano, Oregon. Contrib Mineral Petrol. 168, 1066.

Matjuschkin, V., Blundy, J.D., Brooker, R.A., 2016. The effect of pressure on sulphur speciation in mid-to deep-crustal arc magmas and implications for the formation of porphyry copper deposits. Contrib. Mineral. Petrol. 171, 66.

Mavrogenes, J. A., O'Neill, H. S. C., 1999. The relative effects of pressure, temperature and oxygen fugacity on the solubility of sulfide in mafic magmas. Geochim Cosmochim Acta 63, 1173-1180.

McInnes, B. I., McBride, J. S., Evans, N. J., Lambert, D. D., Andrew, A. S.,1999. Osmium isotope constraints on ore metal recycling in subduction zones. Science 286, 512-516.

Melekhova, E., Annen, C., Blundy, J., 2013. Compositional gaps in igneous rock suites controlled by magma system heat and water content. Nat. Geo. 6, 385.

Melekhova, E., Schlaphorst, D., Blundy, J., Kendall, J. M., Connolly, C., McCarthy, A., Arculus, R., 2019. Lateral variation in crustal structure along the Lesser Antilles arc from petrology of crustal xenoliths and seismic receiver functions. Earth Planet. Sci. 516, 12-24.

Miyashiro, A., 1974. Volcanic rock series in island arcs and active continental margins. Am. J. Sci. 274, 321–355.

Mungall, J. E., 2002. Roasting the mantle: Slab melting and the genesis of major Au and Au-rich Cu deposits. Geology 30, 915-918.

Müntener, O., Ulmer, P., 2018. Arc crust formation and differentiation constrained by experimental petrology. Am. J. Sci. 318, 64-89.

Nandedkar, R. H., Ulmer, P., and Müntener, O., 2014. Fractional crystallization of primitive, hydrous arc magmas: an experimental study at 0.7 GPa. Contrib Mineral Petrol. 167, 1015.

O'Neill, H. S. C., Mavrogenes, J. A., 2002. The sulfide capacity and the sulfur content at sulfide saturation of silicate melts at 1400 C and 1 bar. J. Petrol. 43, 1049-1087.

Otamendi, J. E., Vujovich, G. I., de la Rosa, J. D., Tibaldi, A. M., Castro, A., Martino, R. D., and Pinotti, L. P., 2009. Geology and petrology of a deep crustal zone from the Famatinian paleo-arc, Sierras de Valle Fértil and La Huerta, San Juan, Argentina. J. S. Am. Earth Sci. 27, 258-279.

Park, J. W., Campbell, I. H., Malaviarachchi, S. P., Cocker, H., Hao, H., & Kay, S. M., 2019. Chalcophile element fertility and the formation of porphyry Cu±Au deposits. Min. Dep. 54, 657-670.

Portnyagin, M., Hoernle, K., Plechov, P., Mironov, N., and Khubunaya, S., 2007. Constraints on mantle melting and composition and nature of slab components in volcanic arcs from volatiles (H2O, S, Cl, F) and trace elements in melt inclusions from the Kamchatka Arc. Earth Planet. Sci. 255, 53-69.

Profeta, L., Ducea, M. N., Chapman, J. B., Paterson, S. R., Gonzales, S. M. H., Kirsch, M., Petrescu, L., and DeCelles, P. G., 2015. Quantifying crustal thickness over time in magmatic arcs. Sci. Rep. 5, 17786.

Rezeau, H., Moritz, R., Wotzlaw, J. F., Tayan, R., Melkonyan, R., Ulianov, A., Selby, D., d'Abzac, F. X., Stern, R. A., 2016. Temporal and genetic link between incremental pluton assembly and pulsed porphyry Cu-Mo formation in accretionary orogens. Geology 44, 627-630.

Richards, J. P., 2003. Tectono-magmatic precursors for porphyry Cu-(Mo-Au) deposit formation. Econ. Geol. 98, 1515-1533.

Richards, J.P., 2009. Postsubduction porphyry Cu–Au and epithermal Au deposits: products of remelting of subduction-modified lithosphere. Geology 37, 247–250.

Richards, J. P., 2011a. Magmatic to hydrothermal metal fluxes in convergent and collided margins. Ore Geol. Rev. 40, 1-26.

Richards, J. P., 2011b. High Sr/Y arc magmas and porphyry Cu±Mo±Au deposits: just add water. Econ. Geol. 106, 1075-1081.

Richards, J. P., 2015. The oxidation state, and sulfur and Cu contents of arc magmas: implications for metallogeny. Lithos 233, 27-45.

Richards, J. P., 2018. A shake-up in the porphyry world?. Econ. Geol. 113, 1225-1233.

Ripley, E. M., Li, C., 2013. Sulfide saturation in mafic magmas: Is external sulfur required for magmatic Ni-Cu-(PGE) ore genesis?. Econ. Geol., 108, 45-58.

Rowe, M. C., Kent, A. J., Nielsen, R. L., 2009. Subduction influence on oxygen fugacity and trace and volatile elements in basalts across the Cascade Volcanic Arc. J. Petrol. 50, 61-91.

Schmidt, M. W., Jagoutz, O. 2017. The global systematics of primitive arc melts. Geochem Geophys Geosyst, 18, 2817-2854.

Seedorff, E., J. H. Dilles, J. M. Proffett, M. T. Einaudi, L. Zurcher, W. J. A. Stavast, D. A. Johnson, and M. D. Barton, 2005, Porphyry deposits: characteristics and origin of hypogene features. Economic Geology 100th Anniversary Volume, eds. Jeffrey W. Hedenquist, John F. H. Thompson, Richard J. Goldfarb, Jeremy P. Richards

Sillitoe, R.H., 2010. Porphyry copper systems. Econ. Geol. 105, 3–41.

Sillitoe, R. H., 1997. Characteristics and controls of the largest porphyry copper-gold and epithermal gold deposits in the circum-Pacific region, Aust. J. Earth Sci. 44, 373-388.

Sillitoe, R.H., Hedenquist, J.W., 2003. Linkages between volcanotectonic settings, ore-fluid compositions, and epithermal precious metal deposits. SEG Special Publication 10, 315–343.

Singer, D. A., Berger, V. I., Menzie, W. D., Berger, B. R., 2005. Porphyry copper deposit density. Econ. Geol. 100, 491-514.

Sisson, T. W., Grove, T. L., 1993. Experimental investigations of the role of H2O in calc-alkaline differentiation and subduction zone magmatism. Contrib Mineral Petrol. 113, 143-166.

Sobolev, A. V., and Chaussidon, M., 1996. H_2O concentrations in primary melts from supra-subduction zones and mid-ocean ridges: implications for H_2O storage and recycling in the mantle. Earth Planet. Sci. Lett. 137, 45-55.

Solomon, M., 1990. Subduction, arc reversal, and the origin of porphyry copper-gold deposits in island arcs. Geology 18, 630-633.

Stavast, W. J., Keith, J. D., Christiansen, E. H., Dorais, M. J., Tingey, D., Larocque, A., Evans, N., 2006. The fate of magmatic sulfides during intrusion or eruption, Bingham and Tintic districts, Utah. Econ. Geol. 101, 329-345.

Sun, W., Wang, J. T., Zhang, L. P., Zhang, C. C., Li, H., Ling, M. X., Ding, X., Li, C-y., Liang, H. Y., 2017. The formation of porphyry copper deposits. Acta Geochim, 36, 9-15.

Sun, W., Huang, R. F., Li, H., Hu, Y. B., Zhang, C. C., Sun, S. J., Zhang, L-p., Ding, X., Li, C.Y., Zartman, R.E., Ling, M. X., 2015. Porphyry deposits and oxidized magmas. Ore Geol. Rev. 65, 97-131.

Tatsumi, Y., and Suzuki, T., 2009. Tholeiitic vs calc-alkalic differentiation and evolution of arc crust: constraints from melting experiments on a basalt from the Izu–Bonin–Mariana Arc. J. Petrol. 50, 1575-1603.

Tattitch, B. C., and Blundy, J. D., 2017. Cu-Mo partitioning between felsic melts and saline-aqueous fluids as a function of X NaCleq, f O2, and f S2. Am. Mineral 102, 1987-2006.

Tattitch, B. C., Candela, P. A., Piccoli, P. M., Bodnar, R. J., 2015. Copper partitioning between felsic melt and H_2O–CO_2 bearing saline fluids. Geochim Cosmochim Acta 148, 81-99.

Titley, S.R., 1975, Geological characteristics and environment of some porphyry copper occurrences in the southwestern Pacific. Econ. Geol. 70, 499-514.

Tomkins, A. G., 2010. Windows of metamorphic sulfur liberation in the crust: Implications for gold deposit genesis. Geochim Cosmochim Acta 74, 3246-3259.

Tomkins, A. G., and Evans, K. A., 2015. Separate zones of sulfate and sulfide release from subducted mafic oceanic crust. Earth Planet. Sci. 428, 73-83.

Tosdal, R.M., Richards, J.P., 2001. Magmatic and structural controls on the development of porphyry Cu ± Mo ± Au deposits: Rev. Econ. Geol. 14, p. 157–181.

Turner, S. J., and Langmuir, C. H., 2015. What processes control the chemical compositions of arc front stratovolcanoes?. Geochem Geophys Geosyst, 16, 1865-1893.

Ulmer, P., Kaegi, R., and Müntener, O, 2018. Experimentally derived intermediate to silica-rich arc magmas by fractional and equilibrium crystallization at 1.0 GPa: An evaluation of phase relationships, compositions, liquid lines of descent and oxygen fugacity. J. Petrol. 59, 11-58.

Vasseur, J., and Wadsworth, F. B., 2017. Sphere models for pore geometry and fluid permeability in heterogeneous magmas. Bull. Volcanol. 79, 77.

Villiger, S., Ulmer, P., Müntener, O., and Thompson, A. B., 2004. The liquid line of descent of anhydrous, mantle-derived, tholeiitic liquids by fractional and equilibrium crystallization—an experimental study at 1.0 GPa. J. Petrol. 45, 2369-2388.

Wallace, P. J., 2005. Volatiles in subduction zone magmas: concentrations and fluxes based on melt inclusion and volcanic gas data. J Volcanol Geoth Res 140, 217-240.

Wallace, P. J., and Edmonds, M., 2011. The sulfur budget in magmas: evidence from melt inclusions, submarine glasses, and volcanic gas emissions. Rev Mineral Geochem, 73, 215-246.

Walsh, S. D., and Saar, M. O. 2008. Magma yield stress and permeability: Insights from multiphase percolation theory. . Volcanol. Geotherm. Res. 177, 1011-1019.

Wang, R., Weinberg, R. F., Collins, W. J., Richards, J. P., and Zhu, D. C., 2018. Origin of postcollisional magmas and formation of porphyry Cu deposits in southern Tibet. Earth Sci. Rev. 181, 122-143.

Wilkinson, J.J., 2013. Triggers for the formation of porphyry ore deposits in magmatic arcs. Nat. Geosci. 6, 917.

Zajacz, Z., Halter, W. E., Pettke, T., and Guillong, M., 2008. Determination of fluid/melt partition coefficients by LA-ICPMS analysis of co-existing fluid and silicate melt inclusions: controls on element partitioning. Geochim Cosmochim Acta 72, 2169-2197.

Zelenski, M., Kamenetsky, V. S., Mavrogenes, J. A., Danyushevsky, L. V., Matveev, D., Gurenko, A. A. 2017. Platinum-group elements and gold in sulfide melts from modern arc basalt (Tolbachik volcano, Kamchatka). Lithos 290, 172-188.

Zellmer, G. F., 2008. Some first-order observations on magma transfer from mantle wedge to upper crust at volcanic arcs. Geological Society, London, Special Publications, 304, 15-31.

Zimmer, M. M., Plank, T., Hauri, E. H., Yogodzinski, G. M., Stelling, P., Larsen, J., Singer, B., Jicha, B., Mandeville, C., and Nye, C. J., 2010. The role of water in generating the calc-alkaline trend: new volatile data for Aleutian magmas and a new tholeiitic index. J. Petrol. 51, 2411-2444.

Zheng, Y. C., Liu, S. A., Wu, C. D., Griffin, W. L., Li, Z. Q., Xu, B., Yang, Z. M., Hou, Z-Q., O'Reilly, S. Y., 2018. Cu isotopes reveal initial Cu enrichment in sources of giant porphyry deposits in a collisional setting. Geology 47, 135-138.

HIGHLIGHTS

- Copper (Cu) concentration in primitive arc basalts mainly derived from mantle wedge
- Different evolution of melt Cu concentration in calc-alkaline and tholeiitic magmas
- Large porphyry copper deposits mostly controlled by initial H_2O melt content in arc magmas
- Flux melting in the mantle wedge plays a key role for the ore-forming potential in arc settings.

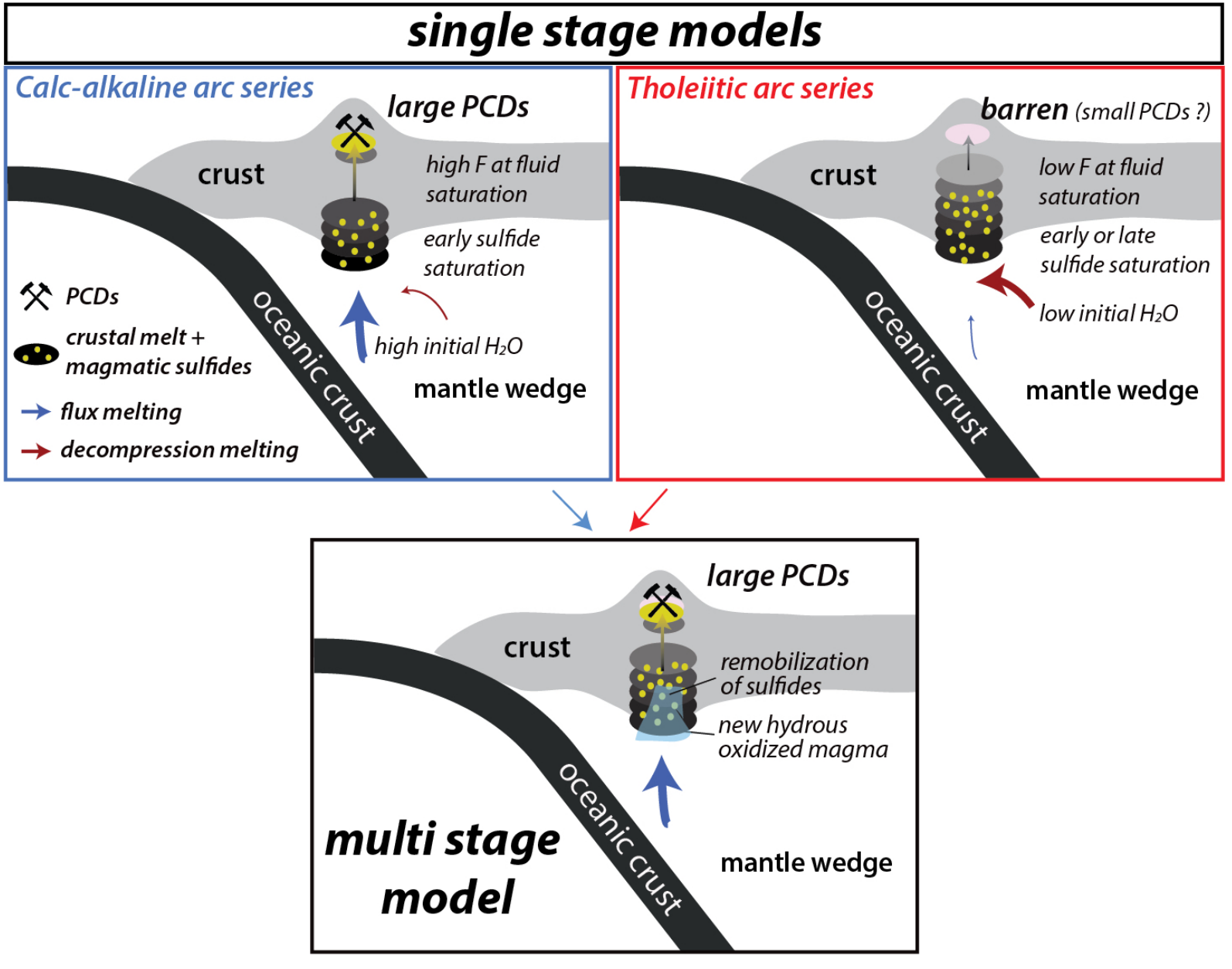
single stage models
Calc-alkaline arc series
large PCDs
crust
high F at fluid saturation
early sulfide saturation
PCDs
crustal melt + magmatic sulfides
flux melting
decompression melting
oceanic crust
high initial H₂O
mantle wedge
Tholeiitic arc series
barren (small PCDs ?)
crust
low F at fluid saturation
early or late sulfide saturation
low initial H₂O
oceanic crust
mantle wedge
large PCDs
crust
remobilization of sulfides
new hydrous oxidized magma
oceanic crust
multi stage model
mantle wedge

The importance of H_2O in arc magmas for the formation of porphyry Cu deposits

Hervé Rezeau† and Oliver Jagoutz

Department of Earth, Atmospheric, and Planetary Sciences, MIT, Cambridge, USA

†Corresponding author: hrezeau@mit.edu

Keywords: Arc magmas; Calc-alkaline and tholeiitic series; Magmatic sulfides; Melt water content; Ore-forming potential; Porphyry copper deposits.

ABSTRACT

Porphyry copper deposits (PCDs) hosted in subvolcanic intrusions at convergent margins are the primary world's copper resources. However, the set of magmatic processes that lead to the generation of ore-bearing magmatic provinces remains unclear. In this paper we review the systematic of Cu evolution during arc magmatic differentiation using new and existing global compilations of whole rock geochemistry data. We trace the Cu evolution from primitive arc magmas through lower crustal plutonic to volcanic rocks. We focus on the well-known tholeiitic and calc-alkaline fractionation sequences, where arc tholeiitic series represents damp primitive melts (<2 wt% H_2O) evolving with iron enrichment, and calc-alkaline series are wet primitive melts (>2 wt% H_2O) that differentiate with iron depletion.

Our study shows that the Cu concentration in primitive arc melts (~80 ppm) is indistinguishable from that of primitive melts formed at mid-ocean ridges (MORBs) implying that Cu is mainly sourced from the mantle wedge in arcs with a limited contribution from the subducted oceanic lithosphere. A global compilation of plutonic rocks whole rock geochemistry (lower crustal cumulates and derivative melts) indicate no systematic difference in Cu concentrations between cumulates associated with tholeiitic or calc-alkaline series. Yet a complementary global compilation of arc volcanic whole rock geochemistry highlights the contrasting behavior of Cu in tholeiitic and calc-alkaline series during magmatic differentiation in arc. In tholeiitic series, Cu shows an incompatible and/or compatible behavior during magma differentiation influenced by the crustal thickness. In calk-alkaline series, Cu is compatible during magma differentiation independently to the crustal thickness. This relates to the timing of sulfide saturation, which is controlled by the

liquid lines of descent (LLD) and/or crustal thickness at redox conditions relevant for arc magmas.

We demonstrate that the initial melt H_2O content in primitive arc melts controls the LLD and the volume of remaining melt mass at fluid saturation. We show that the remaining H_2O-saturated melt mass positively correlates with the total mass of Cu transferred into degassing fluids. The mass of extractable Cu ranges from ~3 to ~10 Mt (i.e., large PCD) for calc-alkaline series, and ranges from ~0.3 to ~2.5 Mt for tholeiitic series. The ore-forming potential of calc-alkaline arc magmas is at least ~4 to ~10 times higher relative to tholeiitic arc magmas. Despite the compatible behavior of Cu during magmatic differentiation, we propose that a single stage model for the formation of large economic PCDs (as opposed to multi-stage model for Cu-sulfides storage and remobilization) is most applicable for the calc-alkaline melts. The importance of the initial melt H_2O content ultimately reflects the key role of flux melting associated with wet calc-alkaline series and high ore-forming potential, in opposition to decompression melting associated with damp tholeiitic series.

1. Introduction

Porphyry copper deposits (PCDs) formed in arc setting represent ~75% of the global copper resources (Sillitoe, 2010). Large economic PCDs are dominantly associated with volatile-rich and oxidized calc-alkaline sub-volcanic intrusions in continental arcs, although some important ones are also formed in oceanic island arcs (Fig. 1; Kesler et al., 1975; Titley, 1975; Solomon, 1990; Richards, 2003, 2011a; Cooke et al., 2005; Sillitoe, 1997, 2010). Magmatic-hydrothermal processes directly associated with the formation of PCDs are reasonably well understood (e.g., Seedorff et al., 2005; Sillitoe, 2010; Kouzmanov and Pokrovski, 2012). In contrast, the role of precursor magmatism (and related source and crustal processes) to generate magmas able to form ore deposits remains less clear (e.g., Audétat and Simon, 2012; Wilkinson, 2013; Richards, 2015). Specifically, the importance of magmatic sulfide crystallization and saturation of a fluid phase acting as the main Cu scavengers during magmatic differentiation is unclear.

Copper is incompatible during magmatic differentiation in thin island arc (<20 km) dominated by tholeiitic series, whereas Cu is compatible during magmatic differentiation in thick continental arc (>30 km) dominated by calc-alkaline series (e.g., Lee et al., 2012;

Chiaradia, 2014). Crustal thickness is proposed to have a first-order control on arc magma differentiation (Miyashiro, 1974; Chiaradia, 2014) and hence the Cu evolution in arc magmas (Chiaradia, 2014; Lee and Tang, 2020). Furthermore, the different tholeiitic and calc-alkaline liquid lines of descent (LLD) control the evolution of the melt redox conditions (expressed in terms of oxygen fugacity, fO_2) in the crust, which in turn impact the solubility of sulfur and Cu through sulfide immiscibility (e.g., Lee et al., 2012), potentially linked to the onset of magnetite crystallization (Jenner et al., 2010; Chiaradia, 2014). Alternative views suggest that the initial H_2O in primitive magma primarily control the LLD (Sisson and Grove, 1993; Tatsumi and Susuki, 2009; Zimmer et al., 2010; Jagoutz et al., 2011; Müntener and Ulmer, 2018), and high initial melt H_2O contents (>4wt% H_2O) combined with high fO_2 in the source region are thought to play a major role for the formation of PCDs (Richards, 2003, 2009, 2011a, 2015; Sun et al., 2015, 2017). As a result, endmember models for PCDs formation in arcs can be grouped in two: (1) multi-stage models envision that early magmatic Cu-sulfide saturation in the deep arc crust represent a key pre-enrichment step to the formation of PCDs in continental arc dominated by calc-alkaline series. Subsequent events within the same or later magmatic cycle remobilize the Cu from these cumulates to form PCDs in the upper crust (e.g., Lee et al., 2012; Wilkinson, 2013; Chiaradia, 2014); alternatively (2) single-stage models consider PCDs formed from metal precipitated from hydrothermal fluids that are exsolved from differentiated mantle-derived, volatile-rich and oxidized calc-alkaline magmas (e.g., Richards, 2009, 2011a, 2015; Sun et al., 2015, 2017).

For both endmember models, a wide range of crucial parameters for the formation of PCDs have been proposed that include the initial metal endowment (McInnes et al., 1999; Mungall, 2002; Sun et al., 2017; Zheng et al., 2018), the melt water concentration (Richards, 2011a,b; Chiaradia et al., 2012; Loucks, 2014; Chiaradia and Caricchi, 2017), the melt redox conditions (Lee et al., 2012; Richards et al., 2015; Sun et al., 2015; Lee and Tang, 2020), the melt metal concentration and/or the melt volume at the time of magmatic fluid saturation (Cline and Bodnar, 1991; Richards, 2009; Park et al., 2019; Chelle-Michou et al., 2017), the duration of the precursor magmatism (Rezeau et al., 2016; Chelle-Michou et al., 2017; Chiaradia and Caricchi, 2017; Richards, 2018) and the overriding plate thickness (i.e.,

pressure of melt differentiation; Chiaradia, 2014; Matjuschkin et al., 2016; Cox et al., 2019; Lee and Tang, 2020).

The evolution of Cu during arc magma differentiation results from a complex interplay of processes occurring in the mantle source region and/or in the crust. Thus, it remains unclear which parameter(s) primarily control the ore-forming potential of arc magmas. This contribution aims to critically evaluate the role of source- and crustal-related magmatic processes related to the ore-forming potential, and examine their respective importance. Here, we use a global compilation of arc volcanic and plutonic (cumulates and derivative melts) whole rock geochemical analyses to systematically characterize the evolution of Cu in arc magmas during magmatic differentiation starting from primitive mantle derived arc magmas. Our global compilation aims to evaluate the role of primitive magma Cu concentration, initial water content, fO_2, pressure of melt differentiation and different LLD for the formation of economic PCDs in the light of the above mentioned two endmember models. Our results emphasize the primary role of the initial melt H_2O content regarding the ore-forming potential of arc magmas, whereas the initial melt Cu content is of secondary importance. We show that a single stage model can explain the formation of large economic PCDs associated with wet calc-alkaline arc series, whereas the multi-stage model is applicable form PCD formed from damp tholeiitic arc series. Ultimately, we propose that the initial melt H_2O content reflect the importance of the melting regime in the mantle wedge, i.e., flux melting in contrast to decompression melting.

2. Copper concentration in primitive arc magmas: implications for the source of Cu

2.1 Dataset and results

Previous studies reported Cu concentration in primitive arc basalts and mid-oceanic ridge basalts (MORBs) ranging from ~50 to ~100 ppm (Jenner et al., 2010; Jenner and O'Neill, 2012; Lee et al., 2012; Chiaradia, 2014; Richards, 2015). Here, we reevaluate the Cu concentration between the different types of primitive arc melts and geodynamic settings. We used the primitive arc melts compilation of Schmidt and Jagoutz (2017) with available whole rock Cu analyses (n=422) from 20 arcs including intra-oceanic, continental and back-arc settings (Supplemental Material Table A1). For this study, we present Cu concentration in primitive arc melts using the same classification scheme as Schmidt and Jagoutz (2017),

with the exception of primitive depleted tholeiitic andesites which are considered fractionated melts. Here, they are classified into five types: (1) primitive calc-alkaline basalts (n=82), (2) primitive tholeiitic basalts (n=50), (3) primitive low-Si basalts (n=64), (4) primitive shoshonites (n=78), and (5) primitive high-Mg andesites (n=148) (Fig. 2; Table A1). For the sake of comparison, we also compiled whole rock Cu analyses (n=58) in primitive MORBs using the data set of Gale et al. (2013). Primitive MORBs were selected based on the same criteria used by Schmidt and Jagoutz (2017) for arc primitive melts, i.e., Mg# of 0.65-0.75, Ni concentrations of 150-500 ppm, and Cr concentrations of < 1200 ppm (Table A1).

Our global compilation indicates that the Cu concentration of primitive arc melts range from 35 to 120 ppm with a global average of 78 ± 31 ppm (1σ) for primitive arc basalts and of 42 ± 17 ppm for primitive high-Mg andesites (Fig. 2). By comparison, the Cu concentration in primitive MORBs display a similar range from 50 to 130 ppm, with a global average of 81 ± 20 ppm (Fig. 2) indistinguishable from primitive arc basalts. Among primitive arc basalts, there is no systematics correlation between the Cu concentrations, the types of primitive melt and/or the geodynamic settings. Only the high-Mg andesites are characterized by systematically lower Cu concentrations.

2.2 The source of Cu in arc magmas

A magmatic origin for Cu in PCDs is widely accepted based on isotopic composition of hydrothermal and magmatic sulfides, ore-forming fluids, and the genetically related igneous intrusions (e.g., Hedenquist and Lowenstern, 1994; Rezeau et al., 2016; Zheng et al., 2018). However, there is no consensus whether Cu in arc magmas is directly derived from the mantle wedge/refertilized sub-continental lithospheric mantle (e.g., McInnes et al., 1999; Richards, 2009; Hou et al., 2017; Wang et al., 2018; Zheng et al., 2018) or dominantly inherited from the subducting oceanic lithosphere by slab-related fluid/melt (e.g., Mungall, 2002; Sun et al., 2017).

2.2.1 Mantle-derived vs. slab-related

The Cu concentrations in primitive arc basalts range from 50 to 120 ppm, with no systematics regarding the types of primitive melt and/or the geodynamic settings (Fig. 2). The range of Cu concentration in primitive arc basalts can be generated after 5 to 30% of melting of a mantle source having an initial Cu concentration of 30 ppm at fO_2 ranging from ΔFMQ = 0 to 2 (Lee et al., 2012), which could be reconciled with primitive arc basalts formed by variable degree of partial melting at different pressure in the mantle wedge (Schmidt and Jagoutz, 2017). Alternatively, the range of Cu in primitive melts may represent variable input of Cu from slab-related fluid and/or melt. In this case, we would expect a positive correlation between incompatible elements and Cu content. Our global compilation lacks of such systematics as demonstrated by similar average Cu contents (and a comparable range of Cu) for the different types of primitive basalts characterized by variable involvement of slab-related fluid and/or melts (Table A1; Schmidt and Jagoutz, 2017). This is consistent with the limited remobilization of chalcophile elements from subducted sulfide ore deposits during dehydration of the subducting oceanic lithosphere (Tomkins, 2010; Giacometti et al., 2015). More importantly, primitive arc basalts and MORBs are characterized by the same global average Cu concentration of ~80 ppm irrespective of the degree of subduction-related inputs (Fig. 2). Therefore, our observations are consistent with previous studies (McInnes et al., 1999; Jenner et al., 2010; Lee et al., 2012; Chiaradia, 2014; Richards, 2015) and strongly suggest the predominant contribution of Cu from the mantle without necessarily requiring additional input from slab-related fluids and/or melts.

2.2.2 Refertilization and Cu enrichment via melt-rock reaction

In arc setting, Cu and Os isotope studies suggest that Cu enrichment is linked to the refertilization of the sub-arc mantle through the redistribution of primary sulfides into sulfide-bearing metasomatic veins by slab-related oxidizing fluids (e.g., McInnes et al., 1999; Zheng et al., 2018). Our compilation reveals that primitive high-Mg andesites are characterized by the lowest Cu concentrations (Fig. 2), which are positively correlated with MgO (Supplemental Figure A1). Primitive high-Mg andesites has been proposed to represent lower temperature derivatives of primitive calc-alkaline basalts through melt-rock reaction (also known as refertilization) in the shallow mantle and/or arc lithosphere (Kelemen et

al.,1995; Kelemen et al., 2014; Schmidt and Jagoutz, 2017). Consequently, we suggest that the low Cu concentrations in primitive high-Mg andesites reflect Cu-sulfide fractionation, which occur during melt-rock reaction. Such mechanism has been documented in a suite of MORBs erupted at the Kane Megamullion, where Cu enrichment in the shallow mantle results from melt-peridotite reaction (Ciazela et al., 2017). Similarly, melt-rock reaction in the arc mantle region could represent an additional mechanism for local Cu enrichment in the sub arc mantle and/or arc lithosphere. We envision that subsequent remelting of these zones may account for unusually high Cu content in primitive arc basalts.

3. Copper concentration in volcanic arc rocks

3.1 Dataset

It has long been recognized that differentiation of arc magmas dominantly follow either a tholeiitic or calc-alkaline series with minor importance of an alkaline series (e.g., Miyashiro, 1974). Global whole rock compilation suggests that the crustal thickness of the overriding plates represents a first-order control on tholeiitic and calc-alkaline differentiation series (Miyashiro, 1974; Chiaradia, 2014, 2015). Yet, tholeiitic and calc-alkaline arc magmas are documented to coexist along the same arc segment from fore-arc to back-arc (e.g., Cascades, Baker et al., 1994; Mandler et al., 2014; Kamchatka, Portnyagin et al., 2007; Izu-Bonin-Mariana, Tatsumi and Susuki, 2009; Brounce et al., 2014; Aleutians, Zimmer et al., 2010). It has been proposed that the geochemical differences between tholeiitic and calc-alkaline series relate to different LLDs controlled by the initial H_2O content of the primitive arc melt (Sisson and Grove 1993; Zimmer et al., 2010; Jagoutz et al., 2011; Melekhova et al., 2013; Müntener and Ulmer, 2018). It has been proposed that primitive arc magmas with high initial H_2O content, that evolve along a calk-alkaline fractionation sequence are related to flux melting in the sub arc mantle (Grove et al., 2002, 2012; Cervantes and Wallace, 2003; Jagoutz et al., 2011). Flux melting occurs because the melting point of peridotite is significantly lowered due to the addition of water in the mantle wedge (e.g., Grove et al., 2012). The influx of slab-derived hydrous melts/fluids hence produces melts with high initial H_2O. Alternatively, the sub arc mantle can melt due to adiabatic decompression, which produces melts with lower initial H_2O content that evolve along a tholeiitic LLD (Grove et al., 2002, 2012).

Here, we produce a global compilation of whole rock analyses with available Cu of arc volcanic rocks from the georoc database (http://georoc.mpch-mainz.gwdg.de/georoc/) to evaluate the Cu evolution between tholeiitic and calc-alkaline magmatic series along individual arc segment. The discrimination between volcanic rock following a calc-alkaline (n=9,275) or tholeiitic (n=6,114) differentiation trend is based on the classical FeO/MgO versus SiO_2 relationship (Supplemental Figure B1; Miyashiro, 1974). Our global compilation includes volcanic rocks from 28 different magmatic arcs for a total of 15,389 entries (Figs. 1, 3, C1 and D1; Supplementary Table B1). The analyses included in the database fulfilled the following criteria: a loss of ignition (LOI) < 2 wt% (if provided), totals of 97-102 wt%, SiO_2 of 50-70 wt%, MgO of 0.5-10 wt% and FeO/MgO ratio < 15 to avoid any exotic melt compositions. Note that we screened and removed analyses from known mineralized porphyry district to avoid high Cu concentration influenced by ore-forming hydrothermal fluids overprint that are unrelated to the original melt Cu endowment. In the following, all the whole rock data have been recalculated on an anhydrous basis.

3.2 Results

Our global compilation of volcanic rocks shows a wide range of Cu concentrations. For MgO ranging from 0.5 to 10 wt%, most of the Cu data ranges from <10 to ~400 ppm in tholeiitic series and from <10 to ~150 ppm in calc-alkaline series (Fig. 3a,d). During magma differentiation (i.e., decreasing MgO concentration), the evolution of Cu concentrations in tholeiitic and calc-alkaline series differs significantly. In tholeiitic series, the Cu concentration increases from the typical primitive arc basalts value of ~80 ppm at 10 wt% MgO, to the highest values between 3.5 and 5 wt% MgO with a maximum median Cu concentration of ~110 ppm at ~4.2 wt% MgO. This is followed by a decrease of Cu concentration down to a median concentration of ~10 ppm at 0.5 wt% MgO (Fig. 3a). FeO_{tot} and V concentrations also exhibit the highest values between 3.5 and 5 wt% MgO (Fig. 3b,c). In calk-alkaline series, the median Cu concentration steadily decreases from the typical primitive arc magma value of ~80 ppm at 10 wt% MgO to ~10 ppm at 0.5 wt% MgO (Fig. 3d). Both FeO_{tot} and V concentration also mimics the evolution trend of Cu (Fig. 3e, f). This suggests an apparent broad correlation between Cu, FeO_{tot} and V for both tholeiitic and calc-alkaline series. Based on this correlation, the switch from incompatible to compatible

behavior of Cu at MgO ~3-5 wt% is ascribed to the late onset of Fe-oxides crystallization in tholeiitic series, whereas the compatible behavior of Cu relates to the early Fe-oxides crystallization in calc-alkaline magmas (Jenner et al., 2010; Chiaradia, 2014). In details, however, the correlation between the three elements is weak for 17 individual representative arc segments characterized by more than 300 whole rock analyses with available Cu (Fig. 4a, b; Fig. C1 and D1; Table B1). For calc-alkaline and tholeiitic series, FeO_{tot} and V are systematically positively correlated (Fig. 4b). Experiments for tholeiitic and calc-alkaline LLDs have demonstrated that the decrease of FeO_{tot} is closely related to the onset of crystallization of Fe-Ti-oxides (spinel hercynite, ilmenite, magnetite; Villiger et al., 2004; Nandedkar et al., 2014; Ulmer et al., 2018) for which V have a high partition coefficient (Kd>>1 up to 130; Luhr and Carmichael, 1980; Latourrette et al. 1991; Canil, 1999). In contrast, the evolution of Cu is generally poorly correlated with FeO_{tot} and V (Fig.4a), although few arcs display positive correlation (e.g., Izu-Bonin, Aleutians; Fig. C1 and D1). Thus, Fe-oxides crystallization may not necessarily have a large effect on Cu depletion.

We use the Cu concentration at MgO~4 wt% (Cu_4) relative to the initial average Cu concentration in primitive arc basalts of ~80 ppm to evaluate the Cu enrichment or depletion during magmatic differentiation (Fig. 4c, d). With the exception of one arc segment (Central America), calc-alkaline series show a systematic depletion of Cu during magma differentiation (Fig. 4c, d), while tholeiitic series are characterized by Cu enrichment and depletion during magmatic differentiation (Fig. 4c, d). For tholeiitic series, we observe a systematic Cu enrichment in thin arcs (<25 km), which ultimately correlates with the highest FeO_{tot} enrichment at MgO~4 wt% (i.e., Fe_4). For tholeiitic series formed in thicker arcs (>25 km), the Cu depletion dominates. These observations indicate that the evolution of Cu during magma differentiation is influenced by the LLD and the pressure of magma differentiation that are further discussed below among other parameters.

3. Copper concentration in plutonic rocks and derivative melts

Finally, based on the compilation of Jagoutz and Kelemen (2015) and Jagoutz and Klein (2018), we produced a compilation of whole rock Cu analyses for lower crustal cumulates and their derivative melts from the Kohistan arc in Pakistan, Talkeetna arc in Alaska, Sierra Valle Fértil–Sierra Famatina complex in Argentina, Fiordland in New Zealand

(Table C1). A complementary whole rock compilation of Cu-bearing cumulates from Chin et al., 2018 is also included in Table C1, which consist of deep crustal cumulates from Arizona and Sierra Nevada (Western USA), Bonanza arc (British Columbia), Colombia (North Volcanic Andean Zone), Kermadec islands (South Pacific Ocean), and Pontides (NE Turkey). The entire dataset consists in 1606 whole rock major elements analyses, of which 985 include Cu analyses (Table C1).

Our compilation of lower crust plutons that are cumulates and frozen melt compositions (Jagoutz, 2010, Jagoutz et al., 2011) is characterized by a range of SiO_2 from 40 to ~76 wt%, Mg# from 0.9 to 0.2, and Cu concentrations from <10 ppm to 250 ppm (Fig. 5, Table C1). The compiled cumulates are associated with differentiated melt of calc-alkaline signature (Famatina arc, e.g., Otamendi et al., 2009; Fiordland arc, e.g., Allibone et al., 2009; Jijal complex in Kohistan arc, e.g., Jagoutz et al., 2011), tholeiitic signature (Chilas complex in Kohistan arc, e.g., Jagoutz et al., 2011), or overlapping the tholeiitic and calc-alkaline fields (Talkeetna arc, e.g., Greene et al., 2006). Most of the compiled lower crustal plutons are characterized by a "Z" shape trend in the Mg# and SiO_2 space, except for the Chilas complex in Kohistan (Fig. 5a). The different patterns are related to different LLD such as the "Z" shape represents wet fractionation associated with calc-alkaline series, whereas the others represent dry fractionation linked to tholeiitic series (Jagoutz, 2010; Jagoutz et al., 2011; Müntener and Ulmer, 2018). Our global compilation of lower crustal cumulates do not show any systematics difference in whole rock Cu concentrations between cumulates associated with calc-alkaline or tholeiitic series (Fig. 5b).

4. Discussion

When melt reaches sulfide or water saturation during magmatic differentiation Cu is strongly partitioned into magmatic sulfides and/or the fluid phase. Therefore, we first discuss the systematic of magmatic sulfide saturation and its role for the different evolutions of Cu concentration observed between tholeiitic and calc-alkaline magmas (Figs. 3 and 4). Subsequently, we focus on the initial melt H_2O content and its role for the ore-forming potential in arc magmas.

4.1 Sulfide saturation in arc magmas

Magmatic sulfide minerals are known to be highly efficient Cu scavengers, and therefore, it is generally assumed that sulfide saturation plays a crucial role in the ore-forming potential of arc magmas. Indeed, magmatic sulfides are ubiquitous in mafic to felsic volcanic and plutonic rocks (e.g., Stavast et al., 2006; Lee et al., 2012; Zelenski et al., 2017; Georgatou and Chiaradia, 2019). The observed volume of magmatic sulfides in igneous rocks range from <0.1 to 0.6 vol% and directly influences the Cu budget during melt differentiation (Kiseeva and Wood, 2015; Georgatou et al., 2018; Cox et al., 2019). As copper is a highly chalcophile element ($D^{sulfide/melt}_{Cu}$ =~250-1000; Li and Audétat, 2012), its solubility in silicate melt strongly depends on sulfide saturation. Experiments have demonstrated a sharp transition from sulfide (S^{2-}) to sulfate (S^{6+}), where sulfide (S^{2-}) is the dominant sulfur species in hydrous silicate melts under more reducing conditions (fO_2), whereas sulfate (S^{6+}) dominates at higher redox conditions (Fig. 6a; Mavrogenes and O'Neill, 1999; O'Neill and Mavrogenes, 2002; Jugo, 2009; Jugo et al., 2010; Botcharnikov et al., 2011; Fortin et al., 2015; Matjuschkin et al., 2016). Furthermore, higher pressure of differentiation shifts the sulfide-sulfate transition towards higher fO_2 (Fig. 6a; Matjuschkin et al., 2016). The sulfur solubility in silicate melts strongly correlates with the sulfide-sulfate transition, such as the S solubility increases as a function of the fraction of oxidized species in the melt (Fig. 6a; Carroll and Rutherford, 1985; Jugo, 2009; Jugo et al., 2010; Botcharnikov et al., 2011; Matjuschkin et al., 2016). At convergent margins, the redox conditions in primitive arc basalts and sub-arc mantle are on average higher than MORBs, but varies over several log units above the fayalite-magnetite-quartz (FMQ) buffer assemblage from ΔFMQ ~0 to +4 (Fig. 6a; e.g., Carmichael, 1991; Lee et al., 2010, 2012; Evans et al., 2012; Kelley and Cottrell, 2012; Brounce et al., 2014; Bénard et al., 2018; Bucholz and Kelemen, 2019). Furthermore, the pressure of differentiation and the volatiles content (H_2O, S) of primitive melt composition vary within and among arcs (e.g., Grove et al., 2002; Rowe et al., 2009; Zimmer et al., 2010; Wallace and Edmonds, 2011; Brounce et al., 2014; Melekhova et al., 2019). In the following, we discuss the importance of sulfide saturation in terms of possible melt evolution paths at different pressures of differentiation, LLD, redox conditions, and initial sulfur concentrations (Fig. 6a-d) that could explain the Cu evolution in tholeiitic and calc-alkaline differentiation series (Fig. 3a, d).

The effect of variable pressure of differentiation on sulfide saturation

The contrasting Cu evolution trends between tholeiitic and calc-alkaline series could be related to different pressures of differentiation, as at low pressure sulfate stability increases towards lower fO_2, whereas higher pressure expands the sulfide stability field (Fig. 6a; e.g., Matjuschkin et al., 2016). Here we discuss arc melts with identical initial fO_2 of ΔFMQ ~ 1.5 and sulfur concentration that differentiate at 0.2 GPa and 1 GPa (Figs. 6a, b). As sulfur is highly incompatible during fractional crystallization (e.g., Ripley and Li, 2013), the sulfur concentration increases with 1/F (F is the remaining melt mass). At 0.2 GPa, hydrous basaltic melt will reach sulfide saturation at S ~0.5 wt% (Figs. 6a; Botcharnikov et al., 2011). At higher pressure, the sulfide-sulfate transition shift towards higher fO_2, and so does the S solubility curve (Matjuschkin et al., 2016). Considering the lack of available experimental data for hydrous basalt at 1 GPa, we shift the experimental sulfur solubility curve obtained at 0.2 GPa and correlate the highest S solubility with the transition of sulfate-only species curve (S^{6+}/S_{tot} =1) at 1 GPa (Figs. 6a). Thus, we can approximate that a hydrous basaltic melt will reach sulfide saturation at S ~0.15 wt%. Assuming the primitive melt has initially 0.12 wt% S (Fig. 6a; Wallace and Edmonds, 2011; Brounce et al., 2014), the high pressure melt will reach sulfur saturation after ~20% fractionation (F=0.8) whereas the low-pressure melt will reach sulfur saturation after 75% differentiation (F=0.25) (Fig. 6b, Table D1). If pressure of differentiation is the controlling parameter, then our data would indicate that tholeiitic melts on average fractionate shallower than calc-alkaline melts. This conclusion is supported by the empirical observation that the overriding plate thickness controls the Cu and FeO enrichment in thin island arc (<20 km) relative to Cu and FeO depletion in thick continental arcs (>30 km) (Chiaradia, 2014). This first-order observation would be consistent with the increase of sulfide stability with pressure (Matjuschkin et al., 2016; Cox et al., 2019). Furthermore, our results highlight that thicker crust and hence possible higher pressure of differentiation prevents Cu enrichment during magma differentiation even for tholeiitic series (Fig. 4d). This observation supports the idea that higher pressure lower crustal melt differentiation plays an important role to trigger early sulfide saturation. Yet, calc-alkaline series are characterized by early Cu depletion independently to the crustal thickness

suggesting that additional parameters control the timing of sulfide saturation during magma differentiation in these series.

The importance of different liquid line of descent on sulfide saturation

For a primitive melt that differentiates at a similar initial pressure, fO_2 and S concentrations, the contrasting Cu evolution trends could be explained by a progressive change of FeO content and redox conditions controlled by the different LLDs (e.g., Lee et al., 2012) due to different initial melt H_2O content (e.g., Sisson and Grove, 1993; Villiger et al., 2004; Nandedkar et al., 2014). Since the variations of redox conditions are sensitive to the melt $Fe^{3+}/\sum Fe$ ratio, the timing of crystallization of Fe-oxides (i.e., Fe^{3+}-bearing minerals) is expected to control the redox trajectories in a closed magmatic system, lowering the melt $Fe^{3+}/\sum Fe$ ratio and hence the oxygen fugacity (e.g., Ghiorso and Carmichael, 1987; Ulmer et al., 2018). The calc-alkaline series is characterized by an early crystallization of Fe-oxides on the LLD compared to the tholeiitic that crystallize Fe-oxide late on the LLD (Sisson and Grove, 1993). We test the evolution of fO_2 using Rhyolite-MELTS (Gualda et al., 2012) to simulate melt crystallization in a thick crust starting from P = 0.8 GPa to 0.15 GPa and in a thin crust starting from P = 0.4 GPa to 0.15 GPa for temperatures ranging from ~1220-1350°C (liquidus varies as a function of initial melt H_2O content) to ~750-800°C (Table D1). Each computation assumes melt differentiation through progressive decompression and cooling followed by cooling once the melt reaches 0.15 GPa (Table D1). We use a starting primitive melt composition of continental arc calc-alkaline basalt (Schmidt and Jagoutz, 2017) having different initial H_2O content of 4 wt%, 1wt% and 0.2 wt% H_2O to account for calc-alkaline and tholeiitic LLDs (e.g., Sisson and Grove 1993; Tatsumi and Susuki, 2009; Zimmer et al., 2010; Melekhova et al., 2013; Table D1).

The modelled melt evolution confirms that the onset of crystallization of ferric bearing minerals (magnetite) triggers the melt to evolve to lower fO_2. The onset of magnetite fractionation is dependent on the melt H_2O content and occurs at F~0.7 for the calc-alkaline series (4 wt% $H_2O_{initial}$) versus F~0.65-0.4 for the tholeiitic series (1 wt% and 0.2 wt% $H_2O_{initial}$). If both calc-alkaline and tholeiitic melt are S undersaturated at the time of magnetite crystallization, the melt evolves toward lower fO_2 as soon as the magnetite appears on the LLD to promotes sulfide saturation, which occur at higher melt fraction for

calc-alkaline magmas compared to tholeiitic ones (Fig. 6c). For tholeiitic series with 1 wt% $H_2O_{initial}$, magnetite crystallization occurs earlier on the LLD (F~0.65) indicative of the concomitant effect of pressure. Our calculations are consistent with Jenner et al. (2010) and Chiaradia (2014) suggestion that difference in Cu depletion trends between the calc-alkaline and tholeiitic differentiation series could be linked to the timing of magnetite crystallization within the respective LLDs, which is ultimately controlled by the initial H_2O content and the pressure of differentiation. This interpretation can explain the Cu enrichment and depletion observed for tholeiitic series in thin arcs (<25 km) and thick arcs (>25 km), while calc-alkaline series consistently displays Cu depletion irrespective of the crustal thickness (Fig. 4c, d).

The importance of variable initial redox conditions on sulfide saturation

The importance of the initial fO_2 of the melt is illustrated by the compatible character of Cu in MORB during differentiation (Jenner and O'Neill, 2012), where the initial fO_2 is ΔFMQ < 0 and sulfide saturation occurs at low S content (Jugo, 2009; Jugo et al, 2010; Botcharnikov et al., 2011; Matjuschkin et al., 2016). In comparison to MORBs, arc-related tholeiitic series are characterized by the early incompatible and compatible character of Cu in thin and thick arcs, respectively (Figs. 3a and 4c,d). According to the experimental sulfide-sulfate transition curves at different pressures (0.2-1 GPa, Fig. 6a), the incompatible character of Cu (i.e. delayed sulfide saturation) in thin arcs could be explained for initial fO_2 conditions of ΔFMQ > ~1 for the primitive arc melt. In contrast, the compatible character of Cu (i.e. early sulfide saturation) in thick arcs could be explained for initial fO_2 conditions of ΔFMQ < ~2 for the primitive arc melt (Figs. 6a,c). Such range of ΔFMQ~1-2 is consistent with estimates for tholeiitic and calc-alkaline arc basalts along the Aleutian arc (ΔFMQ~+0.4-2.1; Zimmer et al., 2010) and Mariana arc (ΔFMQ~+1-1.6; Brounce et al., 2014), for primitive lower crustal ultramafic cumulates in the Talkeetna arc (ΔFMQ~+0.4-2.3; Bucholz and Kelemen, 2019), and for sub-arc mantle xenoliths in Kamchatka arc (ΔFMQ~ +1-1.5; Bénard et al., 2018). If the initial melt fO_2 controls the different behavior of Cu in arc tholeiitic and calc-alkaline series in thin arcs, it would imply that the arc tholeiitic series differentiate at higher initial fO_2 than calc-alkaline series at the same initial S concentrations (Fig. 6c). Although H_2O itself

is a poor oxidant, the oxidation state of arc magmas is mainly affected by the proportion of subduction-related aqueous components added to the mantle wedge (e.g., Kelley and Cottrell, 2009), and more specifically to the chemical components associated with the slab-derived fluids or melts, i.e., Fe^{3+}, S^{6+}, C^{4+} (Mungall, 2002; Tomkins and Evans, 2015; Bénard et al., 2018; Brounce et al., 2019). A positive correlation between H_2O and fO_2 have been shown from mid-ocean ridges to back-arc tectonic settings (Kelley and Cottrell, 2009; Zimmer et al., 2010; Brounce et al., 2014), while melt inclusions from primitive arc basalts from fore-arc to back-arc in the Oregon Cascades do not show any significant differences in fO_2 between tholeiitic and calc-alkaline melts (Rowe et al., 2009). While the role of slab-derived fluids or melts for the oxidation of arc magmas remains unclear, there is no evidence to assume that arc tholeiitic melts have on average higher fO_2 than calc-alkaline melts. Consequently, the early sulfide saturation observed for calc-alkaline series in thin arcs should reflect other processes than a systematic difference in fO_2 in primitive melts.

The importance of variable initial sulfur concentrations on sulfide saturation

It has been proposed that slab-derived fluids/melts appear to be efficient transfer agent for the transport of sulfur from slab to mantle wedge (Jégo and Dasgupta, 2014), which is supported by higher range of S concentrations measured in arc basalts (up to ~0.9 wt%) compared to MORB (up to ~0.2 wt%; e.g., Jugo et al., 2010; Wallace and Edmonds, 2011). In this case, fluid flux melting should be characterized by higher contribution of an external input of S to the mantle wedge via the devolatilization of the subducting oceanic crust relative to decompression melting. Accordingly, we would expect higher initial S concentration in calc-alkaline series promoting early sulfide saturation compared to the tholeiitic series at similar pressure of differentiation and initial fO_2 (Fig. 6d). Positive correlations between melt H_2O content and S exist in arc magmas (e.g., Johnson et al., 2009; Zimmer et al., 2010; Kelley and Cottrell, 2012), although it is not systematic (e.g., Wallace, 2005). Furthermore, any apparent positive correlation from melt inclusions studies could be due to melt degassing (e.g., Wallace and Edmonds, 2011) rather than initial melt conditions. The relationship between the initial H_2O and S content of primitive arc magmas remains uncertain.

In conclusions, this section highlights the complex interplay of different parameters that control sulfide saturation and hence the evolution of melt Cu concentration during magmatic differentiation. Based on our compilation (Fig. 3), we propose that the liquid lines of descent have a large effect on the timing of sulfide saturation in thin arcs (<25 km), whereas the pressure of differentiation becomes the main controlling factor in thicker arcs (>25 km). Finally, more chemical data specifically on the sulfur content of arc magmas and plutons in combination with experimental studies are needed to better understanding sulfide saturation in natural magmatic systems.

4.2 The importance of initial melt H_2O content in arc magmas for the ore-forming potential of magmas

Most of the economic PCDs are preferentially associated with calc-alkaline subvolcanic intrusions (Sillitoe, 2010). Yet, our global compilation shows that the average melt Cu concentration in calc-alkaline series is systematically lower compared to tholeiitic series at a given MgO (Fig. 3a,d). This observation questions the primary importance of melt Cu content in the ore-forming potential. In the following, we evaluate the role of the initial melt water content and the Cu endowment in magmatic fluids for tholeiitic and calc-alkaline series.

4.2.1 Modeling the liquid lines of descent (LLDs)

Compelling lines of evidence suggest that the geochemical differences between tholeiitic and calc-alkaline series relate to different LLDs controlled by the initial H_2O content of the primitive arc melt showing that tholeiitic and calc-alkaline series are best reproduced by LLD of an H_2O-poor and H_2O-rich parental melt, respectively (Sisson and Grove 1993; Chaussidon and Sobolev, 1996; Villiger et al., 2004; Tatsumi and Susuki, 2009; Zimmer et al., 2010; Jagoutz et al., 2011; Melekhova et al., 2013; Brounce et al., 2014; Mandler et al., 2014; Nandedkar et al., 2014; Müntener and Ulmer, 2018). We use Rhyolite-MELTS (Gualda et al., 2012; Ghiorso and Gualda, 2015) to model LLDs with variable initial melt H_2O content from 0.2 wt% to 4 wt% representative of the spectrum of tholeiitic to calc-alkaline series emplaced at convergent margins (e.g., Sisson and Grove 1993; Tatsumi and Susuki, 2009;

Zimmer et al., 2010; Brounce et al., 2014; Melekhova et al., 2013; Mandler et al., 2014). We used an average primitive melt composition of intra-oceanic tholeiitic basalt and continental arc calc-alkaline basalt (Table D1; Schmidt and Jagoutz, 2017). Our models simulate melt differentiation in a thick crust starting from P = 0.8 GPa to 0.15 GPa and in a thin crust starting from P = 0.4 GPa to 0.15 GPa for temperatures ranging from ~1220-1350°C (liquidus varies as a function of initial melt H_2O content) to ~750-800°C at ΔFMQ +1 (Table D1). Each computation assumes melt differentiation through progressive decompression and cooling followed by cooling once the melt reaches 0.15 GPa (Table D1). The modelled LLDs reasonably reproduce the tholeiitic and calc-alkaline trends and show that the amplitude of Fe enrichment decreases as the initial H_2O melt increases (Fig. 7a). Tholeiitic trends are best reproduced by LLDs resulting from the differentiation of intra-oceanic tholeiitic primitive basalt with initial 0.2 to 1.5 wt% H_2O, whereas calc-alkaline trends are best reproduced by LLDs resulting from the differentiation of continental arc calc-alkaline primitive basalt with initial 2 to 4 wt% H_2O (Fig. 7a). For a given initial melt H_2O content, the absolute Fe enrichment depends on the initial melt composition, where LLDs resulting from the differentiation of intra-oceanic tholeiitic primitive basalt show more Fe enrichment compared to continental arc calc-alkaline primitive basalt. Our results also show that an increase of the initial pressure of differentiation slightly reduces the amplitude of Fe enrichment for damp LLDs (Fig. 7a), which is consistent with the broad tendency of having lower Fe_4 at higher crustal thickness (Fig. 4c). Higher redox conditions (ΔFMQ +2-3) significantly limit Fe enrichment and therefore obfuscate the effect of H_2O on the LLDs. Important is that our modeling allows us to quantify the melt composition in respect to the remaining melt fraction (F), the melt water content and the appearance of the aqueous liquid phases (i.e., fluid saturation) for the different LLDs. The latter is based on the fluid saturation model of Ghiorso and Gualda (2015) implemented to Rhyolite-MELT, where thermodynamic properties of the fluid phase are calculated from the model of Duan and Zhang (2006).

We also model the evolution of Cu concentration in the melt using the Rayleigh fractionation equation:

$$C_l = C_0*(F^{D-1}) \qquad [1]$$

where C_l is the concentration of Cu in the fractionated melt, C_0 is the Cu concentration in the parental melt. F is the remaining melt fraction computed from Rhyolite-MELTS. While Cu is incompatible in silicate minerals ($D^{silicates/melt}_{Cu}$ =<0.2; Liu et al., 2014; Hsu et al., 2017), it is highly compatible in sulfides ($D^{sulfide/melt}_{Cu}$ =~250-1000; Li and Audétat, 2012; Jenner, 2017). The bulk-partition coefficient (D) of Cu represents an average of partition coefficients related to the volume percent of saturated magmatic sulfide and rock-forming minerals. Here, we use $D^{sulfide/melt}_{Cu}$ =800 · and $D^{silicates/melt}_{Cu}$ =0.1, and an average of 0.25 vol% of magmatic sulfides (Kiseeva and Wood, 2015; Georgatou et al., 2018) corresponding to a bulk-partition coefficient D of 2.1 at sulfide saturation and a D of 0.1 assuming no sulfide saturation. For tholeiitic series in thin arc (<25 km), the evolution of the Cu is characterized by an initial incompatible behavior followed by a compatible behavior related to late magmatic sulfide saturation (Figs. 3a and 4c,d). In this case, we model the incompatible behavior of Cu assuming no sulfide saturation with an initial Cu concentration of ~80 ppm in the parental melt. The switch from incompatible to compatible behavior of Cu occurs at MgO ~4 wt% (Fig. 3a). At this point, we use the melt Cu concentration at MgO ~4 wt% as the initial Cu concentration in the parental melt (i.e., C_0 ranging from ~130 to 250 ppm) and we assume magmatic sulfide saturation to model the decrease of Cu concentration in tholeiitic series (Fig. 7b; Table D1). For tholeiitic series in thick arc (>25 km) and calc-alkaline series, we assume an early magmatic sulfides saturation to reproduce the steady decrease of Cu concentration (Fig. 7b; Table D1).

For melt differentiation starting at P=4kbars, the computed results indicate that the magmatic fluid phase saturates at H_2O=5.7-6.3 wt%, F=0.35-0.63, P=1.7-2.3 kbars and Cu ~25-50 ppm for the wet series with an initial H_2O content of 2, 2.5, 3, 3.5 and 4 wt%. Damp series with an initial H_2O content of 0.5, 1 and 1.5 wt% saturates magmatic fluid at H_2O=5.4-5.5 wt%, F=0.09-0.26, P=1.5-1.7 kbars and Cu ~15-30/~5-20 ppm (thin/thick arc model) (Figs. 7c,d; Table D1). For melt differentiation starting at P=8kbars, the computed results indicate that the magmatic fluid phase saturates at H_2O=5.5-6.8 wt%, F=0.36-0.59, P=1.8-2.5 kbars and Cu ~25-45 ppm for the wet series, and at H_2O=5.3-5.4 wt%, F=0.11-0.18, P=1.5 kbars and Cu ~15-20/~10 ppm (thin/thick arc model) for the damp series (Figs. 7c,d; Table D1). Independently to the initial pressure of melt differentiation, the wet calc-alkaline LLDs

reach fluid saturation at higher melt fraction, melt H_2O content and melt Cu content compared to damp tholeiitic LLDs (Table D1). Damp melt with initial H_2O content of 0.2 wt% does not reach H_2O saturation, and hence it is not further considered in the next section.

4.2.2 Assessing the ore-forming potential of tholeiitic vs calk alkaline magmas

The Cu endowment of fluids expelled during degassing of H_2O-saturated melt primarily depends on the melt H_2O and Cu content together with the volume of melt presentat fluid saturation (Cline and Bodnar, 1991; Chelle-Michou et al., 2017). As the mass of extractable Cu (Mt) correlates with the volume of water-saturated melt (Chelle-Michou et al., 2017) the remaining melt mass (F) of H_2O-saturated melt is a crucial parameter that determine how much total Cu could be extracted from a magmatic system and hence for the formation of economic PCDs. Because of the different initial H_2O content in the primitive magma, the melt mass remaining at H_2O saturation is different for calk-alkaline vs tholeiitic LLD. Our models presented above have shown that the melt mass remaining at fluid saturation for calk-alkaline LLD is ~1.5 to 7 times that of the tholeiitic LLD.

To illustrate this point, we use a simplified approach of Chelle-Michou et al. (2017) to quantify the mass of extractable Cu in fluids expelled during degassing of H_2O-saturated melt and to estimate the relative Cu endowment in expelled fluids between wet calc-alkaline and damp tholeiitic LLD. We estimate the volume of H_2O-saturated melt according to the Rhyolite-MELTS models presented above as it corresponds to the melt fraction at which an initial volume of primitive magma reached H_2O saturation. Here, we use an initial volume of primitive magma of 189 km^3 km^{-1} Myr^{-1} based on an average arc magma production rate for intra-oceanic arcs (Jicha and Jagoutz, 2015). Once the magma is H_2O-saturated, we calculate the remaining melt fraction of H_2O-saturated melt and the volume of fluids at degassing. Ultimately, the mass of Cu in fluid expelled at degassing corresponds to the volume and density of fluids and the Cu concentration in fluids at degassing. The latter varies according to the melt Cu concentration and the partition coefficient of Cu between the fluid and the melt. The melt Cu concentration is derived from our modelling presented above, while partition coefficients $D_{Cu}^{fluid/melt}$ in the literature range from ~15 to ~300 and strongly depends on the melt salinity, the presence of CO_2, redox conditions, and H_2S content (Zajacz

et al., 2008; Tattitch et al., 2015; Tattitch and Blundy, 2017). We use an intermediate value of $D_{Cu}^{fluid/melt}$ = 140 (Tattitch and Blundy, 2017). Our calculations yield a range of Cu concentration in fluids range from ~0.03 to ~0.1 wt% (Table D1), which correspond to a lower end estimate when compared to fluid inclusions data ranging from 0.002 to 2 wt% Cu with an average of ~0.26 wt% in PCDs (Kouzmanov and Pokrovski, 2012). Magma degassing occurs periodically during crystallization of H_2O-saturated melt, however the first degassing event accounts for ~50 to 75 wt% of the total fluid expelled with fluids enriched in Cu compared to the latest stages of degassing characterized by negligible amount of fluids (<25 wt%) depleted in Cu (Chelle-Michou et al., 2017). For this reason, we consider only a single degassing event, hence providing minimum estimates for the mass of extractable Cu in fluid expelled at degassing. In this simplified approach, we assume fixed parameters (percolation threshold, fluid and melt density, partition coefficient) to assess the role of the initial melt H_2O content and melt Cu concentration at degassing. The reader is referred to the Supplementary Material A1 and Table D1 for a detailed description of the calculations.

The results indicate a positive correlation between the relative mass of extractable Cu in fluids expelled from H_2O-saturated magmas and the initial melt H_2O content (Fig. 8). The mass of extractable Cu ranges from 2.6 to 9.6 Mt for wet calc-alkaline series modelled with initial melt H_2O between 2 and 4 wt%, whereas calculations for damp tholeiitic series modelled with initial melt H_2O between 0.5 and 1.5 wt% yield ranges from 0.3 to 2.3 Mt for and from 0.2 to 1 Mt for thin and thick arc models, respectively. The corresponding volumes of H_2O-saturated melt required to form PCDs >2 to ~10 Mt Cu (i.e., large to giant deposit) range from 50 to 120 km^3, which correspond to reasonable estimates compared to those reported for ore-bearing intrusions (e.g., Cline and Bodnar, 1991; Chelle-Michou et al., 2017; Du and Audétat, 2020). Overall, the ore-forming potential in typical calc-alkaline magmas (initial melt H_2O content of 4 wt%) is ~4-10 times higher relative to damp tholeiitic magmas (initial melt H_2O content of 1.5 wt%), and up to ~20-50 times relative to the dampest tholeiitic magmas (initial melt H_2O content of 0.5 wt%) (Fig. 8). If we assume the same melt Cu content of H_2O-saturated melt, the ore-forming potential in typical calc-alkaline magmas is ~3 to 8 times higher relative to damp tholeiitic magmas (Table D1). Such correlation reflects the crucial importance of the remaining H_2O-saturated melt mass, whereas the melt

Cu concentration is of secondary importance. Of course, higher melt Cu content at the time of fluid saturation increases the ore-forming potential of a given LLD, which can be envision with high fO_2 (e.g., Richards, 2015) and/or a source enriched in Cu (e.g., Zheng et al., 2018). Ultimately, our results are consistent with Chiaradia (2020a) suggesting that the highest ore-forming potential coincides with an initial H_2O content of 4 wt% in the parental basaltic melt, whereas lower ore-forming potential are modelled for initial melt H_2O content <2 wt% and >6 wt%. Although our modelling primarily aims to evaluate the effect of initial melt H_2O content on the ore-forming potential of arc magmas, we acknowledge that additional parameters including favorable tectonics, long-lived thermal sustainability, magma mingling, and metal precipitation efficiency play a complementary and important role to modulate the size of PCDs (Tosdal and Richards, 2001; Richards, 2003, 2011a; Caricchi et al., 2012; Wilkinson, 2013; Chiaradia and Caricchi, 2017; Chiaradia, 2020b).

5. Petrogenetic implications for the formation of giant PCDs

5.1 Models of formation for PCDs

In calc-alkaline series, the compatible behavior of Cu during magmatic differentiation (Fig. 3a,d) does not preclude the transfer of significant mass of Cu into the fluids expelled from H_20-saturated melts to form large economic PCDs in a single stage model (Fig. 9a), where fluid saturation occurs at ~1.5-2.5 kbars with an important volume of fluid-saturated melt at fairly low Cu concentrations of ~25-50 ppm. In contrast, a single stage model for the formation of large economic PCDs associated with damp tholeiitic series is unlikely because fluid saturation occurs late with a small volume of melt remaining and low Cu concentrations (Fig. 9b). Our results are consistent with the fact that large economic PCDs are predominantly associated with subvolcanic fluid-saturated calc-alkaline intrusions emplaced at ~2 kb (Richards, 2003; Sillitoe, 2010), whereas tholeiitic series are barren in the main arc (e.g., Kesler et al., 1977) and/or associated with shallow and smaller epithermal Cu-Au deposits associated with bi-modal suites in rift-related setting (e.g., Sillitoe and Hedenquist, 2003). In the case of the successive emplacement of damp tholeiitic series followed by wet calc-alkaline series, Cu-sulfide segregated in tholeiitic crustal cumulates could represent an additional source of Cu if remelting of lower crustal cumulates occurs during a subsequent hydrous magmatic event (Fig. 9c). Of course, Cu-sulfide segregated in

lower crustal cumulates formed from hydrous melts could equally be remobilized during a subsequent hydrous magmatic event (Fig. 9c; Richards, 2009, 2011a, 2015; Lee et al., 2012; Chiaradia, 2014; Hou et al., 2015). This scenario would increase the ore-forming potential and lead to the formation of large PCDs consistent with a multi-stage model that could occur in both subduction-related and post-subduction settings. In conclusions, we suggest that both scenarios are likely to occur in accretionary orogens, however, Cu-sulfide segregation and remobilization does not appear to be a prerequisite to form economic large PCDs in subduction-related setting.

5.2 Source vs. crustal processes

The importance of the melt H_2O content has long been recognized since large economic PCDs are predominantly associated with subvolcanic calc-alkaline intrusions characterized by high Sr/Y and La/Yb ratios ascribed to the early crystallization of amphibole in the deep crust (± garnet at high pressure) (Richards, 2011b; Chiaradia et al., 2012; Loucks, 2014). Furthermore, these ratios positively correlate with arc crustal thickness (Chiaradia, 2015; Profeta et al., 2015; Lieu and Stern, 2019), which ultimately correlates with tholeiitic and calc-alkaline differentiation series at the global scale (Miyashiro, 1974; Chiaradia, 2014). It has been proposed that the crustal thickness primarily controls the association of large PCDs, calc-alkaline magmas and thicker arc with a limited role for the composition of the mantle source (e.g., Chiaradia, 2014). Yet, at the arc scale, tholeiitic and calc-alkaline arc magmas are temporally and spatially related from fore-arc to back-arc and the different LLDs are controlled by the initial H_2O content of the primitive arc melt independently to the pressure of differentiation (Fig. 7a; Sisson and Grove 1993; Baker et al., 1994; Villiger et al., 2004; Tatsumi and Susuki, 2009; Zimmer et al., 2010; Melekhova et al., 2013; Brounce et al., 2014; Mandler et al., 2014; Nandedkar et al., 2014; Ulmer et al., 2018). Here, we suggest that the importance of the initial melt H_2O content in the ore forming potential of arc magmas reflects the primary role of flux melting in the mantle source associated with wet calc-alkaline series, in opposition to decompression melting associated with damp tholeiitic series (Fig. 9; Grove et al., 2002; Cervantes and Wallace, 2003; Jagoutz et al., 2011). The first order relationship between calc-alkaline

magmas and crustal thicknesses (Miyashiro, 1974; Chiaradia, 2014) illustrates that the crustal thickness controls the height of the mantle column and influences the relative importance of decompression melting versus flux melting (Grove et al., 2002; Jagoutz et al., 2011; Karlstrom et al. 2014; Turner and Langmuir, 2015). This makes intuitively sense as a thicker crust reduces the mantle wedge thickness and hence is associated with a shorter melting column, reducing the capability of the mantle to decompress. At the arc scale, the preferential association of PCDs with the episode of crustal thickening (e.g., Cooke et al., 2005) would be consistent with a shorter melting column and the dominance of flux melting regimes during internal tectonic and magmatic cycles. In conclusions, the role of flux melting at a given arc location remains of primary importance for the ore-forming potential in arc magmas and the formation of economic PCDs.

6. Conclusions

In this study, we reviewed the Cu concentrations in primitive arc melts, plutonic rocks and derivative melts, and volcanic rocks to discuss the role of mantle source and crustal magmatic processes to generate fertile magmatism associated with large economic PCDs. The compilation of primitive arc melt does not indicate any particular Cu endowment for a specific type of primitive arc melt and/or geodynamic setting. Our results are consistent with previous studies (Lee et al., 2012) showing an average Cu concentration in different types of primitive arc basalts similar to MORBs (~80 ppm) indicative of the predominant contribution of Cu from the mantle wedge and limited slab-related fluid/melts input. This suggests that the initial Cu endowment in the primitive arc melt is unlikely to represent a crucial prerequisite to form large economic PCDs. Our global compilation of plutonic rocks illustrates that Cu-rich arc (> 100 ppm) cumulates are associated with both calc-alkaline and tholeiitic series. In contrast, our global compilation of volcanic rocks documents systematically different Cu evolution during magma differentiation in calc-alkaline and tholeiitic series for each arc. The contrasting evolution of Cu in tholeiitic and calc-alkaline systematically correlates with FeO_{tot} and V, which is consistent with previous studies suggesting that the different timing of magmatic sulfide saturation relates to the onset of Fe-oxides crystallization on the respective LLDs (Jenner et al., 2010; Chiaradia, 2014). Additional parameters (pressure of magma differentiation, LLDs, fO_2, and/or sulfur

concentration) may locally play a role and account for the large range of Cu concentration observed in the compiled data. Although the average Cu concentrations during melt differentiation is systematically higher for tholeiitic series compared to calc-alkaline series, we propose that the melt Cu concentrations have minor implications for the ore-forming potential of arc magmas. Instead, we demonstrate that the initial melt H_2O content in primitive arc melts controls the LLD and the volume of remaining melt mass at fluid saturation. We showed that the melt mass remaining is a key parameter for calculating the total mass of Cu transferred into exsolving hydrothermal fluids. We propose that the single stage model for the formation of large economic PCDs is most applicable for melts from the calc-alkaline series. The importance of the initial melt H_2O content ultimately reflects the key role of flux melting associated with wet calc-alkaline series and high ore-forming potential, in opposition to decompression melting associated with damp tholeiitic series.

Acknowledgments

H. R. acknowledges the support by the Swiss National Foundation through the early post-doc mobility research grant P2GEP2_178008. The work of O. J and H. R. was supported by National Science Foundation under grant number EAR-1552202. The authors are grateful for the active discussions during group meetings at MIT that contribute to shape our ideas. The authors thank the reviewers for their insightful comments that helped to clarify and improve the manuscript.

Disclosure Statement

No potential conflict of interest was reported by the authors.

FIGURE CAPTION

Fig. 1: World map showing the distribution of arc magmatism and porphyry copper deposits. The location of calc-alkaline and tholeiitic magmatism compiled in this study is from the Georoc database (http://georoc.mpch-mainz.gwdg.de/georoc/). The location of porphyry copper deposits and the deposit size are from Singer et al. (2005). Phanerozoic felsic magmatism is after Jagoutz and Klein (2018). The location of active margins is from Hayes et al. (2018).

Fig. 2: Compilation of Cu concentrations in primitive arc melts and mid-oceanic ridge basalts (MORBs). (a) Whisker plot showing the Cu concentrations in primitive arc melt based on variable tectonic settings using the classification scheme of Schmidt and Jagoutz (2017). The ranges of Cu values for primitive MORBs are compiled from Gale et al. (2013). (b) Average Cu concentration and associated uncertainties (1 SD) for primitive arc basalts (blue), primitive arc high-Mg andesites (orange), and primitive MORBs (grey). (c) Histogram showing the distribution of Cu concentrations for primitive arc basalts, primitive arc high-Mg andesites (HMA), and primitive MORBs. Abbreviations in (a): C for continental arc, IO for Intra-oceanic arc, and BAB for back-arc basin.

Fig. 3: Plots of Cu, FeO_{tot} and V versus MgO for volcanic rocks of 28 arcs. (a–c) Tholeiitic rocks (n=6,114) (d-f) Calc-alkaline rocks (n=9,275). Median values for each compiled arc are also plotted at every MgO = 0.5 wt% for tholeiitic series (dark red circle) and calc-alkaline series (light blue circle) (see details in Fig. C1). Median values of Cu, FeO_{tot} and V for every MgO = 0.5 wt% are shown for the global compilation of tholeiitic and calc-alkaline series (yellow diamond). The average Cu concentration and associated uncertainties (1 SD) for primitive arc basalts (black bar) is shown in (a) and (d).

Fig. 4: Geochemical relationships between Cu, FeO_{tot}, V and crustal thicknesses for 17 volcanic arcs with representative whole rock geochemical data set (n>300). (a) Cu versus FeO_{tot}. (b) V versus FeO_{tot}. (c) Cu_4 versus Fe_4, where Cu_4 and Fe_4 correspond to the average of median values and associated uncertainties (1 SD) of Cu and Fe between MgO = 3 and MgO = 5 wt% (see Table B1). Circles and squares represent thin (<25 km) and thick arc (>25 km). (d) Cu_4 versus crustal thickness. References for crustal thicknesses and associated uncertainties (1 SD) are available in Table B1. The average Cu concentration and associated uncertainties (1 SD) for primitive arc basalts (black bar) is shown in (c) and (d).

Fig. 5: (a) Plots of Mg# (molar Mg/(Mg+Fe)) versus SiO_2 for compiled whole-rock compositions of plutonic rocks for four crustal sections (Famatina, Fjordland, Kohistan and Talkeetna; Jagoutz and Kelemen, 2015; Jagoutz and Klein, 2018 and references therein) together with other cumulates xenoliths from the Bonanza arc, Sierra Nevada, Arizona, Eastern Pontides and Kermadec (Chin et al., 2018 and references therein). Red dots are used for the Chilas complex in Kohistan arc as it represents a damp tholeiitic fractionation, whereas dots with different shades of blue represent plutonic rocks and cumulates xenoliths associated with wet calc-alkaline fractionation (Jagoutz et al., 2011; Jagoutz and Klein, 2018). (b) Histogram showing the density of Cu concentrations for the four crustal sections and other cumulates xenoliths. See discussion for details and the full data set and references in Table C1.

Fig. 6:

Sulfur speciation in melt and sulfur solubility as a function of oxygen fugacity, expressed log units relative to the fayalite-magnatite-quartz buffer (ΔFMQ). (a) The different black curves illustrates the changes in S6+/Stot in hydrous silicate melts with pressure from Jugo et al., (2010), Botcharnikov et al., (2011) and Matjuschkin et al. (2016). The brown line represents the sulfur solubility curve at sulfide and sulfate saturation at 0.2 GPa after Botcharnikov et al. (2011), whereas the brown dotted line represents an hypothetical similar sulfur solubility curve at higher pressure of 1 GPa. The upper inset indicates the redox ranges for mid-ocean ridge basalt (MORB), sub-arc mantle and arc basalts from Ballhaus (1993), Carmichael (1991), Parkinson and Arculus (1999), Arai and Ishimaru (2008), Wallace and Edmons (2011), Evans et al., (2012) and Bénard et al., (2018). We report a range of sulfur concentrations (orange whisker plot with a median values of 0.12 wt%) measured in olivine-hosted melt inclusions for arc-related basalts and basalt-andesites compiled from the Georoc database (n=456). (b-e) Sulfur solubility curves simplified from Figure 6a to illustrate the effect of different parameters on sulfide saturation, including (b) variable pressure of differentiation, (c) different liquid line of descent, (d) variable initial redox conditions, and (e) variable initial sulfur content $[S]_i$. In (b) and (c), the values of F and the timing of

magnetite is quantified in Table D1. The different scenarios are also discussed in details in the section 4.1 of the manuscript.

Fig. 7: Computed melt composition, melt Cu concentration, melt H_2O content, melt fraction (F), during magmatic differentiation for wet (2 to 4 wt% H_2O - blue) and damp (0.2 to 1.5 wt% H_2O - red) at ΔFMQ =1 for variable starting pressure of differentiation (i.e., 8-1.5 kbars (dotted lines) and 4-1.5 kbars (plain lines)) using Rhyolite-MELTS (Gualda et al., 2012). (a) Computed melt evolution of FeO_{tot} versus MgO. For damp LLDs, the highest and lowest Fe enrichment at MgO ~4-5 wt% corresponds to initial H_2O of 0.2 and 1.5 wt%, respectively. The black line corresponds to modelled LLD with initial H_2O of 1 wt% at ΔFMQ =1 from Zimmer et al. (2010), showing the effect of the initial primitive melt composition for the Fe enrichment. Shaded dots are single data and median data per arc from our global compilation of tholeiitic and calc-alkaline volcanic rocks in Figure 3b,e. (b) Evolution of the Cu concentration versus MgO in wet, damp and dry melt modelled using Rayleigh fractionation assuming 0.25 vol.% sulfide ($D^{sulfide/melt}_{Cu}$ =800) and 99.75 vol.% silicate ($D^{silicate/melt}_{Cu}$ =0.1). Shaded dots are single data and median data per arc from our global compilation of tholeiitic and calc-alkaline volcanic rocks in Figure 3a,d. The steady depletion assumes early sulfide saturation to simulate the trends observed in all calc-alkaline series and some tholeiitic series in thick arcs (>25 km). In contrast, the early enrichment in Cu followed by a sharp depletion simulates late sulfide saturation at MgO ~4 wt% to reproduce the evolution of Cu concentration displayed by tholeiitic series in thin arcs (<25 km). (c, d) Rhyolite-MELTS computed melt H_2O content versus the remaining melt mass (F) and pressure (P). See text for detailed discussion and Table D1 for full data sets.

Fig. 8: Relationship between the initial melt H_2O content and the ore-forming potential for the different liquid lines of descents modelled in Figure 7. The ore-forming potential is expressed as the relative Cu endowment in fluid expelled at degassing of a H_2O-saturated magma normalized to damp tholeiitic melts modelled with an initial H_2O content of 0.5 wt% (circles) and 1.5 wt% (squares) according to the variable pressure of differentiation from 4 to 1.5 kbars (4 kb – filled symbol) from 8 to 1.5 kbars (8 kb – empty symbol). The different

colors reflect melt Cu content at H_2O saturation in tholeiitic series assuming late sulfide saturation in thin arc (grey) and early sulfide saturation in thick arc (yellow). Details of the calculation is provided in Table D1 and Supplementary Material A1. See text for discussion.

Fig. 9: Conceptual cartoon of the single-stage and multi-stage models for the formation of porphyry Cu deposits (PCDs). (a) The single stage model assumes the formation of large economic PCDs associated with the generation of wet calc-alkaline melts, where flux melting is predominant in the main arc. (b) The single stage model assumes the formation of barren upper crustal intrusions associated with the generation of damp tholeiitic melts, where decompression melting is predominant in the main arc. (c) The multi-stage model assumes the remobilization of Cu-sulfide sequestered in crustal cumulates during a later hydrous and oxidized magmatic event in the main arc, which may result in the formation of large PCDs.

Fig. A1: Plots of Cu versus MgO for primitive arc basalts and primitive high-Mg Andesites using the classification scheme of Schmidt and Jagoutz (2017).

Fig. B1: Classification of tholeiitic and calc-alkaline volcanic rocks (n=15,389) based on the FeO/MgO versus SiO_2 after Miyashiro (1974).

Fig. C1: Plots of Cu, FeO_{tot} and V versus MgO for calc-alkaline and tholeiitic volcanic rocks for each compiled arc. Median Cu, FeO_{tot} and V values for each arc are plotted at every MgO = 0.5 wt%.

Fig. D1: Plots of Cu and V versus FeO_{tot} for calc-alkaline and tholeiitic volcanic rocks for each compiled arc.

REFERENCES

Allibone, A. H., Jongens, R., Scott, J. M., Tulloch, A. J., Turnbull, I. M., Cooper, A. F., Powell, N. G., Ladley, E. B., King, R. P., Rattenbury, M. S., 2009. Plutonic rocks of the Median Batholith in eastern and central Fiordland, New Zealand. Field relations, geochemistry, correlation, and nomenclature: New Zeal. J. of Geol. Geop. 52, 101–148.

Arai, S., Ishimaru, S., 2008. Insights into petrological characteristics of the lithosphere of mantle wedge beneath arcs through peridotite xenoliths: a review. J. Petrol. 49, 665-695.

Parkinson, I. J., Arculus, R. J., 1999. The redox state of subduction zones: insights from arc-peridotites. Chem. Geol. 160, 409-423.

Audétat, A., Simon, A. C., 2012. Magmatic Controls on Porphyry Copper Genesis. In Geology and Genesis of Major Copper Deposits and Districts of the World: A Tribute to Richard H. Sillitoe, eds. Jeffrey W. Hedenquist, Michael Harris, Francisco Camus. Society of Economic Geologists, Special Publication 16, 553-572.

Baker, M. B., Grove, T. L., Price, R., 1994. Primitive basalts and andesites from the Mt. Shasta region, N. California: products of varying melt fraction and water content. Contrib Mineral Petrol. 118, 111-129.

Ballhaus, C., 1993. Redox states of lithospheric and asthenospheric upper mantle. Contrib Mineral Petrol. 114, 331-348.

Bénard, A., Klimm, K., Woodland, A. B., Arculus, R. J., Wilke, M., Botcharnikov, R. E., Shimizu, N., Nebel, O., Rivard, C., Ionov, D. A., 2018. Oxidising agents in sub-arc mantle melts link slab devolatilisation and arc magmas. Nat. Commun. 9, 3500.

Botcharnikov, R. E., Linnen, R. L., Wilke, M., Holtz, F., Jugo, P. J., and Berndt, J., 2011. High gold concentrations in sulphide-bearing magma under oxidizing conditions. Nat. Geo. 4, 112-115.

Brounce, M. N., Kelley, K. A., and Cottrell, E., 2014. Variations in Fe3+/∑ Fe of Mariana Arc basalts and mantle wedge fO_2. J. Petrol. 55, 2513-2536.

Brounce, M., Cottrell, E., and Kelley, K. A., 2019. The redox budget of the Mariana subduction zone. Earth Planet. Sci. Lett. 528, 115859.

Bucholz, C. E., Kelemen, P. B., 2019. Oxygen fugacity at the base of the Talkeetna arc, Alaska. Contrib Mineral Petrol. 174, 79.

Canil, D., 1999. Vanadium partitioning between orthopyroxene, spinel and silicate melt and the redox states of mantle source regions for primary magmas Geochim. Cosmochim. Acta 63, 557-572.

Carmichael, I. S., 1991. The redox states of basic and silicic magmas: a reflection of their source regions?. Contrib Mineral Petrol. 106, 129-141.

Caricchi, L., Simpson, G., Schaltegger, U., 2014. Zircons reveal magma fluxes in the Earth's crust. Nature 511, 457-461.

Cervantes, P., and Wallace, P. J., 2003. Role of H2O in subduction-zone magmatism: new insights from melt inclusions in high-Mg basalts from central Mexico. Geology 31, 235-238.

Chelle-Michou, C., Rottier, B., Caricchi, L., Simpson, G., 2017. Tempo of magma degassing and the genesis of porphyry copper deposits. Sci. Rep. 7, 40566.

Chiaradia, M., 2014. Copper enrichment in arc magmas controlled by overriding plate Nat. Geo. 7, 43-46.

Chiaradia, M., 2015. Crustal thickness control on Sr/Y signatures of recent arc magmas: an Earth scale perspective. Sci. Rep. 5, 8115.

Chiaradia, M., 2020a. How much water in basaltic melts parental to porphyry copper deposits?. Frontiers in Earth Sciences, 8, 313.

Chiaradia, M., 2020b. Gold endowments of porphyry deposits controlled by precipitation efficiency. Nat. Commun. 11, 1-10.

Chiaradia, M., Caricchi, L., 2017. Stochastic modelling of deep magmatic controls on porphyry copper deposit endowment. Sci. Rep. 7, 44523.

Chiaradia, M., Ulianov, A., Kouzmanov, K., Beate, B., 2012. Why large porphyry Cu deposits like high Sr/Y magmas? Sci. Rep. 2, 685.

Chin, E.J., Shimizu, K., Bybee, G.M., Erdman, M.E., 2018. On the development of the calc-alkaline and tholeiitic magma series: a deep crustal cumulate perspective. Earth Planet. Sci. Lett. 482, 277–287.

Ciazela, J., Dick, H. J., Koepke, J., Pieterek, B., Muszynski, A., Botcharnikov, R., Kuhn, T., 2017. Thin crust and exposed mantle control sulfide differentiation in slow-spreading ridge magmas. Geology 45, 935-938.

Cline, J. S., Bodnar, R. J., 1991. Can economic porphyry copper mineralization be generated by a typical calc-alkaline melt?. J. Geophys. Res. Solid Earth 96(B5), 8113-8126.

Cooke, D. R., Hollings, P., Walshe, J. L., 2005. Giant porphyry deposits: characteristics, distribution, and tectonic controls. Econ. Geol. 100, 801-818.

Cox, D., Watt, S. F., Jenner, F. E., Hastie, A. R., Hammond, S. J., 2019. Chalcophile element processing beneath a continental arc stratovolcano. Earth Planet. Sci. Lett. 522, 1-11.

Du, J., Audétat, A., 2020. Early sulfide saturation is not detrimental to porphyry Cu-Au formation. Geology, 48, 519-524

Duan, Z., Zhang, Z., 2006. Equation of state of the H_2O, CO_2, and H_2O–CO_2 systems up to 10 GPa and 2573.15 K: molecular dynamics simulations with ab initio potential surface. Geochim Cosmochim Acta 70:2311–2324

Evans, K. A., Elburg, M. A., Kamenetsky, V. S., 2012. Oxidation state of subarc mantle. Geology 40, 783-786.

Fliedner, M. M., Klemperer, S. L., 1999. Structure of an island-arc: Wide-angle seismic studies in the eastern Aleutian Islands, Alaska. Journal of Geophysical Research: Solid Earth, 104(B5), 10667-10694.

Fortin, M. A., Riddle, J., Desjardins-Langlais, Y., Baker, D. R., 2015. The effect of water on the sulfur concentration at sulfide saturation (SCSS) in natural melts. Geochim Cosmochim Acta 160, 100-116.

Gale, A., Dalton, C. A., Langmuir, C. H., Su, Y., Schilling, J. G.,2013. The mean composition of ocean ridge basalts. Geochem Geophys Geosyst. 14, 489-518.

Georgatou, A., Chiaradia, M., 2019. Magmatic sulphides in high-K calc-alkaline to shoshonitic and alkaline rocks. Solid Earth. https://doi.org/10.5194/se-2019-106

Georgatou, A., Chiaradia, M., Rezeau, H., Wälle, M., 2018. Magmatic sulphides in Quaternary Ecuadorian arc magmas. Lithos 296, 580-599.

Ghiorso, M. S., Carmichael, I. S., 1987. Modeling magmatic systems; petrologic applications. Rev Mineral Geochem, 17, 467-499.

Ghiorso, M. S., Gualda, G. A., 2015. An H_2O–CO_2 mixed fluid saturation model compatible with rhyolite-MELTS. Contrib Mineral Petrol., 169, 1-30.

Duan Z, Zhang Z (2006) Equation of state of the H2O, CO2, and H2O–CO2 systems up to 10 GPa and 2573.15 K: molecular dynamics simulations with ab initio potential surface. Geochim Cosmochim Acta 70:2311–2324

Giacometti, F., Evans, K. A., Rebay, G., Cliff, J., Tomkins, A. G., Rossetti, P., Vaggelli, G., Adams, D. T. (2014). Sulfur isotope evolution in sulfide ores from Western Alps: Assessing the influence of subduction-related metamorphism. Geochem Geophys Geosyst 15, 3808-3829.

Greene, A. R., DeBari, S. M., Kelemen, P. B., Blusztajn, J., Clift, P. D., 2006. A detailed geochemical study of island arc crust: the Talkeetna arc section, south–central Alaska. J Petrol, 47, 1051-1093.

Grove, T., Parman, S., Bowring, S., Price, R., Baker, M., 2002. The role of an H_2O-rich fluid component in the generation of primitive basaltic andesites and andesites from the Mt. Shasta region, N California. Contrib Mineral Petrol. 142, 375-396.

Grove, T. L., Till, C. B., Krawczynski, M. J., 2012. The role of H_2O in subduction zone magmatism. Annu. Rev. Earth Planet. Sci, 40, 413-439.

Gualda, A.R., Ghiorso, M.S., Lemons, R. V., Tamara L., Carley, T. L., 2012. Rhyolite-MELTS: a Modified Calibration of MELTS Optimized for Silica-rich, Fluid-bearing Magmatic Systems, J Petrol. 53, 875–890.

Hayes, G. P., Moore, G. L., Portner, D. E., Hearne, M., Flamme, H., Furtney, M., Smoczyk, G. M., 2018. Slab2, a comprehensive subduction zone geometry model. Science 362, 58-61.

Hedenquist, J.W., Lowenstern, J.B., 1994. The role of magmas in the formation of hydrothermal ore deposits. Nature 370, 519.

Hou, Z., Yang, Z., Lu, Y., Kemp, A., Zheng, Y., Li, Q., Tang, J., Yang, Z. and Duan, L., 2015. A genetic linkage between subduction-and collision-related porphyry Cu deposits in continental collision zones. Geology 43, 247-250.

Hsu, Y. J., Zajacz, Z., Ulmer, P., Heinrich, C. A., 2017. Copper partitioning between silicate melts and amphibole: Experimental insight into magma evolution leading to porphyry copper ore formation. Chem. Geol. 448, 151-163.

Jagoutz, O. E., 2010. Construction of the granitoid crust of an island arc. Part II: a quantitative petrogenetic model. Contrib Mineral Petrol. 160, 359-381.

Jagoutz, O., Klein, B., 2018. On the importance of crystallization-differentiation for the generation of SiO_2-rich melts and the compositional build-up of arc (and continental) crust. Am. J. Sci, 318, 29-63.

Jagoutz, O., Kelemen, P. B., 2015. Role of arc processes in the formation of continental crust. Annu. Rev. Earth Planet. Sci, 43, 363-404.

Jagoutz, O., Müntener, O., Schmidt, M. W., Burg, J. P., 2011. The roles of flux-and decompression melting and their respective fractionation lines for continental crust formation: Evidence from the Kohistan arc. Earth Planet Sc Lett. 303, 25-36.

Jégo, S., Dasgupta, R., 2014. The fate of sulfur during fluid-present melting of subducting basaltic crust at variable oxygen fugacity. J. Petrol. 55, 1019-1050.

Jenner, F. E., 2017. Cumulate causes for the low contents of sulfide-loving elements in the continental crust. Nat. Geo. 10, 524-529.

Jenner, F. E., O'Neill, H. S. C., 2012. Analysis of 60 elements in 616 ocean floor basaltic glasses. Geochem, Geophys, Geosyst. 13.

Jenner, F.E., O'Neill, H.S.C., Arculus, R.J., Mavrogenes, J.A., 2010. The magnetite crisis in the evolution of arc-related magmas and the initial concentration of Au, Ag and Cu. J. Petrol. 51, 2445–2464.

Jicha, B. R., Jagoutz, O., 2015. Magma production rates for intraoceanic arcs. Elements 11, 105-111.

Johnson, E. R., Wallace, P. J., Delgado Granados, H., Manea, V. C., Kent, A. J., Bindeman, I. N., and Donegan, C. S., 2009. Subduction-related volatile recycling and magma generation beneath Central Mexico: insights from melt inclusions, oxygen isotopes and geodynamic models. J. Petrol. 50, 1729-1764.

Jugo, P. J., 2009. Sulfur content at sulfide saturation in oxidized magmas. Geology 37, 415-418.

Jugo, P.J., Wilke, M., Botcharnikov, R.E., 2010. Sulfur K-edge XANES analysis of natural and synthetic basaltic glasses: implications for S speciation and S content as function of oxygen fugacity. Geochim. Cosmochim. Acta 74, 5926–5938

Karlstrom, L., Lee, C.T., Manga, M., 2014. The role of magmatically driven lithospheric thickening on arc front migration. Geochem. Geophys. Geosyst. 15, 2655–2675.

Kelemen, P. B., Shimizu, N., Salters, V. J. M., 1995. Formation of harzburgite by pervasive melt/rock reaction in the upper mantle, Nature 358, 635–641.

Kelemen, P., Hanghøj, B., K., Greene, A. R., 2014. One view of the geochemistry of subduction-related magmatic arcs, with an emphasis on primitive andesite and lower crust. In The Crust, Treatise on Geochemistry, edited by H. D. Holland and K. K. Turekian, pp. 669–701, Elsevier-Pergamon, Oxford, U. K.

Kelley, K.A., Cottrell, E., 2009. Water and the oxidation state of subduction zone magmas. Science 325, 605–607

Kelley, K. A., Cottrell, E., 2012. The influence of magmatic differentiation on the oxidation state of Fe in a basaltic arc magma. Earth Planet. Sci. 329, 109-121.

Kesler, S.E., Jones, L.M., Walker, R.L., 1975, Intrusive rocks associates with porphyry copper mineralization in island arc areas. Econ. Geol. 70, 515-526.

Kesler, S. E., Sutter, J. F., Issigonis, M. J., Jones, L. M., Walker, R. L., 1977. Evolution of porphyry copper mineralization in an oceanic island arc; Panama. Econ. Geol. 72, 1142-1153.

Kiseeva, E. S., Wood, B. J., 2015. The effects of composition and temperature on chalcophile and lithophile element partitioning into magmatic sulphides. Earth Planet. Sci. 424, 280-294.

Kouzmanov, K., Pokrovski, G. S., 2012. Hydrothermal controls on metal distribution in porphyry Cu(–Au–Mo) systems. In Geology and Genesis of Major Copper Deposits and Districts of the World: A Tribute to Richard H. Sillitoe, eds. Jeffrey W. Hedenquist, Michael Harris, Francisco Camus. Society of Economic Geologists, Special Publication 16, 573–618.

La Tourrette, T. Z., Burnett, D. S., and Bacon, C. R., 1991. Uranium and minor-element partitioning in Fe-Ti oxides and zircon from partially melted granodiorite, Crater Lake, Oregon. Geochim. Cosmochim. Acta 55, 457-469.

Lee, C. T. A., Tang, M., 2020. How to make porphyry copper deposits. Earth Planet. Sci. 529, 115868.

Lee, C. T. A., Luffi, P., Le Roux, V., Dasgupta, R., Albaréde, F., Leeman, W. P., 2010. The redox state of arc mantle using Zn/Fe systematics. Nature 468, 681-685.

Lee, C.-T.A., Luffi, P., Chin, E.J., Bouchet, R., Dasgupta, R., Morton, D.M., Le Roux, V., Yin, Q.-z., Jin, D., 2012. Copper systematics in arc magmas and implications for crust–mantle differentiation. Science 336, 64–68.

Li, Y. Audétat, A., 2012. Partitioning of V, Mn, Co, Ni, Cu, Zn, As, Mo, Ag, Sn, Sb, W, Au, Pb, and Bi between sulfide phases and hydrous basanite melt at upper mantle conditions. Earth Planet. Sci. Lett. 355–356, 327–340.

Lieu, W. K., Stern, R. J., 2019. The robustness of Sr/Y and La/Yb as proxies for crust thickness in modern arcs. Geosphere 15, 621-641.

Liu, X., Xiong, X., Audétat, A., Li, Y., Song, M., Li, L., Sun, W., Ding, X., 2014. Partitioning of copper between olivine, orthopyroxene, clinopyroxene, spinel, garnet and silicate melts at upper mantle conditions. Geochim. Cosmochim. Acta 125, 1–22.

Loucks, R., 2014. Distinctive composition of copper–ore-forming arc magmas. Aust. J. Earth Sci. 61, 5–16.

Luhr, J. F., Carmichael, I. S., 1980. The colima volcanic complex, Mexico. Contrib Mineral Petrol. 71, 343-372.

Mandler, B. E., Donnelly-Nolan, J. M., Grove, T. L., 2014. Straddling the tholeiitic/calc-alkaline transition: the effects of modest amounts of water on magmatic differentiation at Newberry Volcano, Oregon. Contrib Mineral Petrol. 168, 1066.

Matjuschkin, V., Blundy, J.D., Brooker, R.A., 2016. The effect of pressure on sulphur speciation in mid-to deep-crustal arc magmas and implications for the formation of porphyry copper deposits. Contrib. Mineral. Petrol. 171, 66.

Mavrogenes, J. A., O'Neill, H. S. C., 1999. The relative effects of pressure, temperature and oxygen fugacity on the solubility of sulfide in mafic magmas. Geochim Cosmochim Acta 63, 1173-1180.

McInnes, B. I., McBride, J. S., Evans, N. J., Lambert, D. D., Andrew, A. S.,1999. Osmium isotope constraints on ore metal recycling in subduction zones. Science 286, 512-516.

Melekhova, E., Annen, C., Blundy, J., 2013. Compositional gaps in igneous rock suites controlled by magma system heat and water content. Nat. Geo. 6, 385.

Melekhova, E., Schlaphorst, D., Blundy, J., Kendall, J. M., Connolly, C., McCarthy, A., Arculus, R., 2019. Lateral variation in crustal structure along the Lesser Antilles arc from petrology of crustal xenoliths and seismic receiver functions. Earth Planet. Sci. 516, 12-24.

Miyashiro, A., 1974. Volcanic rock series in island arcs and active continental margins. Am. J. Sci. 274, 321–355.

Mungall, J. E., 2002. Roasting the mantle: Slab melting and the genesis of major Au and Au-rich Cu deposits. Geology 30, 915-918.

Müntener, O., Ulmer, P., 2018. Arc crust formation and differentiation constrained by experimental petrology. Am. J. Sci. 318, 64-89.

Nandedkar, R. H., Ulmer, P., and Müntener, O., 2014. Fractional crystallization of primitive, hydrous arc magmas: an experimental study at 0.7 GPa. Contrib Mineral Petrol. 167, 1015.

O'Neill, H. S. C., Mavrogenes, J. A., 2002. The sulfide capacity and the sulfur content at sulfide saturation of silicate melts at 1400 C and 1 bar. J. Petrol. 43, 1049-1087.

Otamendi, J. E., Vujovich, G. I., de la Rosa, J. D., Tibaldi, A. M., Castro, A., Martino, R. D., and Pinotti, L. P., 2009. Geology and petrology of a deep crustal zone from the Famatinian paleo-arc, Sierras de Valle Fértil and La Huerta, San Juan, Argentina. J. S. Am. Earth Sci. 27, 258-279.

Park, J. W., Campbell, I. H., Malaviarachchi, S. P., Cocker, H., Hao, H., & Kay, S. M., 2019. Chalcophile element fertility and the formation of porphyry Cu±Au deposits. Min. Dep. 54, 657-670.

Portnyagin, M., Hoernle, K., Plechov, P., Mironov, N., and Khubunaya, S., 2007. Constraints on mantle melting and composition and nature of slab components in volcanic arcs from volatiles (H2O, S, Cl, F) and trace elements in melt inclusions from the Kamchatka Arc. Earth Planet. Sci. 255, 53-69.

Profeta, L., Ducea, M. N., Chapman, J. B., Paterson, S. R., Gonzales, S. M. H., Kirsch, M., Petrescu, L., and DeCelles, P. G., 2015. Quantifying crustal thickness over time in magmatic arcs. Sci. Rep. 5, 17786.

Rezeau, H., Moritz, R., Wotzlaw, J. F., Tayan, R., Melkonyan, R., Ulianov, A., Selby, D., d'Abzac, F. X., Stern, R. A., 2016. Temporal and genetic link between incremental pluton assembly and pulsed porphyry Cu-Mo formation in accretionary orogens. Geology 44, 627-630.

Richards, J. P., 2003. Tectono-magmatic precursors for porphyry Cu-(Mo-Au) deposit formation. Econ. Geol. 98, 1515-1533.

Richards, J.P., 2009. Postsubduction porphyry Cu–Au and epithermal Au deposits: products of remelting of subduction-modified lithosphere. Geology 37, 247–250.

Richards, J. P., 2011a. Magmatic to hydrothermal metal fluxes in convergent and collided margins. Ore Geol. Rev. 40, 1-26.

Richards, J. P., 2011b. High Sr/Y arc magmas and porphyry Cu±Mo±Au deposits: just add water. Econ. Geol. 106, 1075-1081.

Richards, J. P., 2015. The oxidation state, and sulfur and Cu contents of arc magmas: implications for metallogeny. Lithos 233, 27-45.

Richards, J. P., 2018. A shake-up in the porphyry world?. Econ. Geol. 113, 1225-1233.

Ripley, E. M., Li, C., 2013. Sulfide saturation in mafic magmas: Is external sulfur required for magmatic Ni-Cu-(PGE) ore genesis?. Econ. Geol., 108, 45-58.

Rowe, M. C., Kent, A. J., Nielsen, R. L., 2009. Subduction influence on oxygen fugacity and trace and volatile elements in basalts across the Cascade Volcanic Arc. J. Petrol. 50, 61-91.

Schmidt, M. W., Jagoutz, O. 2017. The global systematics of primitive arc melts. Geochem Geophys Geosyst, 18, 2817-2854.

Seedorff, E., J. H. Dilles, J. M. Proffett, M. T. Einaudi, L. Zurcher, W. J. A. Stavast, D. A. Johnson, and M. D. Barton, 2005, Porphyry deposits: characteristics and origin of hypogene features. Economic Geology 100th Anniversary Volume, eds. Jeffrey W. Hedenquist, John F. H. Thompson, Richard J. Goldfarb, Jeremy P. Richards

Sillitoe, R.H., 2010. Porphyry copper systems. Econ. Geol. 105, 3–41.

Sillitoe, R. H., 1997. Characteristics and controls of the largest porphyry copper-gold and epithermal gold deposits in the circum-Pacific region, Aust. J. Earth Sci. 44, 373-388.

Sillitoe, R.H., Hedenquist, J.W., 2003. Linkages between volcanotectonic settings, ore-fluid compositions, and epithermal precious metal deposits. SEG Special Publication 10, 315–343.

Singer, D. A., Berger, V. I., Menzie, W. D., Berger, B. R., 2005. Porphyry copper deposit density. Econ. Geol. 100, 491-514.

Sisson, T. W., Grove, T. L., 1993. Experimental investigations of the role of H2O in calc-alkaline differentiation and subduction zone magmatism. Contrib Mineral Petrol. 113, 143-166.

Sobolev, A. V., and Chaussidon, M., 1996. H_2O concentrations in primary melts from supra-subduction zones and mid-ocean ridges: implications for H_2O storage and recycling in the mantle. Earth Planet. Sci. Lett. 137, 45-55.

Solomon, M., 1990. Subduction, arc reversal, and the origin of porphyry copper-gold deposits in island arcs. Geology 18, 630-633.

Stavast, W. J., Keith, J. D., Christiansen, E. H., Dorais, M. J., Tingey, D., Larocque, A., Evans, N., 2006. The fate of magmatic sulfides during intrusion or eruption, Bingham and Tintic districts, Utah. Econ. Geol. 101, 329-345.

Sun, W., Wang, J. T., Zhang, L. P., Zhang, C. C., Li, H., Ling, M. X., Ding, X., Li, C-y., Liang, H. Y., 2017. The formation of porphyry copper deposits. Acta Geochim, 36, 9-15.

Sun, W., Huang, R. F., Li, H., Hu, Y. B., Zhang, C. C., Sun, S. J., Zhang, L-p., Ding, X., Li, C.Y., Zartman, R.E., Ling, M. X., 2015. Porphyry deposits and oxidized magmas. Ore Geol. Rev. 65, 97-131.

Tatsumi, Y., and Suzuki, T., 2009. Tholeiitic vs calc-alkalic differentiation and evolution of arc crust: constraints from melting experiments on a basalt from the Izu–Bonin–Mariana Arc. J. Petrol. 50, 1575-1603.

Tattitch, B. C., and Blundy, J. D., 2017. Cu-Mo partitioning between felsic melts and saline-aqueous fluids as a function of X NaCleq, f O2, and f S2. Am. Mineral 102, 1987-2006.

Tattitch, B. C., Candela, P. A., Piccoli, P. M., Bodnar, R. J., 2015. Copper partitioning between felsic melt and H_2O–CO_2 bearing saline fluids. Geochim Cosmochim Acta 148, 81-99.

Titley, S.R., 1975, Geological characteristics and environment of some porphyry copper occurrences in the southwestern Pacific. Econ. Geol. 70, 499-514.

Tomkins, A. G., 2010. Windows of metamorphic sulfur liberation in the crust: Implications for gold deposit genesis. Geochim Cosmochim Acta 74, 3246-3259.

Tomkins, A. G., and Evans, K. A., 2015. Separate zones of sulfate and sulfide release from subducted mafic oceanic crust. Earth Planet. Sci. 428, 73-83.

Tosdal, R.M., Richards, J.P., 2001. Magmatic and structural controls on the development of porphyry Cu ± Mo ± Au deposits: Rev. Econ. Geol. 14, p. 157–181.

Turner, S. J., and Langmuir, C. H., 2015. What processes control the chemical compositions of arc front stratovolcanoes?. Geochem Geophys Geosyst, 16, 1865-1893.

Ulmer, P., Kaegi, R., and Müntener, O, 2018. Experimentally derived intermediate to silica-rich arc magmas by fractional and equilibrium crystallization at 1.0 GPa: An evaluation of phase relationships, compositions, liquid lines of descent and oxygen fugacity. J. Petrol. 59, 11-58.

Vasseur, J., and Wadsworth, F. B., 2017. Sphere models for pore geometry and fluid permeability in heterogeneous magmas. Bull. Volcanol. 79, 77.

Villiger, S., Ulmer, P., Müntener, O., and Thompson, A. B., 2004. The liquid line of descent of anhydrous, mantle-derived, tholeiitic liquids by fractional and equilibrium crystallization—an experimental study at 1.0 GPa. J. Petrol. 45, 2369-2388.

Wallace, P. J., 2005. Volatiles in subduction zone magmas: concentrations and fluxes based on melt inclusion and volcanic gas data. J Volcanol Geoth Res 140, 217-240.

Wallace, P. J., and Edmonds, M., 2011. The sulfur budget in magmas: evidence from melt inclusions, submarine glasses, and volcanic gas emissions. Rev Mineral Geochem, 73, 215-246.

Walsh, S. D., and Saar, M. O. 2008. Magma yield stress and permeability: Insights from multiphase percolation theory. . Volcanol. Geotherm. Res. 177, 1011-1019.

Wang, R., Weinberg, R. F., Collins, W. J., Richards, J. P., and Zhu, D. C., 2018. Origin of postcollisional magmas and formation of porphyry Cu deposits in southern Tibet. Earth Sci. Rev. 181, 122-143.

Wilkinson, J.J., 2013. Triggers for the formation of porphyry ore deposits in magmatic arcs. Nat. Geosci. 6, 917.

Zajacz, Z., Halter, W. E., Pettke, T., and Guillong, M., 2008. Determination of fluid/melt partition coefficients by LA-ICPMS analysis of co-existing fluid and silicate melt inclusions: controls on element partitioning. Geochim Cosmochim Acta 72, 2169-2197.

Zelenski, M., Kamenetsky, V. S., Mavrogenes, J. A., Danyushevsky, L. V., Matveev, D., Gurenko, A. A. 2017. Platinum-group elements and gold in sulfide melts from modern arc basalt (Tolbachik volcano, Kamchatka). Lithos 290, 172-188.

Zellmer, G. F., 2008. Some first-order observations on magma transfer from mantle wedge to upper crust at volcanic arcs. Geological Society, London, Special Publications, 304, 15-31.

Zimmer, M. M., Plank, T., Hauri, E. H., Yogodzinski, G. M., Stelling, P., Larsen, J., Singer, B., Jicha, B., Mandeville, C., and Nye, C. J., 2010. The role of water in generating the calc-alkaline trend: new volatile data for Aleutian magmas and a new tholeiitic index. J. Petrol. 51, 2411-2444.

Zheng, Y. C., Liu, S. A., Wu, C. D., Griffin, W. L., Li, Z. Q., Xu, B., Yang, Z. M., Hou, Z-Q., O'Reilly, S. Y., 2018. Cu isotopes reveal initial Cu enrichment in sources of giant porphyry deposits in a collisional setting. Geology 47, 135-138.

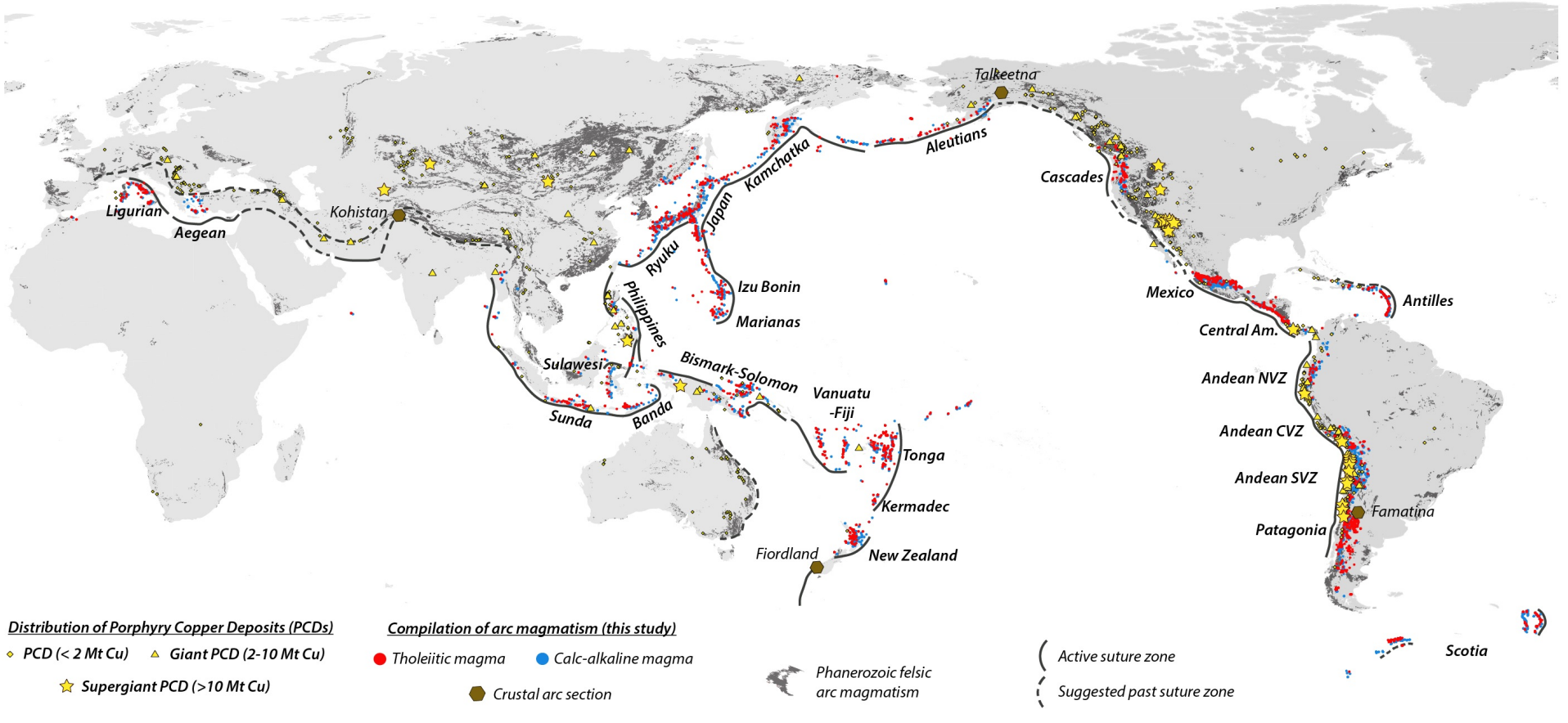
Talkeetna
Aleutians
Kamchatka
Japan
Ryuku
Izu Bonin
Marianas
Philippines
Sulawesi
Bismark-Solomon
Vanuatu
-Fiji
Tonga
Kermadec
New Zealand
Fiordland
Sunda
Banda
Kohistan
Ligurian
Aegean
Cascades
Mexico
Central Am.
Antilles
Andean NVZ
Andean CVZ
Andean SVZ
Patagonia
Famatina
Scotia
Distribution of Porphyry Copper Deposits (PCDs)
PCD (< 2 Mt Cu)
Giant PCD (2-10 Mt Cu)
Supergiant PCD (>10 Mt Cu)
Compilation of arc magmatism (this study)
Tholeiitic magma
Calc-alkaline magma
Crustal arc section
Phanerozoic felsic
arc magmatism
Active suture zone
Suggested past suture zone

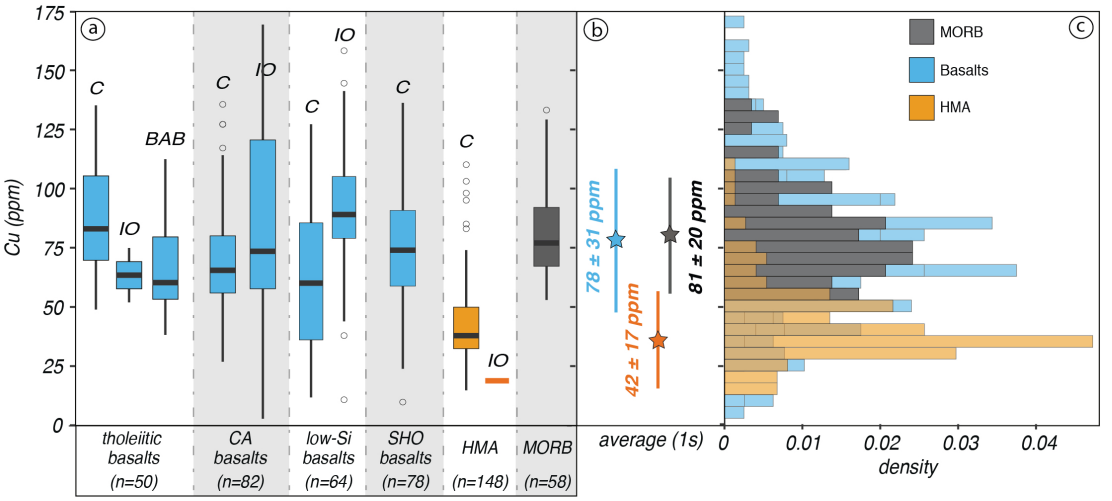
a
b
c
Cu (ppm)
175
150
125
100
75
50
25
0
C
IO
BAB
C
IO
C
IO
C
C
IO
tholeiitic basalts (n=50)
CA basalts (n=82)
low-Si basalts (n=64)
SHO basalts (n=78)
HMA (n=148)
MORB (n=58)
78 ± 31 ppm
42 ± 17 ppm
81 ± 20 ppm
average (1s)
MORB
Basalts
HMA
0
0.01
0.02
0.03
0.04
density

Figure 2

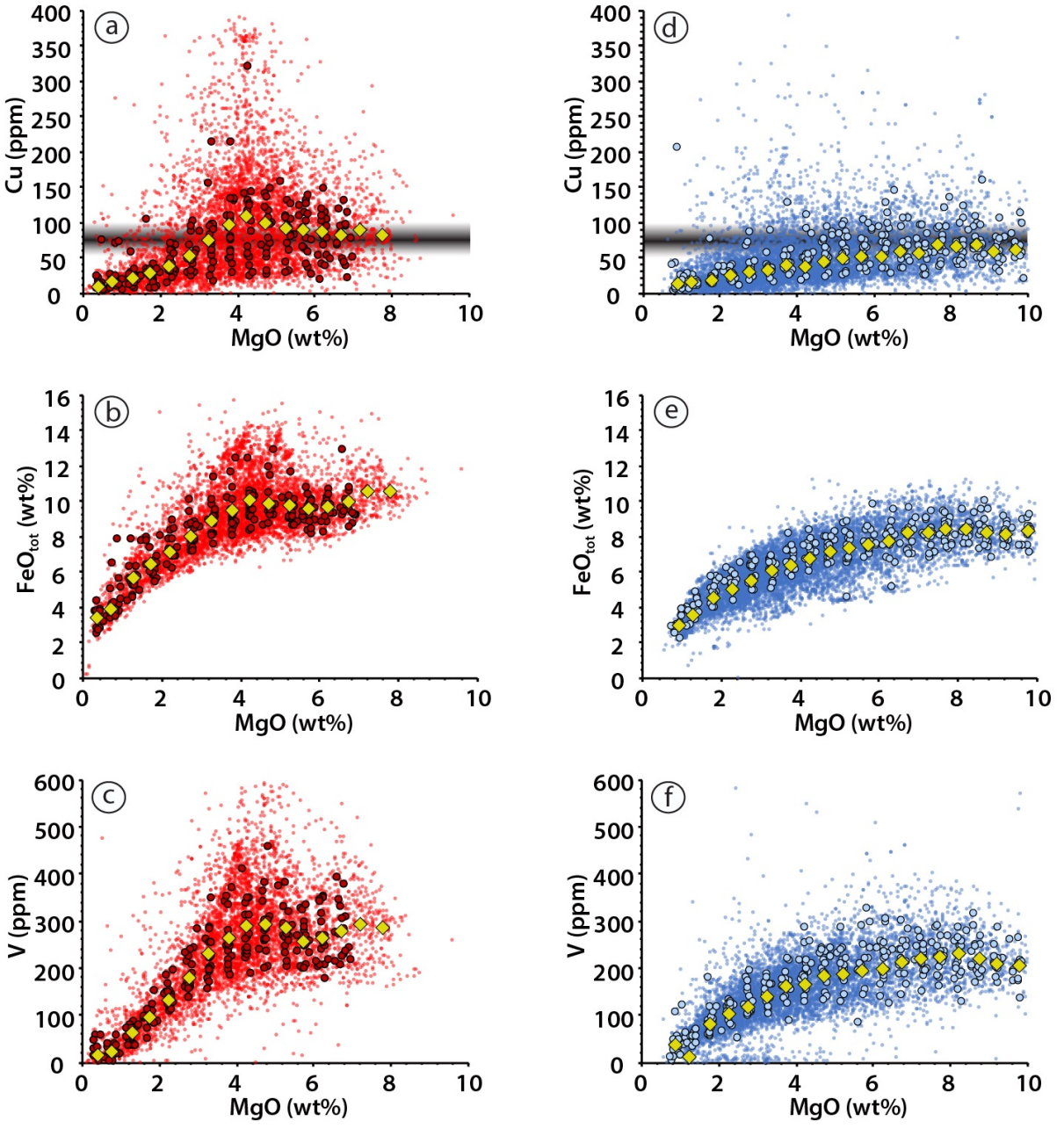

Figure 3

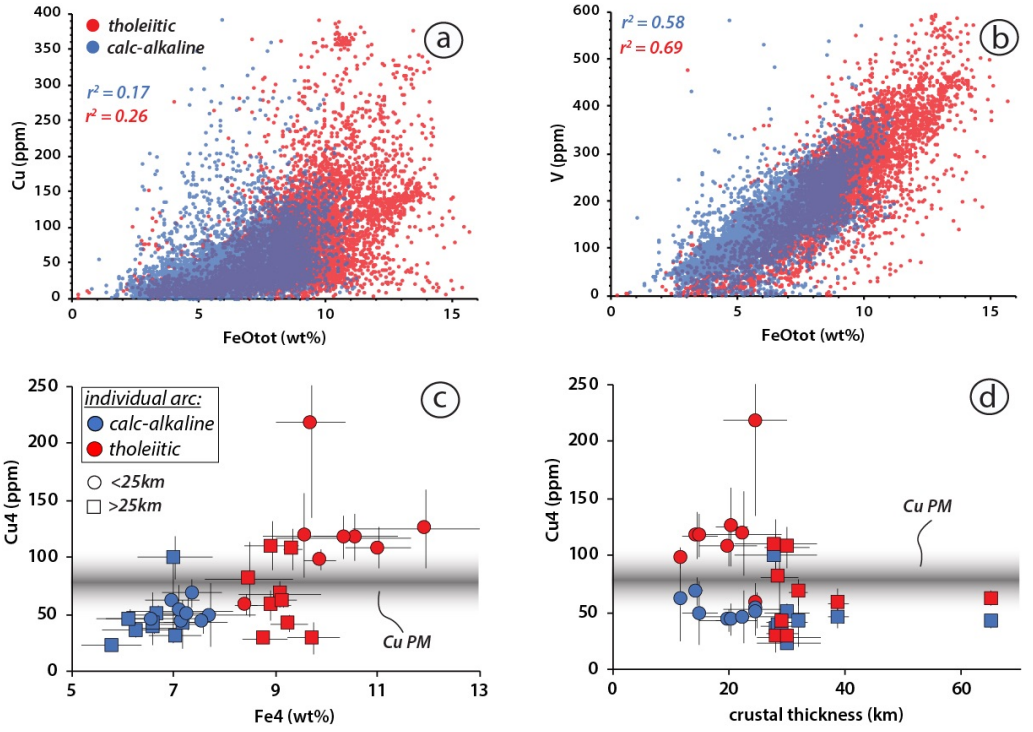
a
tholeiitic
calc-alkaline
r² = 0.17
r² = 0.26
Cu (ppm)
FeOtot (wt%)
b
r² = 0.58
r² = 0.69
V (ppm)
FeOtot (wt%)
c
individual arc:
calc-alkaline
tholeiitic
<25km
>25km
Cu4 (ppm)
Fe4 (wt%)
Cu PM
d
Cu4 (ppm)
crustal thickness (km)
Cu PM

Figure 4

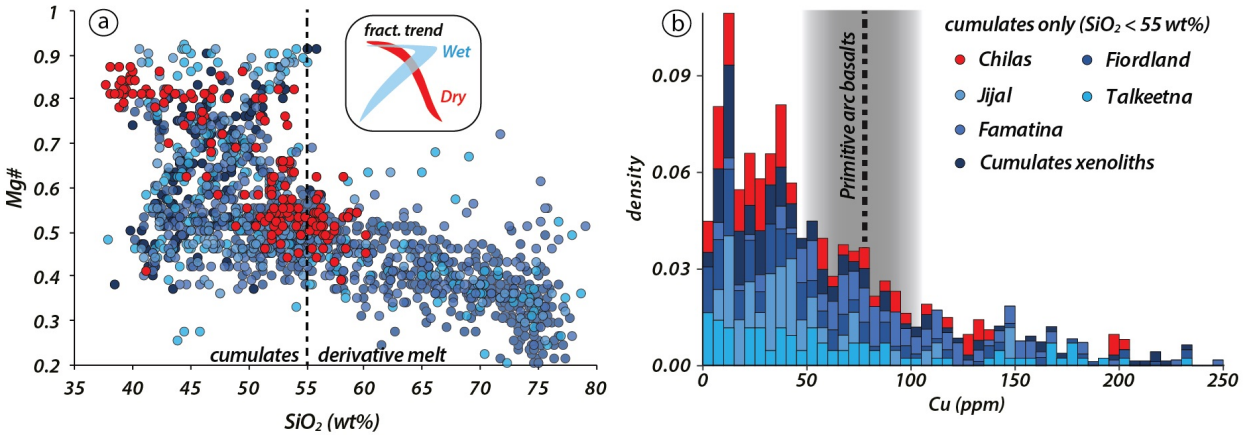
a
fract. trend
Wet
Dry
Mg#
cumulates
derivative melt
SiO₂ (wt%)
b
cumulates only (SiO₂ < 55 wt%)
Chilas
Fiordland
Jijal
Talkeetna
Famatina
Cumulates xenoliths
Primitive arc basalts
density
Cu (ppm)

Figure 5

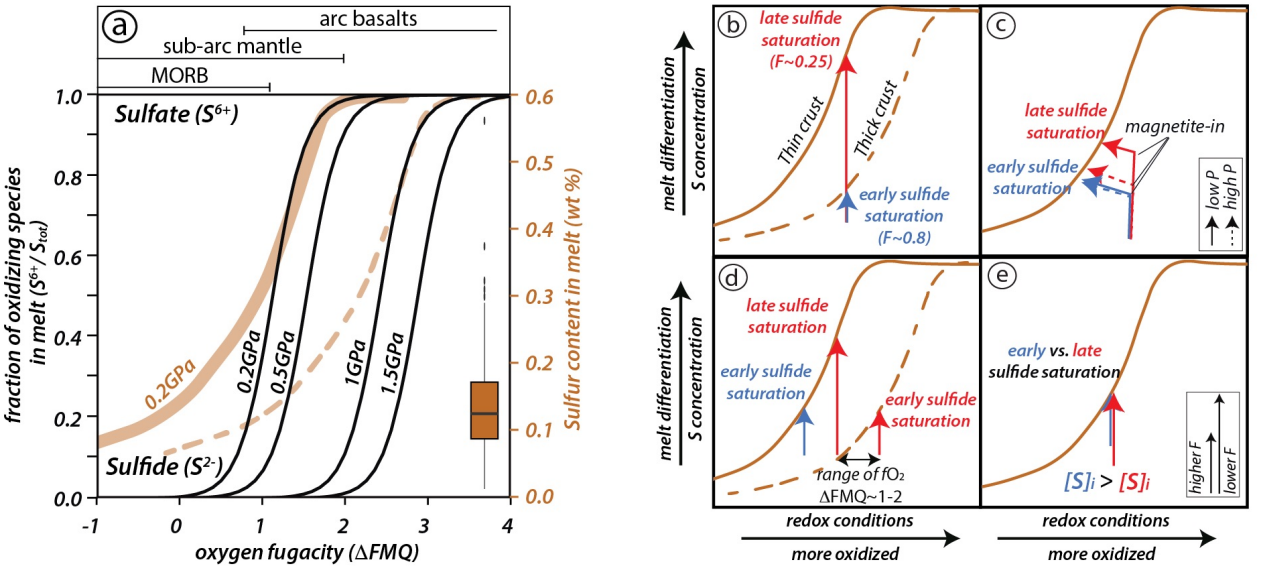
a
arc basalts
sub-arc mantle
MORB
Sulfate (S6+)
Sulfide (S2-)
0.2GPa
0.2GPa
0.5GPa
1GPa
1.5GPa
fraction of oxidizing species in melt (S6+ / Stot)
Sulfur content in melt (wt %)
oxygen fugacity (ΔFMQ)
b
late sulfide saturation (F~0.25)
Thin crust
Thick crust
early sulfide saturation (F~0.8)
c
late sulfide saturation
magnetite-in
early sulfide saturation
low P
high P
d
late sulfide saturation
early sulfide saturation
early sulfide saturation
range of fO2
ΔFMQ~1-2
e
early vs. late sulfide saturation
[S]i > [S]i
higher F
lower F
melt differentiation
S concentration
redox conditions
more oxidized

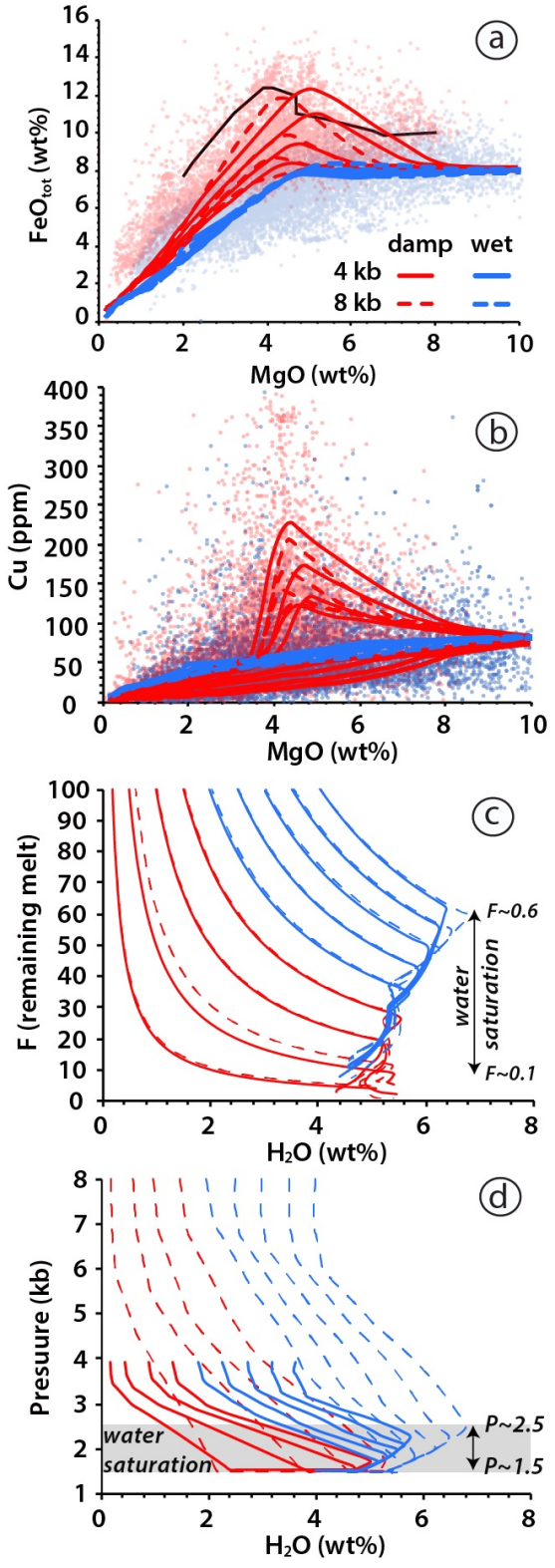
a
FeOtot (wt%)
MgO (wt%)
damp
wet
4 kb
8 kb
b
Cu (ppm)
MgO (wt%)
c
F (remaining melt)
H2O (wt%)
F~0.6
water
saturation
F~0.1
d
Presuure (kb)
H2O (wt%)
water
saturation
P~2.5
P~1.5

Figure 7

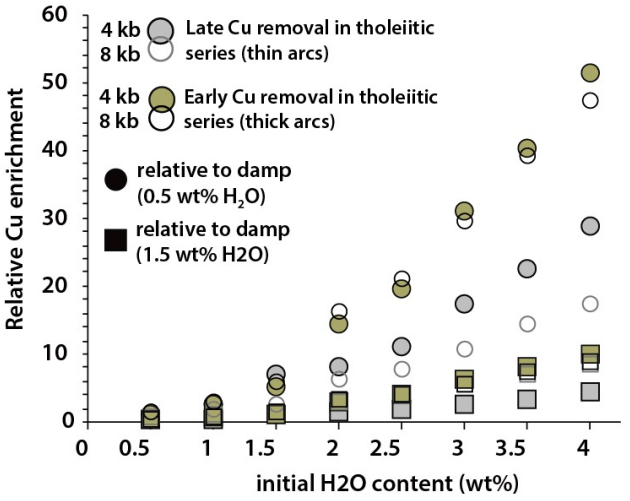
4 kb
8 kb
Late Cu removal in tholeiitic series (thin arcs)
4 kb
8 kb
Early Cu removal in tholeiitic series (thick arcs)
relative to damp (0.5 wt% H_2O)
relative to damp (1.5 wt% H2O)
Relative Cu enrichment
initial H2O content (wt%)
0
10
20
30
40
50
60
0
0.5
1
1.5
2
2.5
3
3.5
4

Figure 8

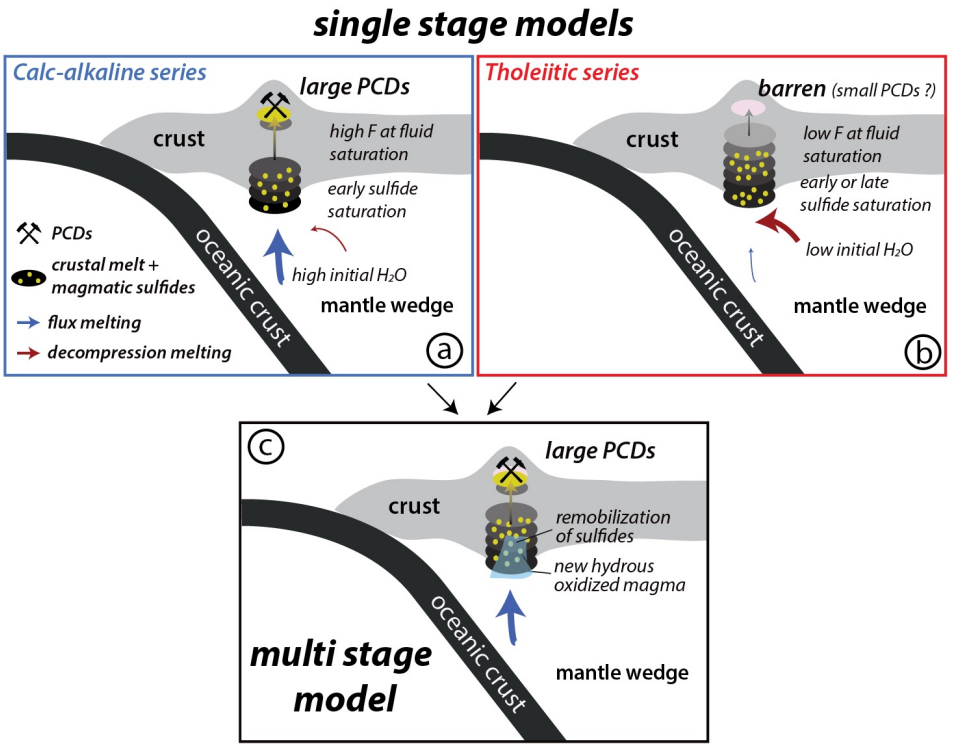
single stage models
Calc-alkaline series
large PCDs
crust
high F at fluid saturation
early sulfide saturation
PCDs
crustal melt + magmatic sulfides
flux melting
decompression melting
oceanic crust
high initial H2O
mantle wedge
a
Tholeiitic series
barren (small PCDs ?)
crust
low F at fluid saturation
early or late sulfide saturation
low initial H2O
oceanic crust
mantle wedge
b
c
large PCDs
crust
remobilization of sulfides
new hydrous oxidized magma
oceanic crust
multi stage model
mantle wedge

Figure 9

Declaration of interests

 The authors declare that they have no known competing financial interests or personal relationships that could have appeared to influence the work reported in this paper.

☐The authors declare the following financial interests/personal relationships which may be considered as potential competing interests:

I declare that we have no competing interests.

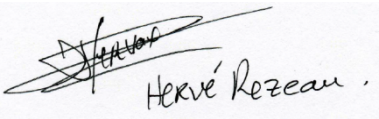

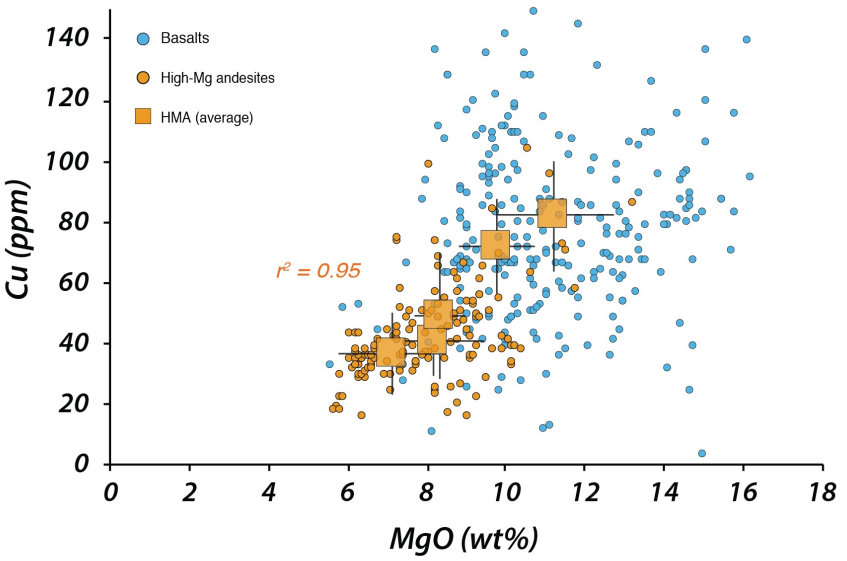
Basalts
High-Mg andesites
HMA (average)
$r^2 = 0.95$
Cu (ppm)
MgO (wt%)
0
20
40
60
80
100
120
140
0
2
4
6
8
10
12
14
16
18

Figure A1

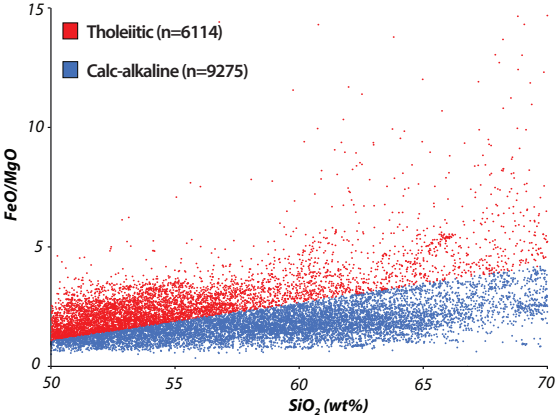
Tholeiitic (n=6114)
Calc-alkaline (n=9275)
FeO/MgO
15
10
5
0
50
55
60
65
70
SiO2 (wt%)

Figure A1

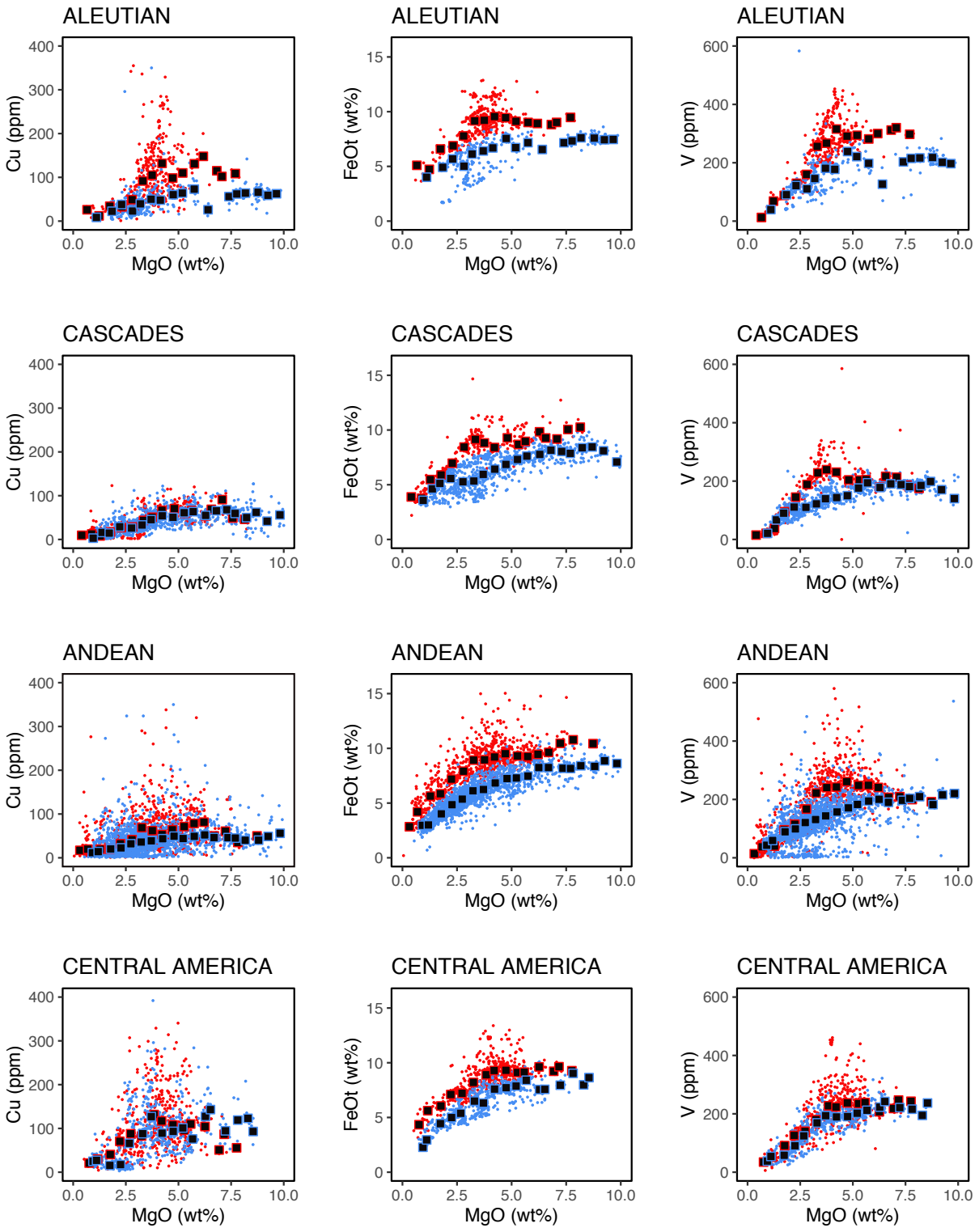
ALEUTIAN
Cu (ppm)
MgO (wt%)
ALEUTIAN
FeOt (wt%)
MgO (wt%)
ALEUTIAN
V (ppm)
MgO (wt%)
CASCADES
Cu (ppm)
MgO (wt%)
CASCADES
FeOt (wt%)
MgO (wt%)
CASCADES
V (ppm)
MgO (wt%)
ANDEAN
Cu (ppm)
MgO (wt%)
ANDEAN
FeOt (wt%)
MgO (wt%)
ANDEAN
V (ppm)
MgO (wt%)
CENTRAL AMERICA
Cu (ppm)
MgO (wt%)
CENTRAL AMERICA
FeOt (wt%)
MgO (wt%)
CENTRAL AMERICA
V (ppm)
MgO (wt%)

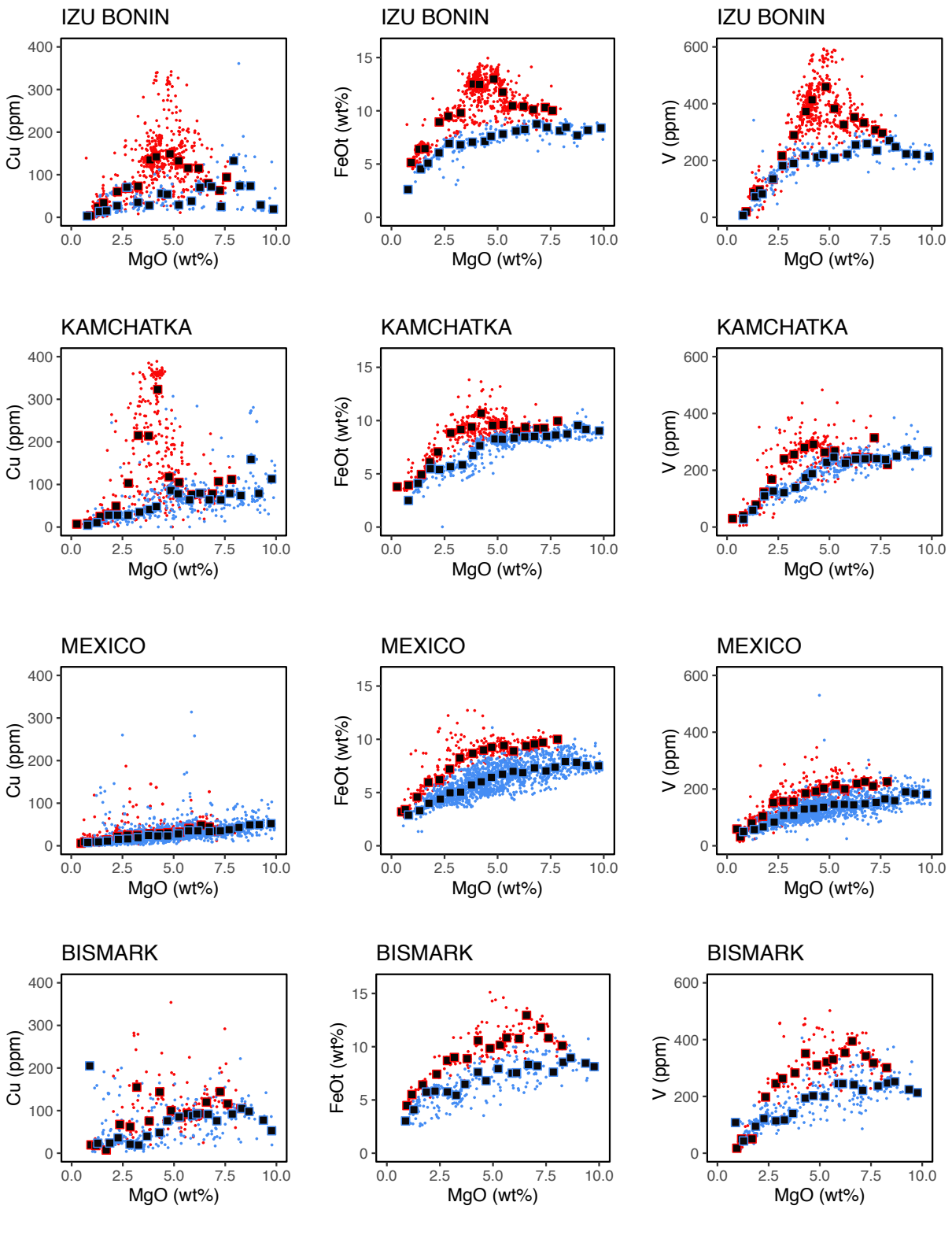
IZU BONIN
Cu (ppm)
MgO (wt%)
IZU BONIN
FeOt (wt%)
MgO (wt%)
IZU BONIN
V (ppm)
MgO (wt%)
KAMCHATKA
Cu (ppm)
MgO (wt%)
KAMCHATKA
FeOt (wt%)
MgO (wt%)
KAMCHATKA
V (ppm)
MgO (wt%)
MEXICO
Cu (ppm)
MgO (wt%)
MEXICO
FeOt (wt%)
MgO (wt%)
MEXICO
V (ppm)
MgO (wt%)
BISMARK
Cu (ppm)
MgO (wt%)
BISMARK
FeOt (wt%)
MgO (wt%)
BISMARK
V (ppm)
MgO (wt%)

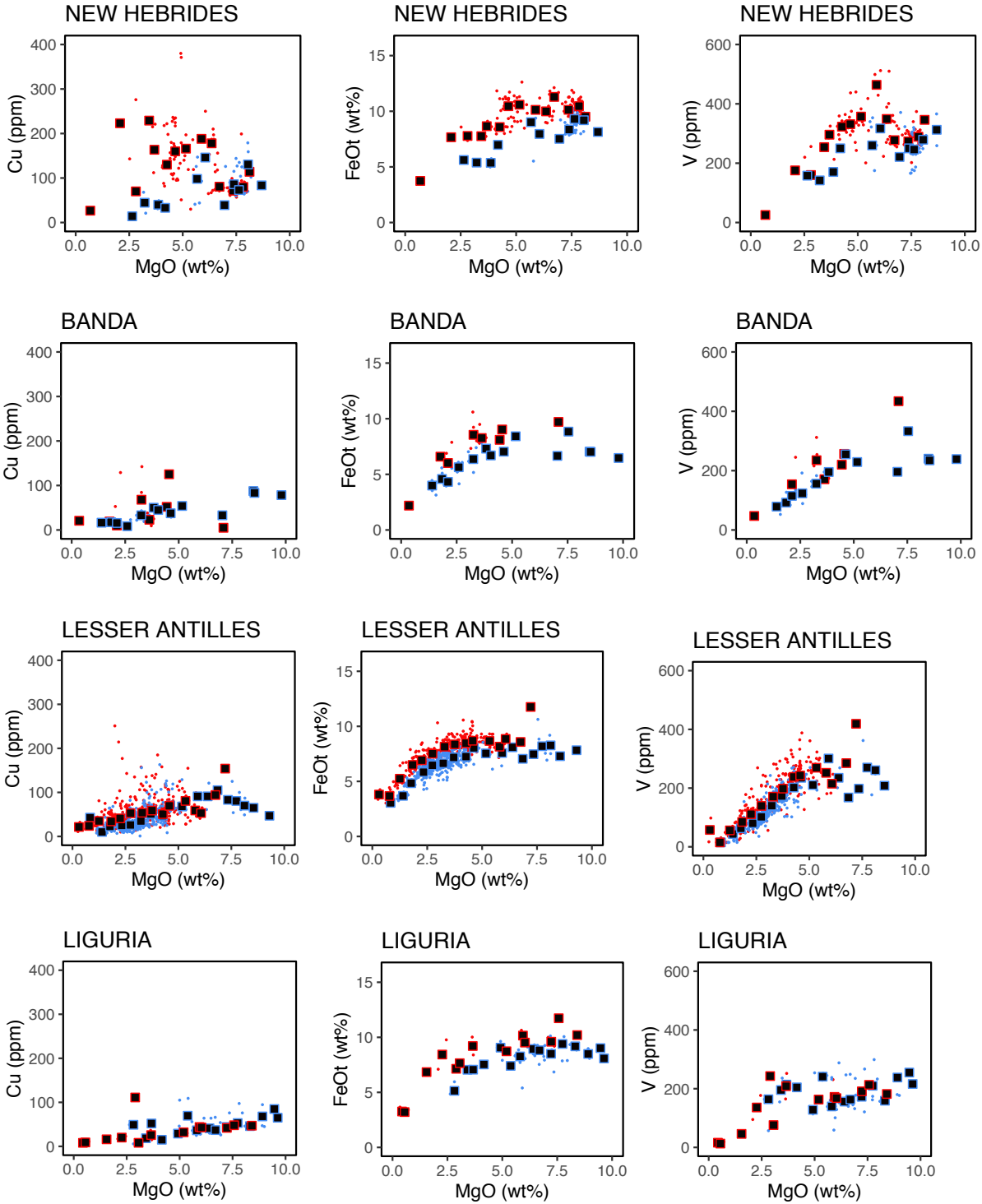
NEW HEBRIDES
Cu (ppm)
MgO (wt%)
NEW HEBRIDES
FeOt (wt%)
MgO (wt%)
NEW HEBRIDES
V (ppm)
MgO (wt%)
BANDA
Cu (ppm)
MgO (wt%)
BANDA
FeOt (wt%)
MgO (wt%)
BANDA
V (ppm)
MgO (wt%)
LESSER ANTILLES
Cu (ppm)
MgO (wt%)
LESSER ANTILLES
FeOt (wt%)
MgO (wt%)
LESSER ANTILLES
V (ppm)
MgO (wt%)
LIGURIA
Cu (ppm)
MgO (wt%)
LIGURIA
FeOt (wt%)
MgO (wt%)
LIGURIA
V (ppm)
MgO (wt%)

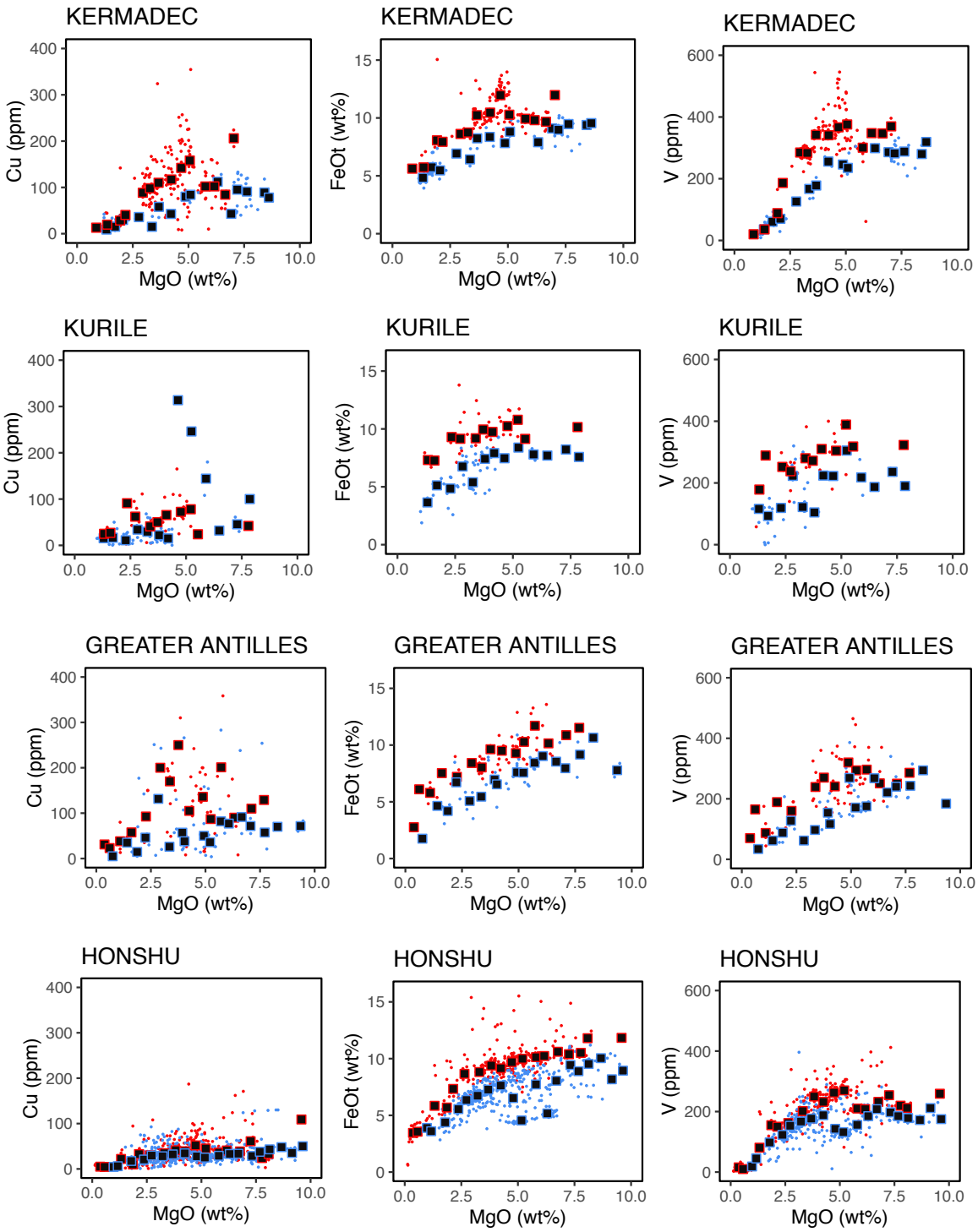
KERMADEC
Cu (ppm)
MgO (wt%)
KERMADEC
FeOt (wt%)
MgO (wt%)
KERMADEC
V (ppm)
MgO (wt%)
KURILE
Cu (ppm)
MgO (wt%)
KURILE
FeOt (wt%)
MgO (wt%)
KURILE
V (ppm)
MgO (wt%)
GREATER ANTILLES
Cu (ppm)
MgO (wt%)
GREATER ANTILLES
FeOt (wt%)
MgO (wt%)
GREATER ANTILLES
V (ppm)
MgO (wt%)
HONSHU
Cu (ppm)
MgO (wt%)
HONSHU
FeOt (wt%)
MgO (wt%)
HONSHU
V (ppm)
MgO (wt%)

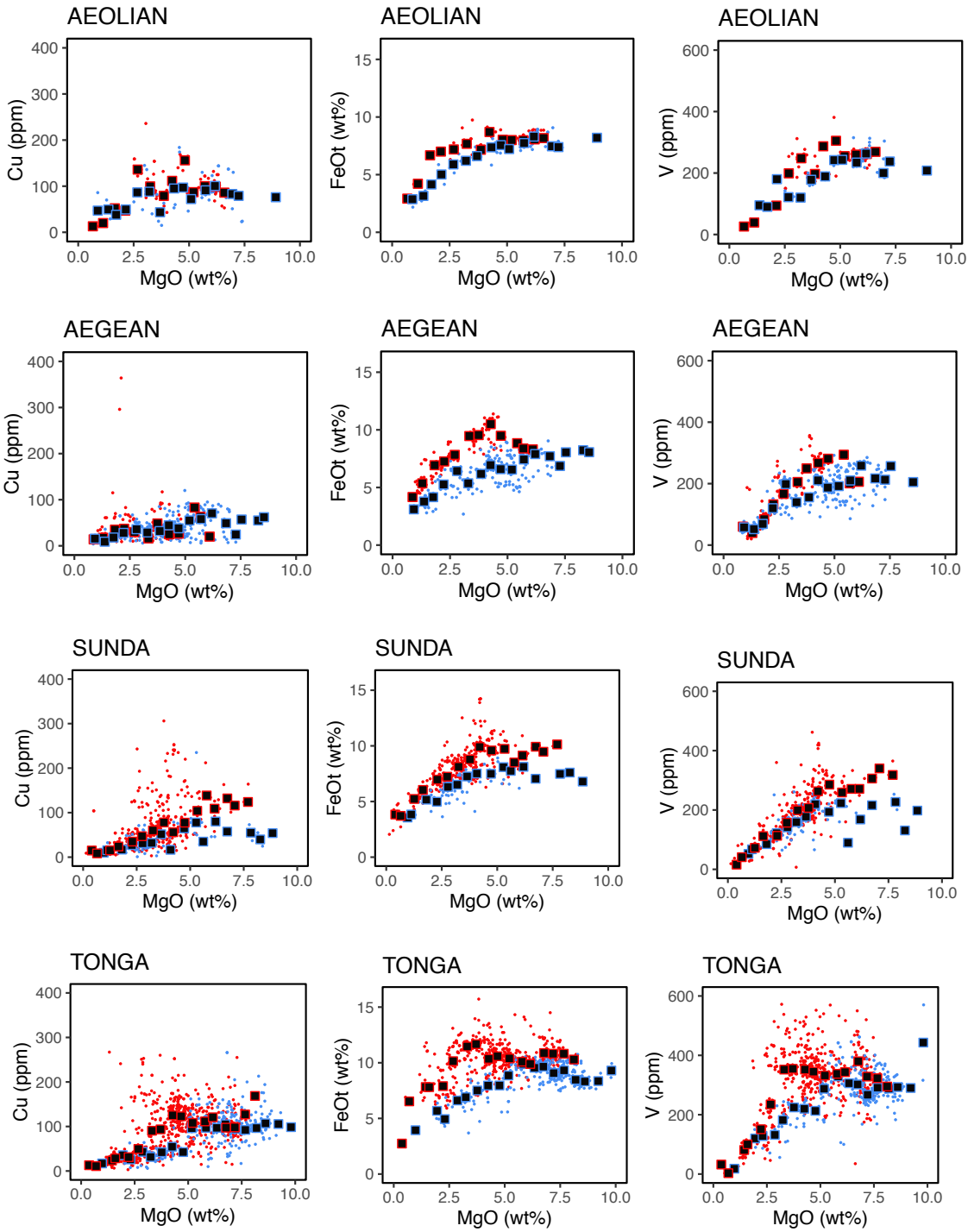
AEOLIAN
Cu (ppm)
MgO (wt%)
AEOLIAN
FeOt (wt%)
MgO (wt%)
AEOLIAN
V (ppm)
MgO (wt%)
AEGEAN
Cu (ppm)
MgO (wt%)
AEGEAN
FeOt (wt%)
MgO (wt%)
AEGEAN
V (ppm)
MgO (wt%)
SUNDA
Cu (ppm)
MgO (wt%)
SUNDA
FeOt (wt%)
MgO (wt%)
SUNDA
V (ppm)
MgO (wt%)
TONGA
Cu (ppm)
MgO (wt%)
TONGA
FeOt (wt%)
MgO (wt%)
TONGA
V (ppm)
MgO (wt%)

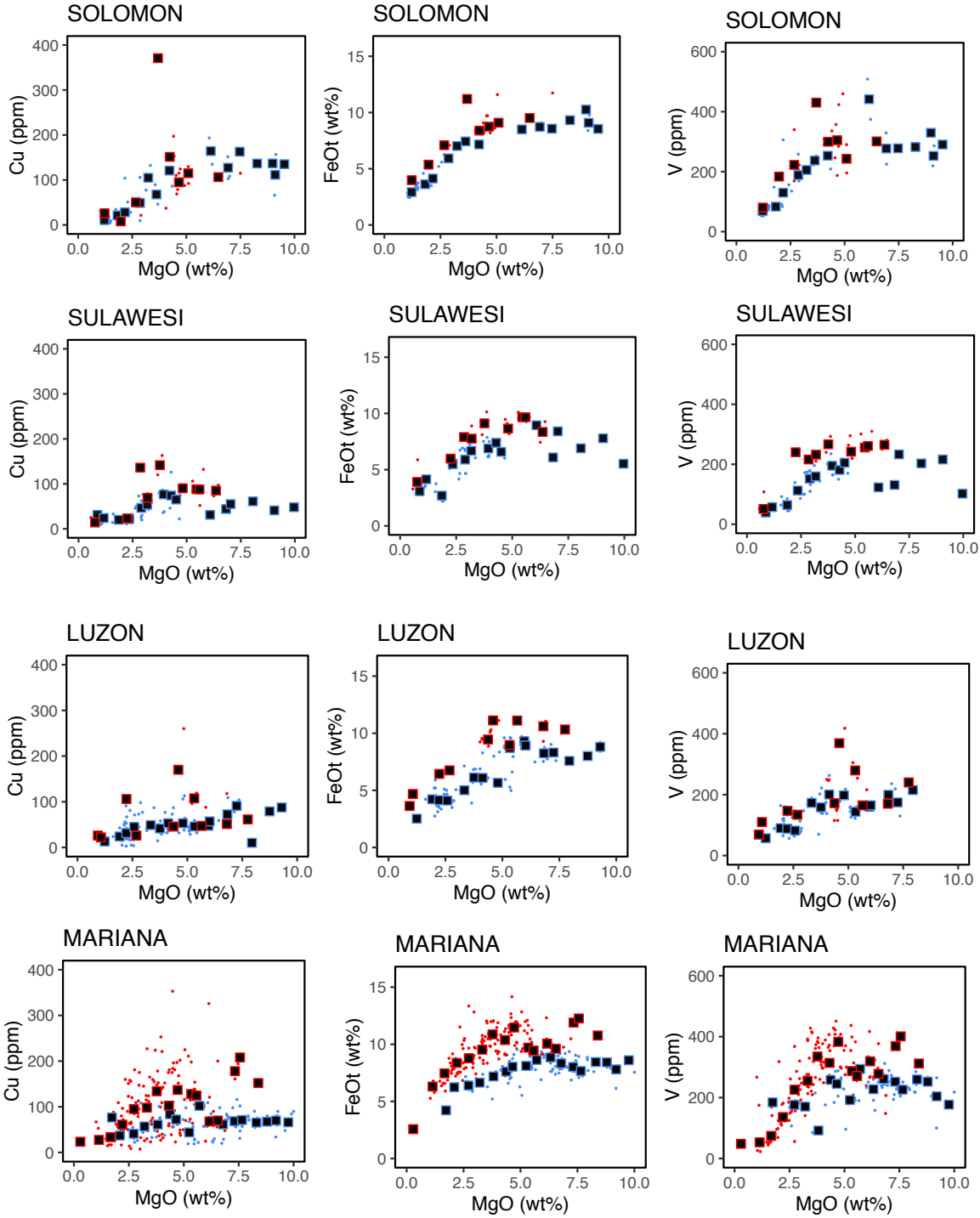
SOLOMON
Cu (ppm)
MgO (wt%)
SOLOMON
FeOt (wt%)
MgO (wt%)
SOLOMON
V (ppm)
MgO (wt%)
SULAWESI
Cu (ppm)
MgO (wt%)
SULAWESI
FeOt (wt%)
MgO (wt%)
SULAWESI
V (ppm)
MgO (wt%)
LUZON
Cu (ppm)
MgO (wt%)
LUZON
FeOt (wt%)
MgO (wt%)
LUZON
V (ppm)
MgO (wt%)
MARIANA
Cu (ppm)
MgO (wt%)
MARIANA
FeOt (wt%)
MgO (wt%)
MARIANA
V (ppm)
MgO (wt%)

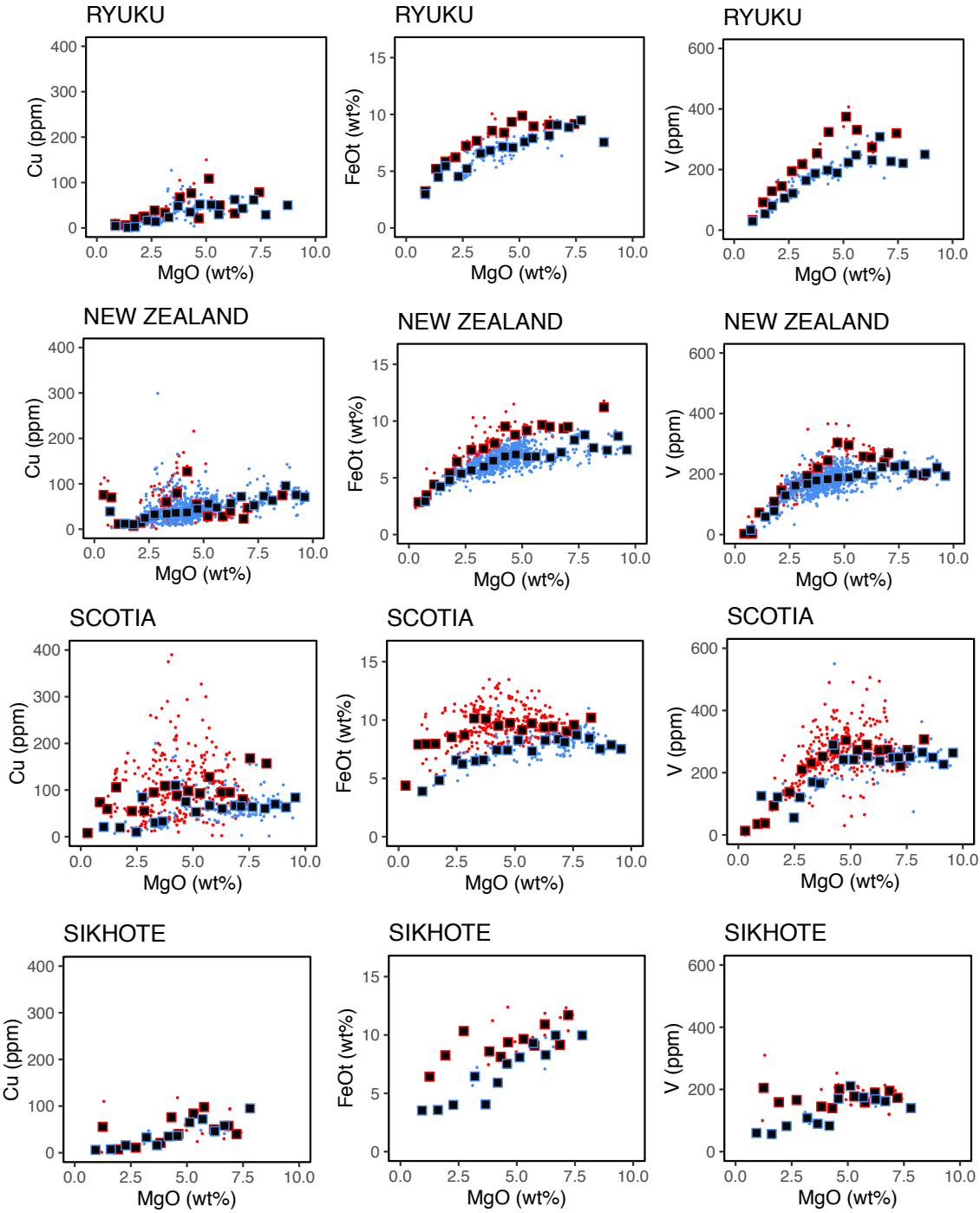
RYUKU
RYUKU
RYUKU
NEW ZEALAND
NEW ZEALAND
NEW ZEALAND
SCOTIA
SCOTIA
SCOTIA
SIKHOTE
SIKHOTE
SIKHOTE
Cu (ppm)
FeOt (wt%)
V (ppm)
MgO (wt%)
0.0
2.5
5.0
7.5
10.0
0
100
200
300
400
5
10
15
600

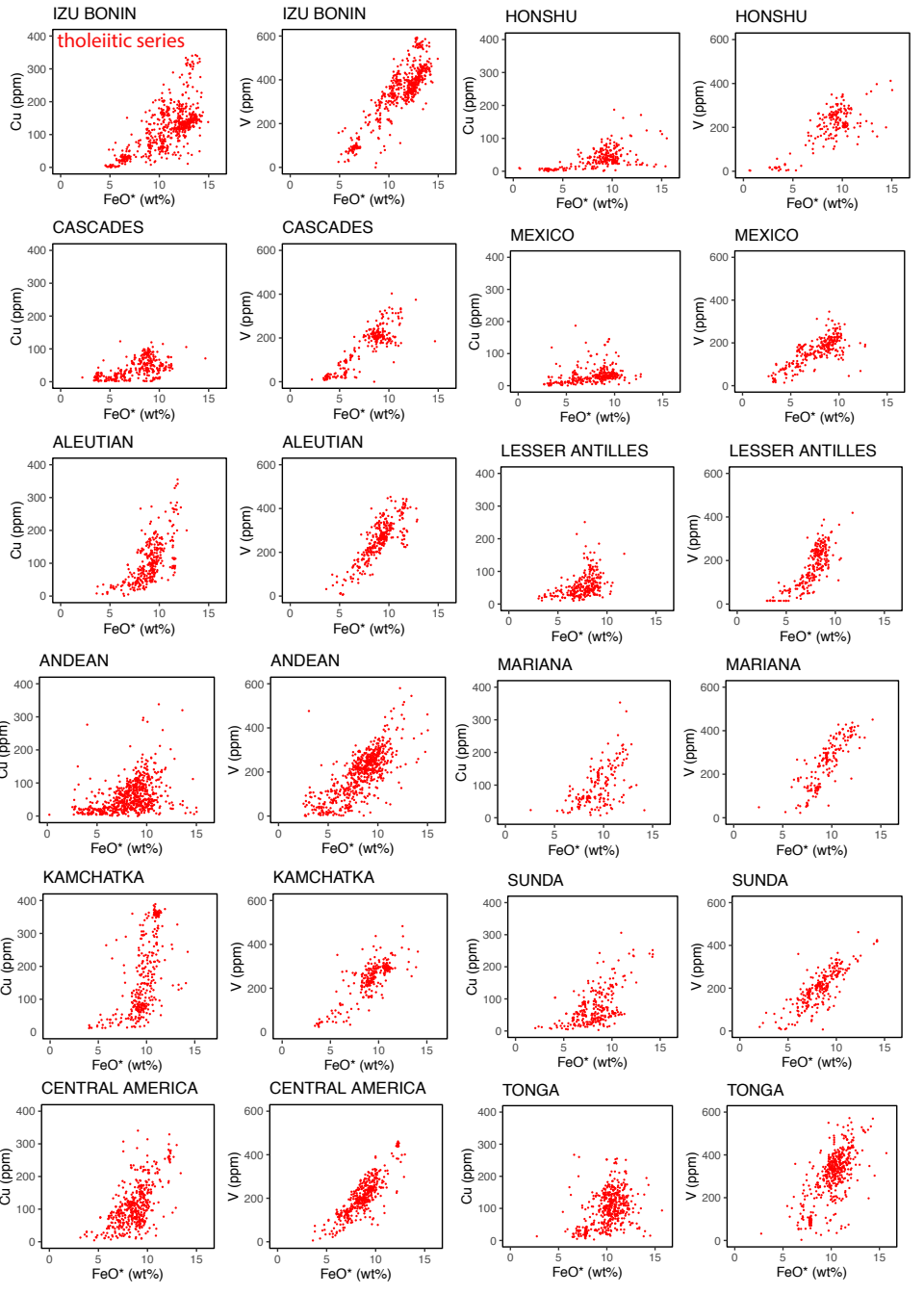
tholeiitic series
IZU BONIN
IZU BONIN
HONSHU
HONSHU
CASCADES
CASCADES
MEXICO
MEXICO
ALEUTIAN
ALEUTIAN
LESSER ANTILLES
LESSER ANTILLES
ANDEAN
ANDEAN
MARIANA
MARIANA
KAMCHATKA
KAMCHATKA
SUNDA
SUNDA
CENTRAL AMERICA
CENTRAL AMERICA
TONGA
TONGA
Cu (ppm)
V (ppm)
FeO* (wt%)

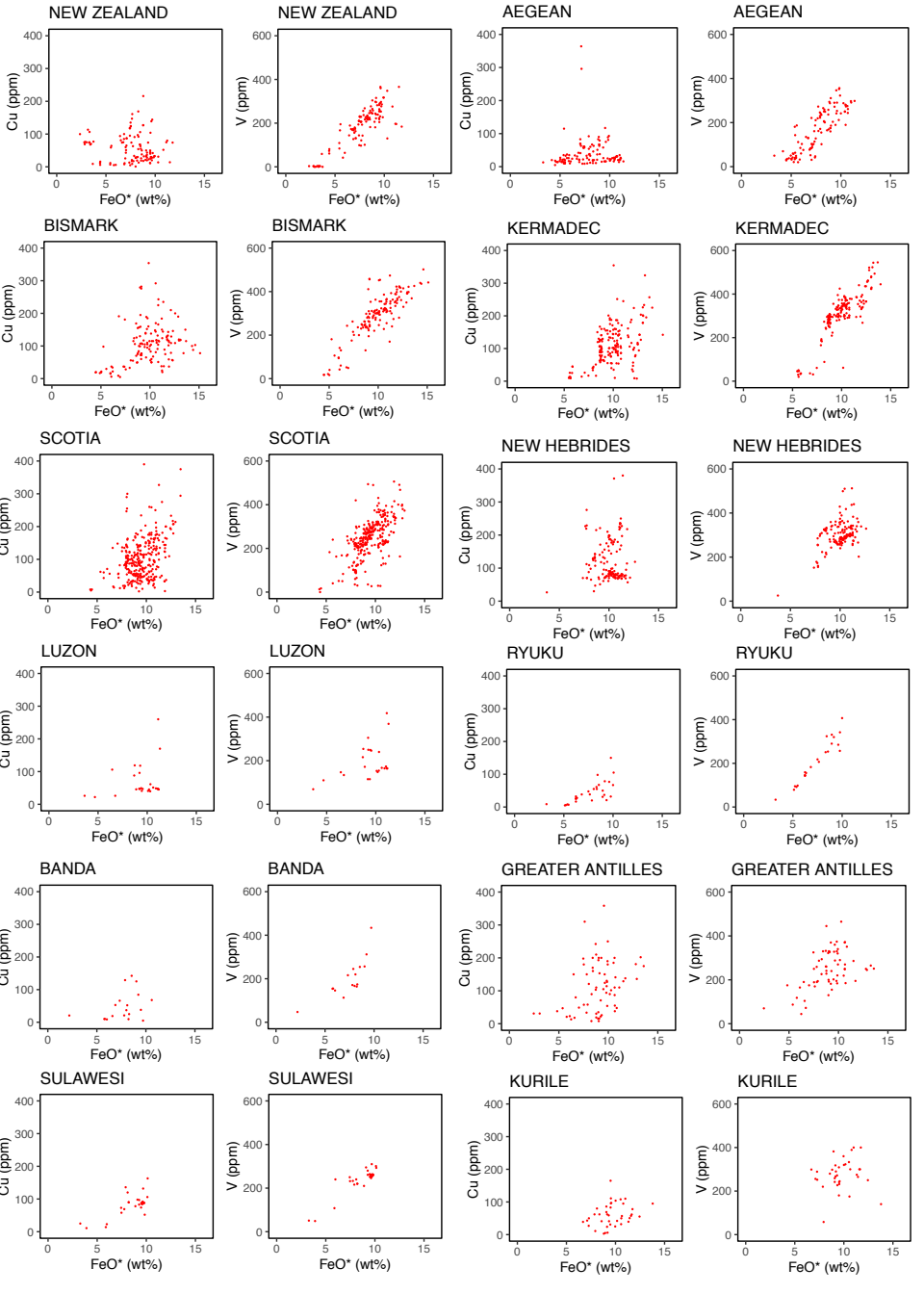
NEW ZEALAND
Cu (ppm)
FeO* (wt%)
NEW ZEALAND
V (ppm)
FeO* (wt%)
AEGEAN
Cu (ppm)
FeO* (wt%)
AEGEAN
V (ppm)
FeO* (wt%)
BISMARK
Cu (ppm)
FeO* (wt%)
BISMARK
V (ppm)
FeO* (wt%)
KERMADEC
Cu (ppm)
FeO* (wt%)
KERMADEC
V (ppm)
FeO* (wt%)
SCOTIA
Cu (ppm)
FeO* (wt%)
SCOTIA
V (ppm)
FeO* (wt%)
NEW HEBRIDES
Cu (ppm)
FeO* (wt%)
NEW HEBRIDES
V (ppm)
FeO* (wt%)
LUZON
Cu (ppm)
FeO* (wt%)
LUZON
V (ppm)
FeO* (wt%)
RYUKU
Cu (ppm)
FeO* (wt%)
RYUKU
V (ppm)
FeO* (wt%)
BANDA
Cu (ppm)
FeO* (wt%)
BANDA
V (ppm)
FeO* (wt%)
GREATER ANTILLES
Cu (ppm)
FeO* (wt%)
GREATER ANTILLES
V (ppm)
FeO* (wt%)
SULAWESI
Cu (ppm)
FeO* (wt%)
SULAWESI
V (ppm)
FeO* (wt%)
KURILE
Cu (ppm)
FeO* (wt%)
KURILE
V (ppm)
FeO* (wt%)

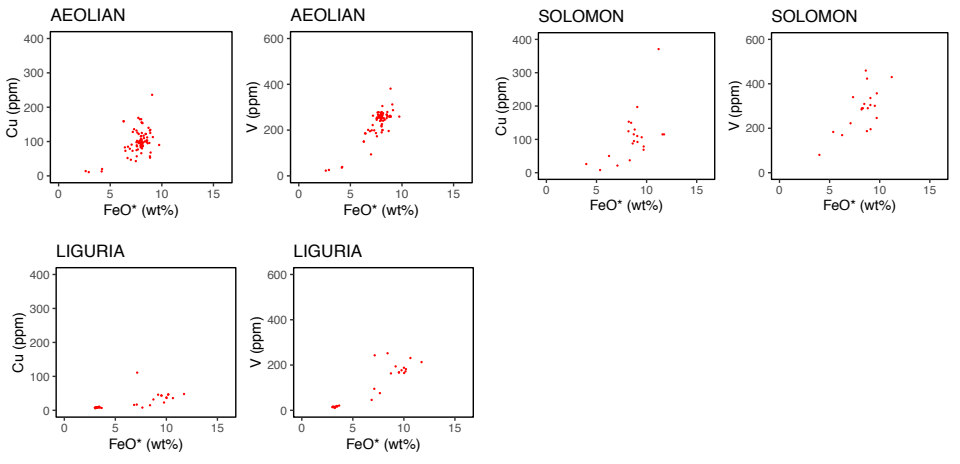
AEOLIAN
Cu (ppm)
FeO* (wt%)
AEOLIAN
V (ppm)
FeO* (wt%)
SOLOMON
Cu (ppm)
FeO* (wt%)
SOLOMON
V (ppm)
FeO* (wt%)
LIGURIA
Cu (ppm)
FeO* (wt%)
LIGURIA
V (ppm)
FeO* (wt%)

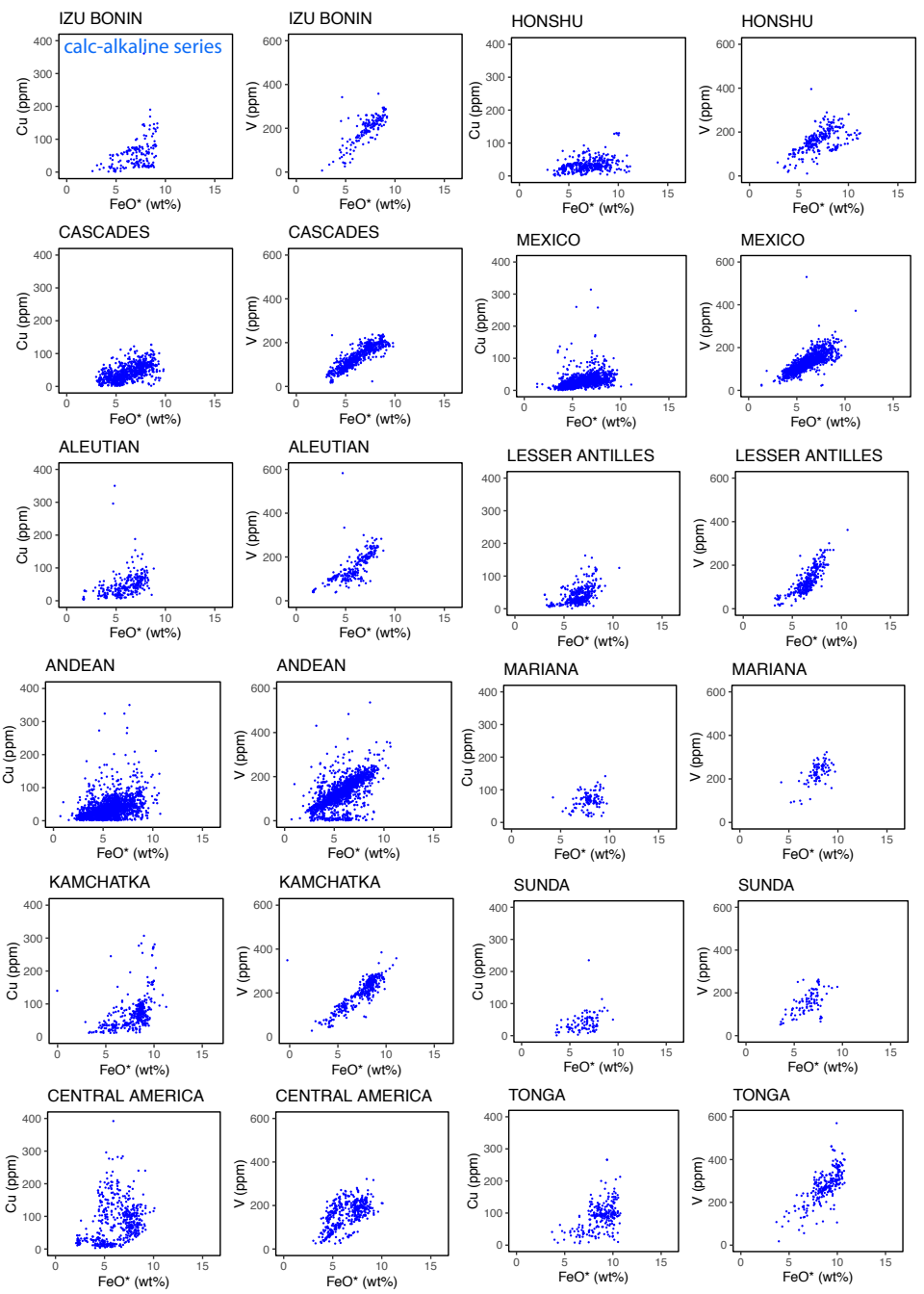
IZU BONIN
calc-alkaline series
Cu (ppm)
FeO* (wt%)
IZU BONIN
V (ppm)
FeO* (wt%)
HONSHU
Cu (ppm)
FeO* (wt%)
HONSHU
V (ppm)
FeO* (wt%)
CASCADES
Cu (ppm)
FeO* (wt%)
CASCADES
V (ppm)
FeO* (wt%)
MEXICO
Cu (ppm)
FeO* (wt%)
MEXICO
V (ppm)
FeO* (wt%)
ALEUTIAN
Cu (ppm)
FeO* (wt%)
ALEUTIAN
V (ppm)
FeO* (wt%)
LESSER ANTILLES
FeO* (wt%)
LESSER ANTILLES
V (ppm)
FeO* (wt%)
ANDEAN
Cu (ppm)
FeO* (wt%)
ANDEAN
V (ppm)
FeO* (wt%)
MARIANA
Cu (ppm)
FeO* (wt%)
MARIANA
V (ppm)
FeO* (wt%)
KAMCHATKA
Cu (ppm)
FeO* (wt%)
KAMCHATKA
V (ppm)
FeO* (wt%)
SUNDA
Cu (ppm)
FeO* (wt%)
SUNDA
V (ppm)
FeO* (wt%)
CENTRAL AMERICA
Cu (ppm)
FeO* (wt%)
CENTRAL AMERICA
V (ppm)
FeO* (wt%)
TONGA
Cu (ppm)
FeO* (wt%)
TONGA
V (ppm)
FeO* (wt%)

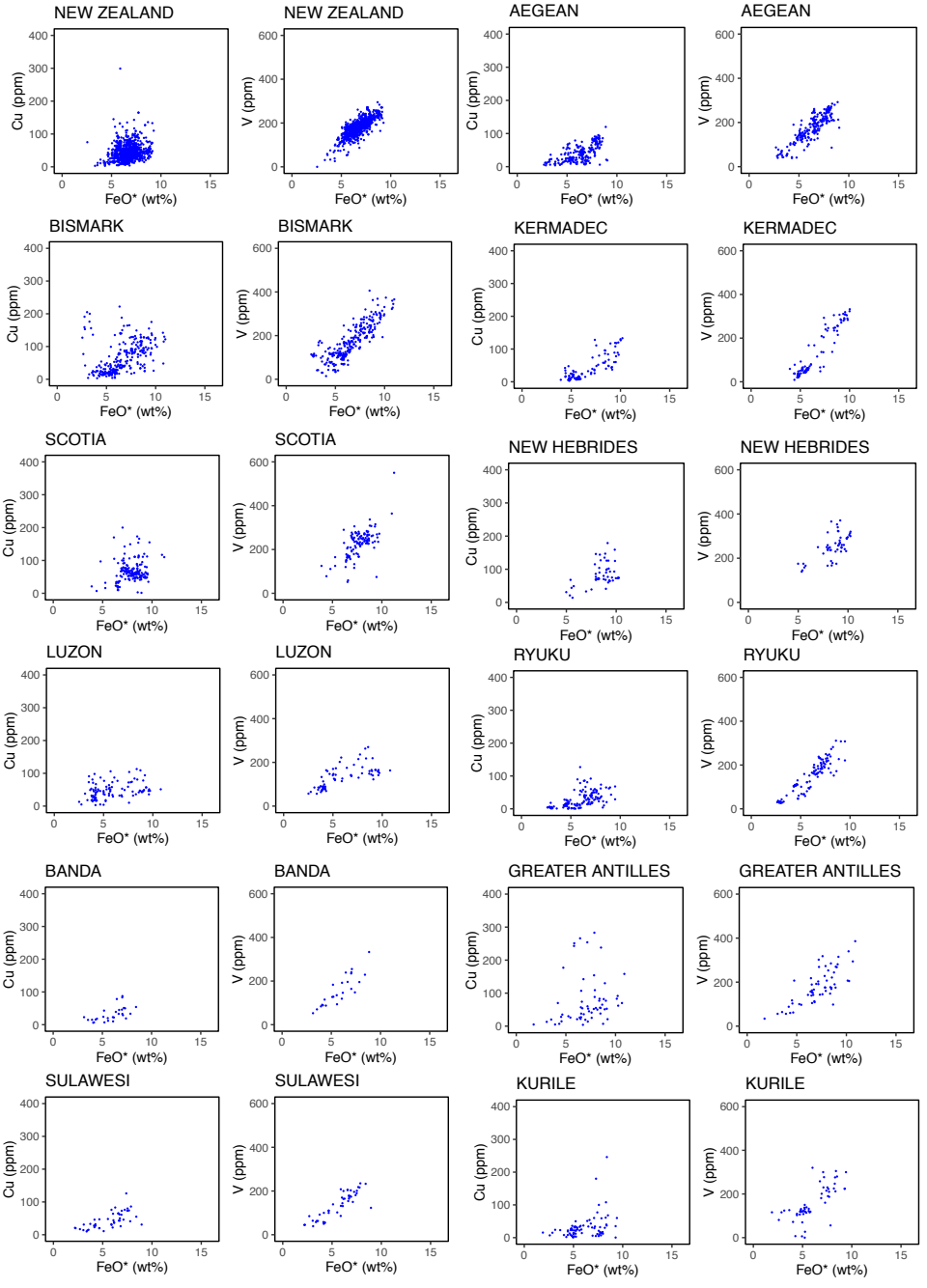
NEW ZEALAND
Cu (ppm)
FeO* (wt%)
NEW ZEALAND
V (ppm)
FeO* (wt%)
AEGEAN
Cu (ppm)
FeO* (wt%)
AEGEAN
V (ppm)
FeO* (wt%)
BISMARK
Cu (ppm)
FeO* (wt%)
BISMARK
V (ppm)
FeO* (wt%)
KERMADEC
Cu (ppm)
FeO* (wt%)
KERMADEC
V (ppm)
FeO* (wt%)
SCOTIA
Cu (ppm)
FeO* (wt%)
SCOTIA
V (ppm)
FeO* (wt%)
NEW HEBRIDES
Cu (ppm)
FeO* (wt%)
NEW HEBRIDES
V (ppm)
FeO* (wt%)
LUZON
Cu (ppm)
FeO* (wt%)
LUZON
V (ppm)
FeO* (wt%)
RYUKU
Cu (ppm)
FeO* (wt%)
RYUKU
V (ppm)
FeO* (wt%)
BANDA
Cu (ppm)
FeO* (wt%)
BANDA
V (ppm)
FeO* (wt%)
GREATER ANTILLES
Cu (ppm)
FeO* (wt%)
GREATER ANTILLES
V (ppm)
FeO* (wt%)
SULAWESI
Cu (ppm)
FeO* (wt%)
SULAWESI
V (ppm)
FeO* (wt%)
KURILE
Cu (ppm)
FeO* (wt%)
KURILE
V (ppm)
FeO* (wt%)

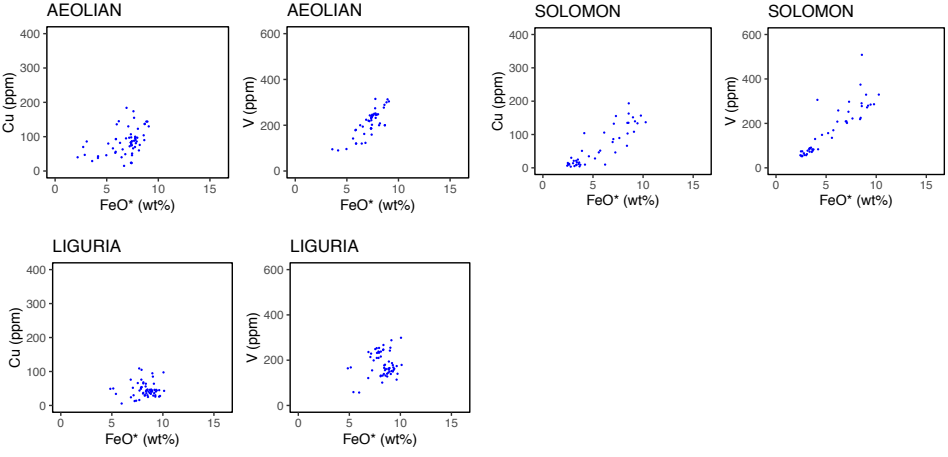
AEOLIAN
Cu (ppm)
FeO* (wt%)
AEOLIAN
V (ppm)
FeO* (wt%)
SOLOMON
Cu (ppm)
FeO* (wt%)
SOLOMON
V (ppm)
FeO* (wt%)
LIGURIA
Cu (ppm)
FeO* (wt%)
LIGURIA
V (ppm)
FeO* (wt%)

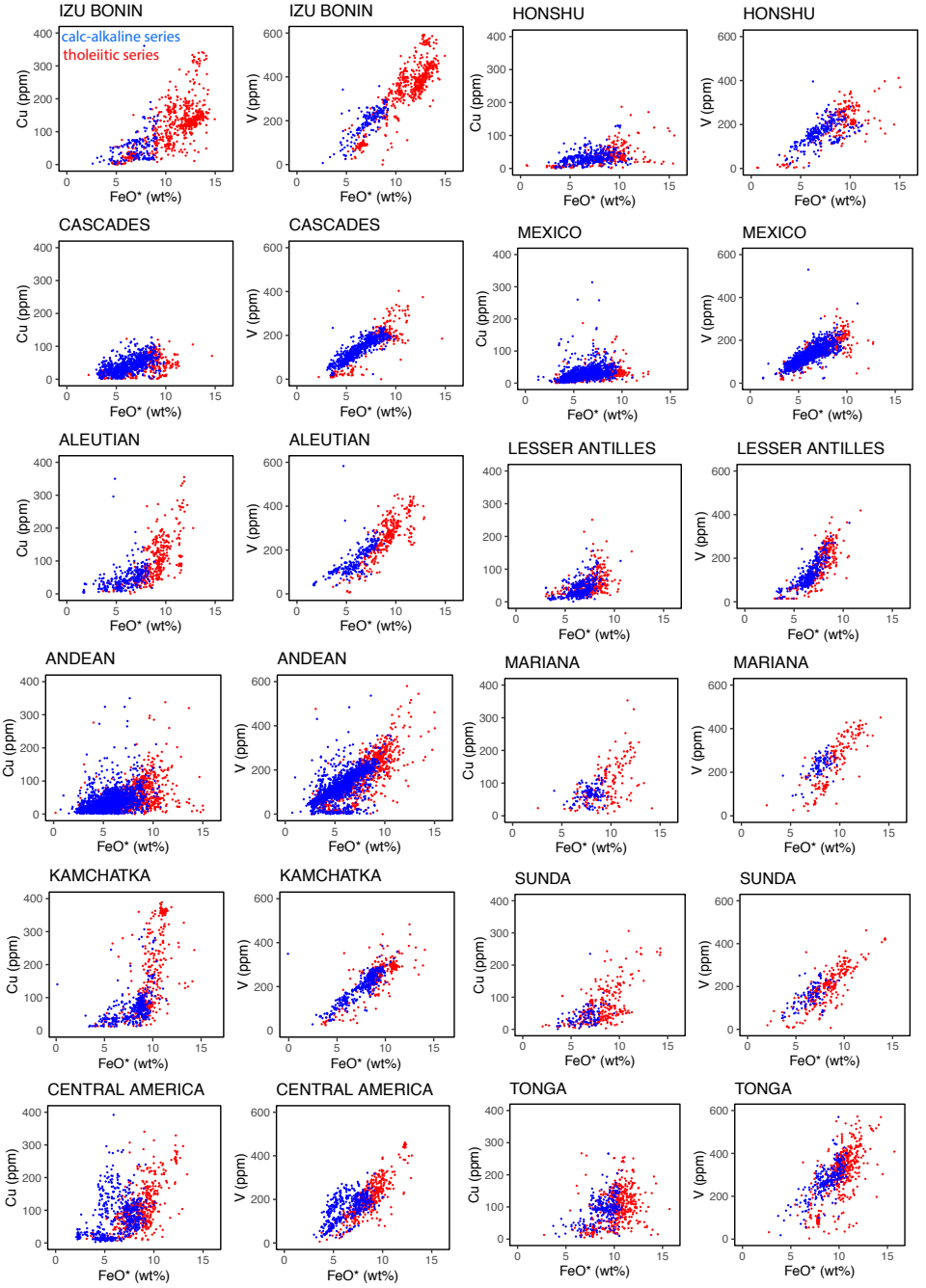
calc-alkaline series
tholeiitic series
IZU BONIN
IZU BONIN
HONSHU
HONSHU
CASCADES
CASCADES
MEXICO
MEXICO
ALEUTIAN
ALEUTIAN
LESSER ANTILLES
LESSER ANTILLES
ANDEAN
ANDEAN
MARIANA
MARIANA
KAMCHATKA
KAMCHATKA
SUNDA
SUNDA
CENTRAL AMERICA
CENTRAL AMERICA
TONGA
TONGA
Cu (ppm)
V (ppm)
FeO* (wt%)

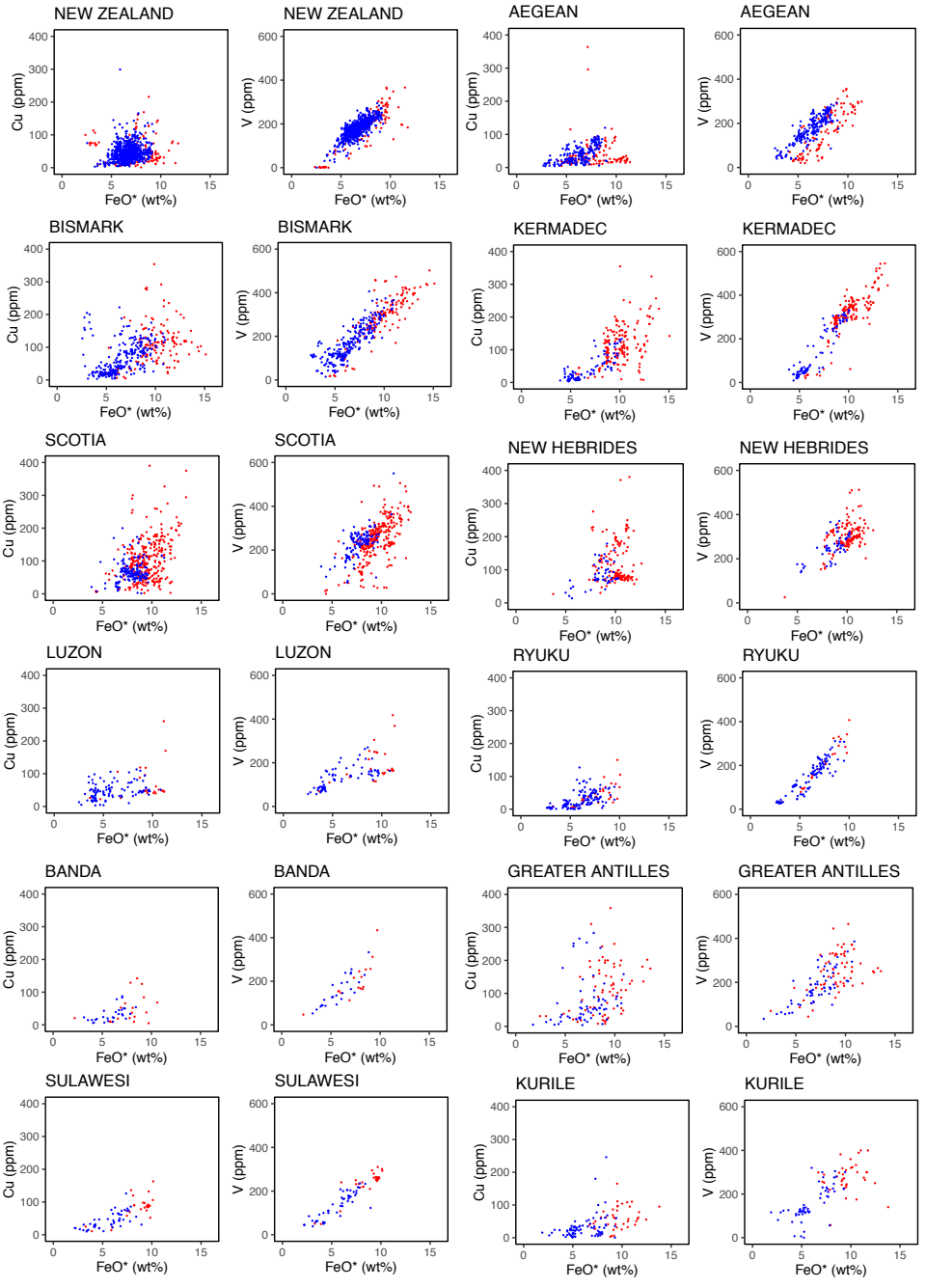
NEW ZEALAND
Cu (ppm)
FeO* (wt%)
NEW ZEALAND
V (ppm)
FeO* (wt%)
AEGEAN
Cu (ppm)
FeO* (wt%)
AEGEAN
V (ppm)
FeO* (wt%)
BISMARK
Cu (ppm)
FeO* (wt%)
BISMARK
V (ppm)
FeO* (wt%)
KERMADEC
Cu (ppm)
FeO* (wt%)
KERMADEC
V (ppm)
FeO* (wt%)
SCOTIA
Cu (ppm)
FeO* (wt%)
SCOTIA
V (ppm)
FeO* (wt%)
NEW HEBRIDES
Cu (ppm)
FeO* (wt%)
NEW HEBRIDES
V (ppm)
FeO* (wt%)
LUZON
Cu (ppm)
FeO* (wt%)
LUZON
V (ppm)
FeO* (wt%)
RYUKU
Cu (ppm)
FeO* (wt%)
RYUKU
V (ppm)
FeO* (wt%)
BANDA
Cu (ppm)
FeO* (wt%)
BANDA
V (ppm)
FeO* (wt%)
GREATER ANTILLES
Cu (ppm)
FeO* (wt%)
GREATER ANTILLES
V (ppm)
FeO* (wt%)
SULAWESI
Cu (ppm)
FeO* (wt%)
SULAWESI
V (ppm)
FeO* (wt%)
KURILE
Cu (ppm)
FeO* (wt%)
KURILE
V (ppm)
FeO* (wt%)

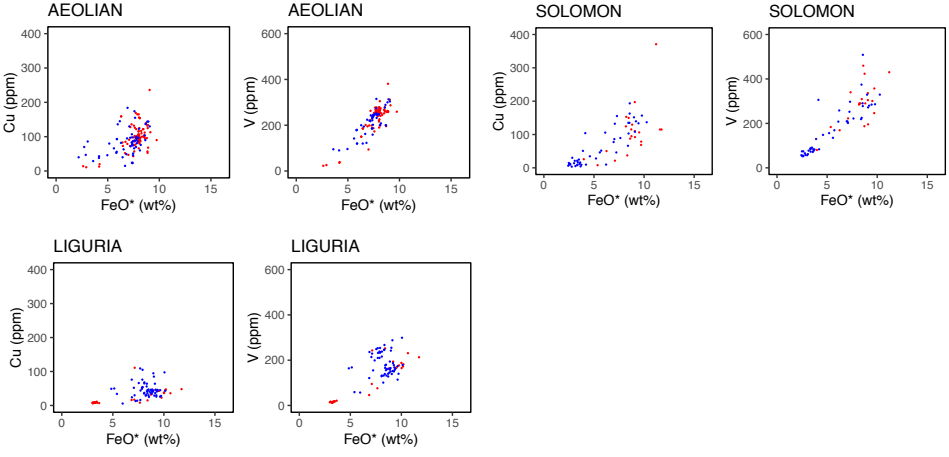
AEOLIAN
Cu (ppm)
FeO* (wt%)
AEOLIAN
V (ppm)
FeO* (wt%)
SOLOMON
Cu (ppm)
FeO* (wt%)
SOLOMON
V (ppm)
FeO* (wt%)
LIGURIA
Cu (ppm)
FeO* (wt%)
LIGURIA
V (ppm)
FeO* (wt%)

Calculation of Cu endowment in fluid

The volume of the H_2O-saturated melt (V_{ini}) corresponds to the melt fraction at which an initial volume of magma (V_0) reached H_2O saturation (F_{ini})

$$V_{ini}^{melt} = V_0^{melt} * F_{ini}$$

Where V_0 is the initial volume of magma based on an average arc magma production rate of 189 km^3 km^{-1} Myr^{-1} in intra-oceanic arcs (Jicha and Jagoutz, 2015) and F_{ini} is determined from the Rhyolite-MELT modeling (Table. D1). The remaining melt fraction of H_2O-saturated melt at degassing depends on the H_2O dissolved in the melt (W), the percolation threshold (ϕ_c), and the density of melt (d_{melt}) and fluid (d_{fluid}):

$$F_{degas} = \frac{W}{d_{fluid}} / \left(\frac{\phi c}{d_{melt}\,(1 - \phi c)} + \frac{W}{d_{fluid}} \right)$$

Where, the percolation threshold (Φc) correspond to the critical porosity at which the transition from an impermeable to permeable magma allowing degassing occurs and fixed at 0.3 based on percolation theory for overlapping spheres that predict Φc~0.28-0.35 (Walsh and Saar, 2008; Vasseur and Wadsworth, 2017), W and density (Mt/km^3) of melt and fluid are obtained from the Rhyolite-MELT modeling (Table. D1).

The volume (km^3) of H_2O-saturated melt and fluid at degassing corresponds to

$$V_{degas}^{melt} = V_{ini}^{melt} * F_{degas}$$

$$V_{degas}^{fluid} = V_{ini}^{melt} * W * (F_{n-1} - F_{degas}) \frac{d_{melt}}{d_{fluid}}$$

where F_{n-1}=1.

The concentration of Cu (wt%) in the melt and fluid at degassing corresponds to

$$C_{Cudegas}^{melt} = \frac{C_{Cuini}^{melt}}{D_{Cu} + F_{degas}\,(1 - D_{Cu})}$$

$$D_{Cu} = D^{crystals/melt}_{Cu}(1 - W) + D_{fluid/melt}^{Cu} W$$

$$C^{fluid}_{Cu} = C_{Cudegas}^{melt} * D^{fluid/melt}_{Cu}$$

Where C^{melt}_{Cuini} is the melt copper content at fluid saturation obtained from the Rhyolite-MELT modeling (Table D1), $D^{crystals/melt}_{Cu}$ and $D^{fluid/melt}_{Cu}$ are the partition coefficient of Cu between fractionated phases (silicates, oxides, phosphates, sulfide) or fluid with respect to the melt. $D^{crystals/melt}_{Cu}$ = 2.1 corresponds to the one used in the Rayleigh fractionation model (Table D1), whereas $D^{fluid/melt}_{Cu}$ = 140 (Tattitch and Blundy, 2017).

The mass (Mt) of Cu transferred in expelled fluids corresponds to

$$m^{fluid}_{Cu} = V^{fluid}_{degas} * d_{fluid} * C^{fluid}_{Cu}$$

References

Chelle-Michou, C., Rottier, B., Caricchi, L., Simpson, G., 2017. Tempo of magma degassing and the genesis of porphyry copper deposits. *Sci. Rep. 7*, 40566.

Jicha, B. R., Jagoutz, O., 2015. Magma production rates for intraoceanic arcs. *Elements 11*, 105-111.

Kouzmanov, K., Pokrovski, G. S., 2012. Hydrothermal controls on metal distribution in porphyry Cu(–Au–Mo) systems. *Society of Economic Geologists*, Special Publication 16, 573–618.

Tattitch, B. C., Blundy, J. D., 2017. Cu-Mo partitioning between felsic melts and saline-aqueous fluids as a function of XNaCleq, fO_2, and fS_2. *Am. Miner*. 102, 1987-2006.

Vasseur, J., Wadsworth, F. B., 2017. Sphere models for pore geometry and fluid permeability in heterogeneous magmas. *Bull. Volcanol.*79, 77.

Walsh, S. D., and Saar, M. O. 2008. Magma yield stress and permeability: Insights from multiphase percolation theory. . Volcanol. Geotherm. Res. 177, 1011-1019.